AN ABSTRACT OF THE THESIS OF

Suvimol Sujjavanich for the degree of Doctor of Philosophy in Civil Engineering presented on November 27,1996. Title Early Age Performance of Latex-Modified Concrete Bridge Deck Overlays.

Redacted for privacy

James R.Lundy

Environmental factors and physical properties of latex modified concrete (LMC) are hypothesized to contribute to early age cracking in bridge deck overlays. Cracking permits the ingress of moisture and aggressive solutions into the substrate and may contribute to other subsequent distresses. Understanding the material properties and mechanisms involved is necessary to minimize these distresses.

This research consisted of a two part study: first, the development of LMC strength and fracture properties at ages ranging from 5 hours to 28 days was studied, and secondly, the effects of the environment on LMC distresses were modelled. Environmental conditions: temperature, solar energy, and wind speed were determined from weather records. A fracture mechanics based model, the Fictitious Crack Model (FCM), incorporating finite element analyses and superposition techniques was employed with material properties from the first part of study on LMC performance. Different bilinear strain softening diagrams were used to predict fracture performance at different ages. The predictions agreed well with the test data. The impacts of temperature differentials on crack development were studied. The shrinkage effect was also indirectly incorporated through the temperature analysis.

The material properties study indicated significant changes in strength, deformability and fracture properties, particularly during the early age. The developments differ slightly from conventional concrete. Test results indicated a significant improvement in reducing and bridging microcracks, especially in the prepeak-load region. Fracture toughness and deformability increased significantly with time. Fracture energy varied from 2.3 to 133.1 N/m, depending on age, and to some degree, on notch depth ratio.

In the second stage, the FCM provided a reasonable prediction for crack initiation and propagation when only temperature effects are of concern. Age, surface conditions and structural restraint strongly affect crack resistance of the overlays. Only slight effects were observed from the overlay thickness in the study range (51-76mm). Shallow pre-existing cracks possibly reduce the crack resistance of the overlay about 30 percent. A prolonged moist cure for 48 hours after placing is suggested to reduce the risk of cracking. With available environmental information, it is possible to develop guidelines for appropriate environmental conditions for LMC bridge deck construction to minimize the risk of early age cracking.

Early Age Performance of Latex-Modified Concrete Bridge Deck Overlays

by

Suvimol Sujjavanich

A THESIS

submitted to

Oregon State University

in partial fulfillment of
the requirements for the
degree of

Doctor of Philosophy

Presented November 27, 1996
Commencement June 1997

Doctor of Philosophy thesis of Suvimol Sujjavanich presented on November 27,1996

APPROVED:

Redacted for privacy

Major Professor, representing Civil, Construction and Environmental Engineering

Redacted for privacy

Head of Department of Civil, Construction and Environmental Engineering

Redacted for privacy

Dean of Graduate School

I understand that my thesis will become part of the permanent collecton of Oregon State University libraries. My signature below authorizes release of my thesis to any reader upon request.

Redacted for privacy

Suvimol Sujjavanich, Author

ACKNOWLEDGEMENT

The author is grateful to Dr.James R.Lundy, the major advisor for the precious time of continuous advice as well as acknowledgment for many fruitful discussions with Professor Methi Wecharatana of the New Jersey Institute of Technology, Professor Timothy Kennedy and Dr.Thomas Miller of the Oregon State University. The valuable instrumentation assistance of Mr.Andy Brickman of OSU is grateful acknowledged. Also, the financial support of the Departments of Civil Engineering, Oregon State University and Kasetsart University, and material supplied by Dow Chemical Company are appreciated. Finally, the author also wishes to thank the following for their support: Dr. Bob Leichti, Mr.Cherdchai Udom, Ms.Sharon Hope, Dr. Ye Shun Tien, Mr.veerachai Siripunvaraporn, Mr.Larry Ilg, friends and family. Without these supports, this research would not be finished.

TABLE OF CONTENTS

Page

1. INTRODUCTION 1
   1.1 Background 1
   1.2 Objectives 4
   1.3 Scope 4
   1.4 Research Significance 5

2 MATERIALS AND PROBLEM DEVELOPMENT 6
   2.1 Material: Latex Modified Concrete (LMC) 6
   2.2 Material Properties 12
      2.2.1 Plastic Concrete 12
      2.2.2 Hardened Concrete 13
   2.3 Problem Development 16
   2.4 Cause of Distresses 18
      2.4.1 Construction Procedure 19
      2.4.2 Structural Loading 19
      2.4.3 Environmental Impacts 20
      2.4.4 Shrinkage 21
   2.5 Cracking Characteristics 23
      2.5.1 Random Cracks 23
      2.5.2 Transverse Cracks 24
      2.5.3 Longitudinal Cracks 25
   2.6 Contributing Factors to Early Age Cracking 25
      2.6.1 Temperature 26
      2.6.2 Solar Radiation 27
   2.6.3 Wind 29
   2.6.4 Shrinkage 30

3. TOOLS AND MODELING TECHNIQUES 32
   3.1 Introduction to Fracture Mechanics 32
   3.2.Linear Elastic Fracture Mechanics (LEFM) 36
   3.3 Fictitious Crack Model (FCM) 42
      3.3.1 Principles and Assumptions 43
      3.3.2 Methodology 47
      3.3.3 Strain Softening Diagram 49
   3.4 Finite Element Model 53
   3.5 Heat Flow Conditions 53

TABLE OF CONTENTS (CONTINUED)

Page

4. EXPERIMENTS AND RESULTS 56
4.1 Material and Test Setup 57
4.1.1 Compressive Strength 62
4.1.2 Tensile Strength 62
4.1.3 Modulus of Elasticity 62
4.1.4 Fracture Energy 63
4.1.5 Shrinkage 67
4.2 Test Results and Discussions 70
4.2.1 General Strength Properties 70
4.2.2 Fracture Properties 73
4.2.3 Shrinkage Properties 91
4.3 Summary 97

5. ANALYSIS AND MODELLING 100
5.1 Approaches Verification 100
5.2 The Chosen Strain Softening Diagram 106
5.3 Environmental Effects 111
5.3.1 Case Study 111
5.3.2 Unit Temperature Differential 113
5.3.3 Temperature Distribution 116
5.3.4 Temperature Differential Effect 120
5.4 Shrinkage Effect 128

6. CONCLUSIONS 132
6.1 Conclusions 132
6.2 Recommendations 137

REFERENCES 140

LIST OF FIGURES

Figure Page

2.1 Polymer classification....7

2.2 The processes developed in latex modified concrete....10

2.3 Pore size distribution of unmodified concrete and LMC....11

2.4 Change in compressive strength, LMC and normal concrete comparison....14

2.5 Comparison of shrinkage performance between LMC and conventional concrete...22

3.1 Stress distribution around an elliptical hole in an infinitely large plate....32

3.2 Energy change between crack and uncracked plate....36

3.3 Crack tip coordinates and stress system....39

3.4 Three modes of fracture in a material....40

3.5 Behavior comparison between concrete and metal....41

3.6 Principle of Fictitious Crack Model Concept applied to Tension member....44

3.7 Stress-elongation of cracked and uncracked portion....44

3.8 Stress state at cracking area by FCM....46

3.9 Flow chart for the calculation steps, using superposition technique and FCM....50

LIST OF FIGURES (Continued)

Figure Page

3.10 Fictitious Crack Model Concept applied to three point bending beam incorporating bilinear strain softening diagram.....51

3.11 Proposed shapes of strain softening diagrams.....51

4.1 Test setup for fracture test.....59

4.2 Three point bending set up for flexure and fracture energy test.....60

4.3 Special Plexiglas mold for flexure and fracture test at early age.....60

4.4 Test setup for Plexiglas mold calibration.....61

4.5 LMC early age test setup.....61

4.6 Typical load vs mid span deflection for mold calibration.....66

4.7 Wood mold for shrinkage testing.....69

4.8 Shrinkage test specimens in controlled environmental chamber.....69

4.9 Strength and modulus development of LMC.....71

4.10 The development of f_c/f_t vs time.....72

4.11 Development of LMC flexural stress with time.....72

4.12 Development of notch sensivity with time.....74

4.13 The effect of notch depth ratio on notch sensitivity.....74

LIST OF FIGURES (Continued)

Figure Page

4.14 Development of deformability with time....75

4.15 Typical load vs mid span deflection and load vs crack mouth opening displacement (cmod) relationships for notched beams....75

4.16 Determination of the elastic limit, Pe....76

4.17 Relationship of Pe/Pmax. with time....77

4.18 Relationship of Pe/Pmax. with notch depth ratio....78

4.19 Typical bilinear relationship between mid span deflection and crack mouth opening....80

4.20 The relationship between slope S2 and time....81

4.21 Typical load vs mid span for notched and unnotched beams....81

4.22 Development of LMC fracture energy with time....82

4.23 Relationship between load and displacement at different ages....82

4.24 Relationship between load and displacement at different notch depth ratios....83

4.25 Effect of dead weight on fracture energy development....84

4.26 Effect of age and notch depth ratio on LMC fracture energy....87

4.27 Typical load vs midspan deflection of unnotched beam....87

4.28 Relationship of LMC fracture energy with compressive strength....88

LIST OF FIGURES (Continued)

Figure Page

4.29 Development of LMC characteristic length with time....88

4.30 Difference of crack pattern of test specimen....89

4.31 Difference failure mechanism at different ages....90

4.32 Development of LMC and normal concrete shrinkage with time for two temperatures....94

4.33 Severe cracking under low temperature/humidity condition....95

4.34 Shrinkage performance under control condition for 10 days....95

4.35 Shrinkage performance under cyclic temperature change between 160-250 hours....96

4.36 Influence of temperature of concrete(at an air temperature of 4.5 °C on the loss of water from concretein the early stages after placing relative humidity of air 100 percent, wind velocity 4.5 m/s)....96

4.37 Relationbetween shrinkage and loss of water from specimens, cured for 7 days at 21 °C and then dried....97

5.1 Superposition model verification....102

5.2 The comparison of load-deflection curves between Wittman's data and predictions using the superposition method....104

5.3 Prediction of temperature effect for bridge deck....105

5.4 Comparison of load vs midspan deflection for linear and bilinear relationships at various ages....107

LIST OF FIGURES (Continued)

Figure Page

5.5 Effects of strain softening diagram on load-deflection curve....108

5.6 Comparison of load-deflection curves between test and the predicted results from the chosen strain softening diagram....111

5.7 Variation of solar radiation from case study in Oregon....114

5.8 Temperature variation from the study case....114

5.9 Unit temperature distribution....115

5.10 Variation of solar radiation, air and deck temperature with time....117

5.11 Comparison of environmental variations between predicted and field measurements....118

5.12 Temperature distribution through deck depth....119

5.13 F.E. model for deck with different condition....121

5.14 Crack performance of the 51 mm overlay, for a continuous span at different ages and conditions....123

5.15 Model for simple support condition....124

5.16 Comparison of 51 mm overlay performances with different restraint conditions....125

5.17 Performance comparison between two thickness overlays with different ages and conditions....126

5.18 Comparison of crack resistance for similar age overlays witth different thicknesses....127

LIST OF FIGURES (Continued)

Figure Page

5.19 Stress distribution through the deck depth..... 127

LIST OF TABLES

Table Page

1.1 Composition of a Styrene Butadiene Copolymer Latex.....8

4.1 Mix proportions of latex modified concrete 58

4.2 Mechanical properties of coarse and fine aggregates.....58

4.3 Load-Deflection relationship for early-age test molds.....67

4.4 Regression equations for LMC mechanical properties 71

Glossary

A	cross sectional area
E	modulus of elasticity
ECS	Environmental Control System
FCM	Fictitious Crack Model, a fracture mechanics-based model which stress transfer ability is assumed in a partial damaged zone
FPZ	Fracture process zone, a partial damaged zone with assumed stress transfer ability
G	Strain energy release rate, dU/da
G_c	critical strain energy release rate
G_f	Fracture energy, a required energy to create a new unit area of crack surface, calculated from the area under σ-w curve
G_{IC}	Critical energy release rate
K_{IC}	Stress intensity factor
L	element length
L'	total thickness of the medium
LEFM	Linear Elastic Fracture Mechanics, a mean to characterize fracture behavior of structural material, based on stress analyses, flaw effect, material toughness and assumed homogenous elastic material
LMC	latex-modified concrete, a mixture of portland cement, fine and coarse aggregates combined with organic polymers that are dispersed in water during mixing
R	crack resistance, dw/da
R_S	bridge temperature on absolute scale
R_*	air temperature on absolute scale

S	total daily solar radiation, Watt hr/m^2/hr
S_2	changing rate rate of crack mouth opening displacement to mid span deflection
T_{SL}	length of the solar day
T_{max}	maximum temperature in the day, °C
T_{min}	minimum temperature in the day, °C
T_s	tensile stress in the far region
T	temperature
U	strain energy
a	half length of ellipse along major axis
b	half length of ellipse along minor axis
c	specific heat, 960 J/kg°C
dA	area increment
dx	crack propagation increment
f_c	compressive strength
f_t	tensile strength
h_1	heat transfer coefficient including convective and radiative heat losses
h_2	heat transfer coefficient at bottom surface
h_c	convection
k	conductivity of the medium, 1.4w/m°C for concrete
l_1, l_2	excess deformation of gauge lengths in zone B and A, respectively
l_0	gauge length

l_{ch}	Characteristic length, a fracture parameter which is a function of modulus of elasticity, tensile strength and fracture energy
q	boundary heat input(lost)/unit area
r,θ	polar coordinates
s_1	defined ordinate of the strain softening diagram
t	time
t'	thickness
v_v	wind velocity, mph
v	vertical opening of a crack length 2a
w	additional deformation due to fracture zone or crack width
w_c	Critical crack width, w-value for $\sigma = 0$
w_1	defined abscissa of the strain softening diagram at any stress level
w_2	defined abscissa of the strain softening diagram at zero stress level
w(x)	crack width at distance x
x	measured distance from the fictitious crack tip (x=0), based on a moving coordinate system with the origin at the tip. x increases in the direction opposite to the direction of crack propagation
ρ	density of the medium, 2400 kg/m^2 for concrete
α	$\pi t/T_{SL}$
ε	strain
ε_{sh}	shrinkage strain at time t
σ	stress at edge of ellipse
σ_{SB}	Stefan-Boltzman's constant
$\sigma_x, \sigma_y, \tau_{xy}$	stresses acting on the element

$\sigma_0(0)$	normal stress at crack tip due to a unit external load
$\sigma_i(0)$	normal stress at crack tip due to a unit internal load at node i in the process zone
υ	Poisson ratio
μ	shear modulus
α	absorptivity coefficient of top surface
α_0, α_i	load multiplication factor for unit external and unit internal loads respectively, applied at node i in the process zone

DEDICATION

This thesis is dedicated to the loving memory of my mother and father who taught me "never give up".

Early Age Performance of Latex-Modified Concrete Bridge Deck Overlays

1. INTRODUCTION

1.1 Background

Transportation systems strongly influence national development, economics, lifestyle, and defense. Roads and bridges provide important links for population movement and conveying goods and technology from place to place. Enormous sums have been invested in the construction and maintenance of these national systems.

The system must be well maintained to maximize its benefit, both in terms of economics and safety. However, deterioration of the system is inevitable. Infrastructure deterioration may be due to environmental conditions, age, material degradation and/or increased loading spectra.

Bridge deck deterioration is one major concern because it affects the service life and maintenance costs of the bridge as well as user safety and convenience. The deterioration, which is often manifested in surface cracking and spalling, is often related to corrosion of the reinforcing steel. Several factors are believed to contribute to this type of deterioration such as the quality of concrete and workmanship, environment, and cracking as well as increasing traffic density and loading.

Furthermore, most existing bridges have no protection systems for salt infiltration. Intruded salt accumulation through the open-pore structure of concrete may initiate and certainly exacerbates steel corrosion. This action is followed by concrete cracking, spalling,

or delamination resulting from the increased volume of corroded steel (1). These factors reduce the service lives of concrete pavements and bridge decks. Therefore, good performing repair materials and cost-effective application of these materials are of interest.

Repair materials must serve two purposes. First, effective materials and efficient repair techniques reduce public inconvenience, and, as a result, user costs. Secondly, materials that reduce the bridge deck permeability provide a protection system against aggressive solution seepage. The reduced permeability is believed to delay the corrosion of reinforcing steel, a major factor in bridge deck deterioration. In 1990, FHWA estimated the cost to rehabilitate and replace 40 percent of all bridges in the United States at about 50 billion dollars. Half of the rehabilitation /replacement cost of bridge decks could be related to deterioration problems caused by steel corrosion (2, 3).

Impermeability and durability are two important factors that are used to judge the effectiveness of bridge deck overlays. Although normal concrete is extensively used for structural members, it is not appropriate for such overlays due to relatively high material permeability. Lower permeability materials that provide a more effective protection system against the ingress of aggressive solutions are of interest.

Improved concrete properties, particularly lower permeability, can be achieved by adding admixtures such as latex to modify the concrete matrices. Latex modified concrete (LMC) is the most common overlay material used for bridge decks over the last decade (4). Many highway agencies continue to use this material and recognize its beneficial qualities. These modified materials generally perform well, however, distress continues to be

reported. Often, distresses are reported soon after construction. The most common early age distresses are cracking and delamination.

These early age distresses are related to several factors, some of which can be controlled. Construction procedures and environmental conditions are believed to significantly influence these distresses. However, it is difficult to predict performance of bridge deck overlays from combinations of these factors, since performance is influenced by material properties and environmental effects which are both time-dependent.

Although much research has been conducted on the impact of material properties, environmental conditions, construction procedures and traffic on long term bridge deck performance, little information is available on early age performance. However, early age performance is critical to the long term performance of the bridge deck. Concrete must be protected from stresses in excess of its developed tensile strength to prevent cracking and delamination.

Cracking and delamination permit the ingress of moisture or aggressive solutions into the substrate. These actions may contribute to other subsequent distresses. The consequences of early age deficiencies are, for example, corrosion in the steel and moisture accumulation in cracks that may lead to spalling after sufficient freezing and thawing. These actions contribute significantly to a reduced deck life. Therefore, to avoid or minimize these distresses and achieve better long term performance, a study is necessary to investigate and understand the material properties and mechanisms involved.

Fracture mechanics provides more realistic descriptions of crack development in a composite material like concrete, compared to the conventional stress criteria which

assumes an immediate drop to zero stress after peak stress (5). Therefore, a Fictitious Crack Model (FCM) was employed to investigate cracking in this study. In order to apply this fracture mechanics-based model to early age crack propagation, some fracture parameters must be investigated.

1.2 Objectives

Many agencies recognize the beneficial qualities of LMC and continue to use this material despite reported problems. This research focuses on the early age performance of LMC bridge deck overlays and particularly, cracking. In order to realize these objectives it is necessary:

1. To investigate the development of LMC early age properties including strength development, deformability, fracture properties and shrinkage.

2. To study the LMC early age cracking performance, using fracture mechanics of concrete incorporating the superposition technique.

3. To predict the effect of material properties and the environment on the early age performance of LMC bridge deck overlays, using the proposed model.

1.3 Scope

The scope of this research is limited to a study of early age performance of LMC bridge deck overlays. "Early age" is defined as the first seven days following placement. Experimental limitations preclude obtaining material properties at ages less than 5 hours.

This study focuses on two types of stresses that are hypothesized to have a strong influence on early age distresses. These are thermal and shrinkage-induced stresses.

1.4 Research Significance

This work provides an understanding of crack formation and performance of early age LMC overlays, as affected by environmental conditions and material properties. The results from this study may be used to develop guidelines for construction specifications to minimize early age distresses in latex-modified concrete although these guidelines have not been developed herein.

2. MATERIALS AND PROBLEM DEVELOPMENT

2.1 Material: Latex Modified Concrete (LMC)

Polymers were first introduced to hydraulic-cement systems in 1923 due to an increased need for a durable construction material. In 1924, Lefebure, using conventional concrete mixture proportioning, produced latex modified concrete (LMC) and latex modified mortar (LMM)(4). After WWII, natural latex was replaced with several types of chemical polymers, both thermoplastic (vinyl-type) and elastomeric (styrene-butadiene copolymer) based. These polymers were developed and commercialized to modify the structure of concrete systems. A classification is shown in Figure 2.1.

American Concrete Institute Committee 548 defines LMC as a mixture of Portland cement, fine and coarse aggregates combined with organic polymers that are dispersed in water during mixing (4). Typical LMC mixes have water to cement (w/c) ratios of about 0.30-0.40. The range of latex to cement (p/c) ratios between 0.05 to 0.20 strongly affects the mixture properties. However, a ratio of 0.15 is normally used, based on economics. Generally, the properties of most commercially-available latexes are similar. Only slight differences in working performance have been reported (7).

Since the 1960s when latexes based on thermoelastic polymers were first introduced, some improved latexes such as styrene butadiene have been widely used in the concrete industry, especially in bridge deck overlays. This material provides satisfactory protective/preventive systems for bridge decks due in part to its excellent properties, especially lower permeability and improved bond strength (4,7,8,9).

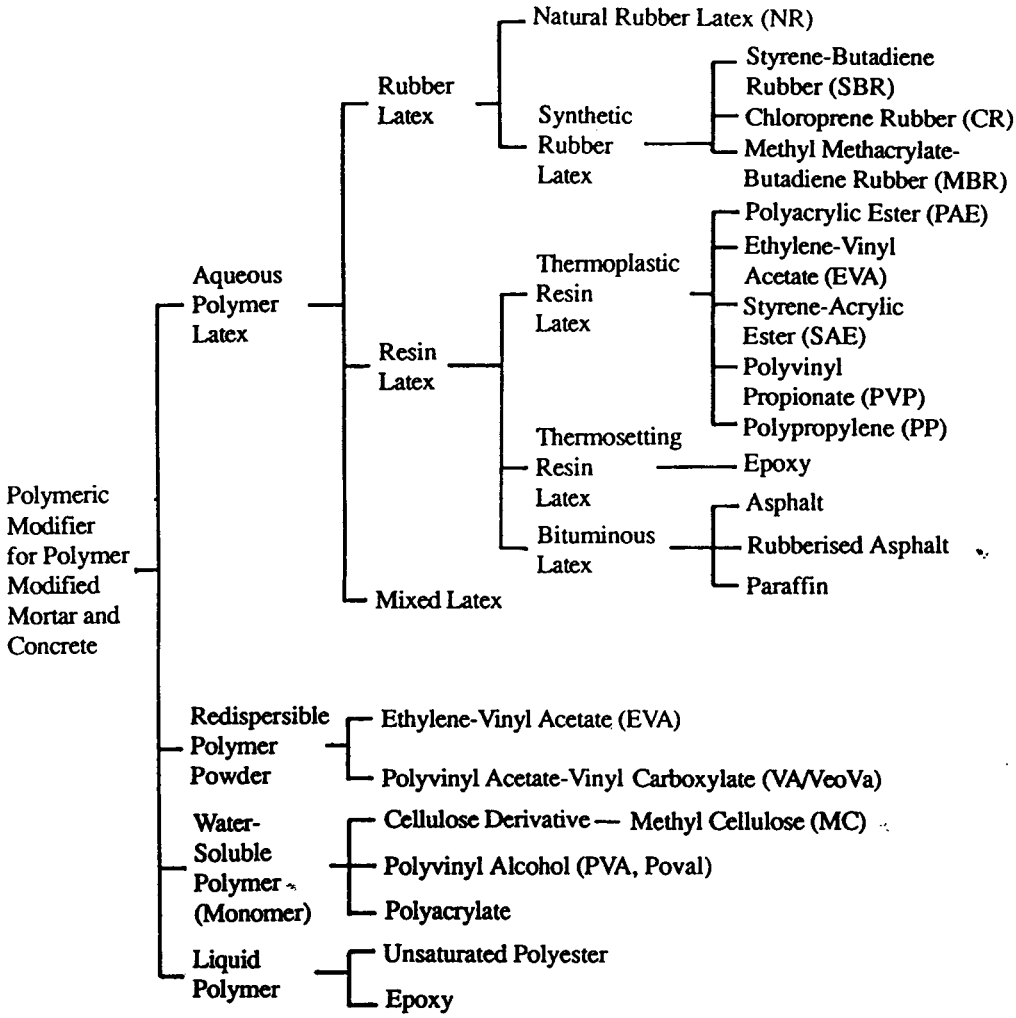

Figure 2.1 Polymer classification (6)

Styrene butadiene, an elastomeric polymer, is the copolymerized product of two monomers, styrene and butadiene. The composition of the mixture is shown in Table 1.1 (10). In addition to the two major components, other constituents also contribute to the properties of the latex and modified concrete. For example, the surfactant contributes to

increased concrete workability. The anionic and nonionic surfactants on particle surfaces helps stabilize the product in water. This addition prevents particle agglomeration in the presence of polyvalent ions in Portland cement systems. These components also prevent particle coagulation under high shear forces during mixing (11).

Table 1.1 Composition of a Styrene Butadiene Copolymer Latex (10)

substance	parts by weight
Styrene	64.0
Butadiene	35.0
A vinyl carboxylic acid	1.0
Non ionic surfactant	7.0+
Anionic surfactant	0.1*
Ammonium persulfate	0.2
water	105

Note: + The nonionic surfactants may be nonyl phenols react wiith 20 to 40 molecule of ethylene oxide.
* The low levels of anionic surfactants are used to control the rate of polymerization.

Latex is typically introduced in concrete in the form of a colloidal polymer suspension in water. This polymer latex, usually a milky-white fluid, contains small, spherical, copolymer particles that vary in diameter from approximately 0.05 to 5 microns (4). The modified structure of LMC is a result of two processes, cement hydration and film formation. Ohama modeled and explained these processes in three steps as shown in Figure 2.2 (10). A brief summary follows.

First, the polymer particles uniformly disperse in the fresh mix. As the cement gel forms during the hydration reaction. calcium hydroxide reacts with the silica surface of aggregates to form calcium silicate hydrate. Some polymer particles deposit on the unhydrated cement gel particle surface or on the silicate surface of the aggregates.

Second, as the matrix is developing, water drains and is lost through hydration and evaporation. The polymer particles confine the capillary pores gradually. A chemical reaction possibly occurs on the surfaces between particles or between particle surfaces and the developed silicate surface of the aggregates. This reaction may contribute to the improved properties of LMC. Finally, after proper curing time under appropriate conditions, these particles will coalesce and form a continuous film on the surface of the cement gel and unhydrated cement. This monolithic network with a polymer phase interpenetrates throughout the cement hydrate phase also forms a comatrix that will bind the aggregate and hydrated product together.

Wide variation in polymer particle size results in an effective void filling and a closely-packed film system. A continuous film forms on the surface of the cement gel-unhydrated cement particle mixture effectively retaining internal moisture and enhancing curing. The continuous matrix also bridges some capillary pores and microcracks. The result is a significant improvement in some concrete properties such as tensile strength, flexural strength and permeability (4,6,10).

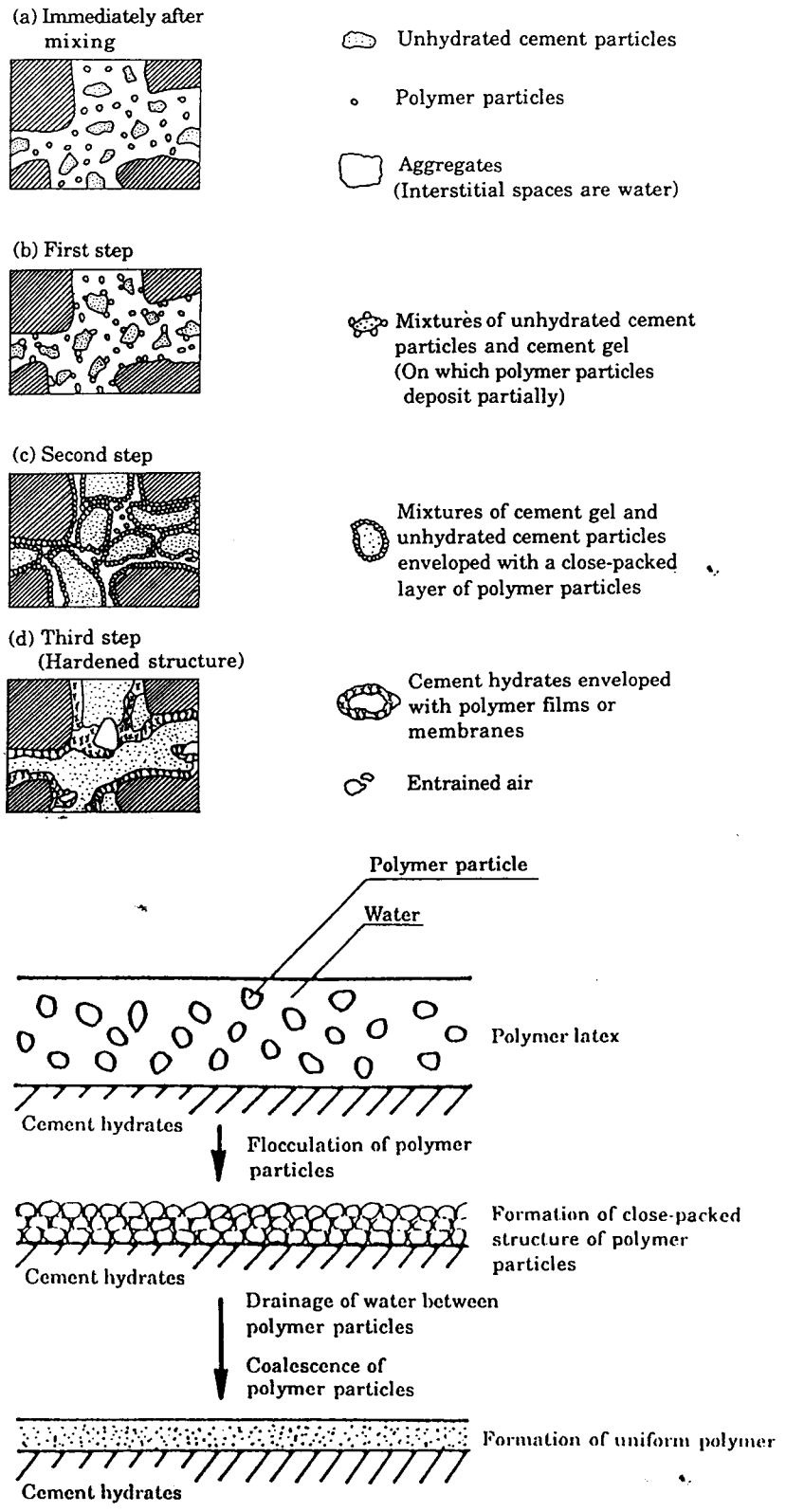

Figure 2.2 The processes developed in latex modified concrete (6)

A clear model describing modification of the interface zone between aggregate and cement paste does not exist. However, the microcracks in the aggregate-cement paste interface zone in LMC, are believed to be effectively bridged by the pore filling and the interface zone is improved by the bonding effect (12). Compared to normal concrete, these effects reduce microcrack intensity in LMC at every load level, and even before any load is applied. However, sudden increases in microcrack intensity are still reported as in conventional concrete in spite of latex modification (12).

The typical LMC pore structure differs from that of conventional concrete (13). The hardened LMC contains a relatively small number of single pores. Pores with radii of 0.2 μm or more are significantly reduced. However, smaller radii pores (≤ 75nm) are increased. (6,14,15). The total porosity tends to decrease by as much as 50 percent as the polymer-cement ratio (p/c) increases as shown in Figure 2.3 (10). The effects of filling and sealing large voids with polymer reduces gas and water vapor transmission. This phenomenon increases material resistance to liquid intrusion. Permeability tends to continue decreasing after 28 days as a function of age (9,15).

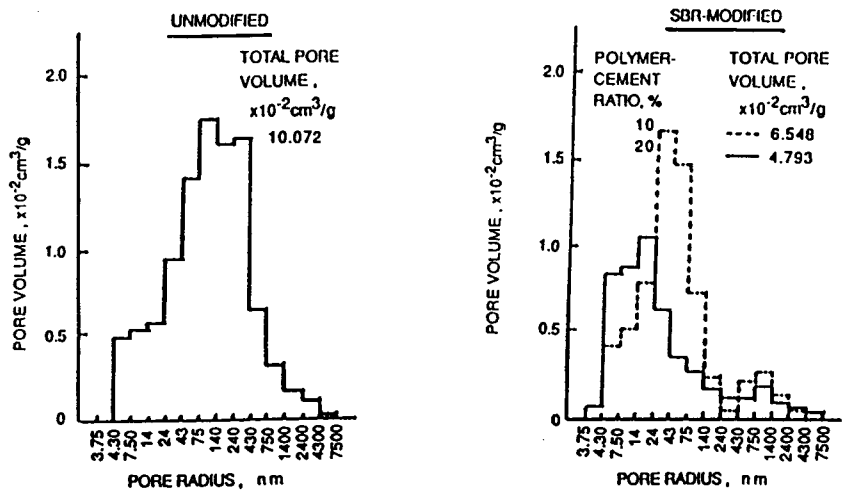

Figure 2.3 Pore size distribution of unmodified concrete and LMC (10)

2.2 Material Properties

A comatrix structure from cement hydration and the continuous film formation process improves properties of LMC both in the plastic and hardened states. Improved properties include fluidity, adhesion, microcrack reduction and increased strength. Factors that contribute to these effects are polymer type, polymer-cement ratio, water-cement ratio, air content, and curing conditions (6).

2.2.1 Plastic Concrete

1. Workability. The coated surfactants on the polymer particle surfaces influence the interaction both between polymer particles and between particles and the material to which the latex has been added. This notably improves the workability even when the mixture has a low w/c ratio (6). Compared to conventional concrete with the same consistency and workability, 20-35 percent less water is normally required for the same workability in LMC (16).

2. Air entrainment. The latex surfactants, which act as both emulsifiers and stabilizers, also increase the entrained air. This improves consistency and freeze-thaw durability. However, anti-foaming or air detraining admixtures may be necessary in some cases to control air content in the mixture, thereby preventing strength reduction from excessive entrained air(17).

3. Bleeding and segregation. The air-entraining and water reducing effects as well as the hydrophobic colloidal properties of latex result in less bleeding and segregation within the material (10).

4. Setting time. Slightly longer setting times for LMC, compared to conventional concrete have been reported (4). This is possibly related to the delayed hydration effect. The variation appears to depend on the latex-cement ratio of the mixture.

Working time is another issue for LMC. A crust formation at the surface may occur due to the effects of temperature, wind and humidity. This formation determines the working time of LMC, generally reported to be 15-30 minutes (4).

2.2.2 Hardened Concrete

1. Strength. In conventional concrete, the development of ettringite crystals shortly after mixing is believed to contribute to early age strength and the developed C-S-H gel contributes to the later strength (18). The microstructure of LMC is developed in a similar way, however some differences may result from the film formation of latex particles.

Compared to conventional concrete, the addition of latex significantly increases tensile, flexural, shear and bond strength but not compressive strength. The modified structure of LMC improves dry strength characteristics by mobilizing polymer tensile strength and by improving the cement hydrate-aggregate bond. The ductile bond from the coated plastic film also increases flexural strength and reduces the modulus of elasticity. Compressive strength may be slightly reduced as shown in Figure 2.4 (10). A higher ratio of tensile to compressive strength of about 1/6 to 1/8 for LMC, compared to 1/9 to 1/15 for conventional concrete is reported (19).

Both excellent bond and impact strength are typical for LMC. The chemical bond that develops when latex particles deposit on the silicate surface of aggregates is believed to

be irreversible and imparts an improved bond strength (11). Strength estimates of about two times for shear bond or 3-5 times for bonding with the existing substrate are expected beyond that of conventional concrete. Impact strength as high as ten times that of unmodified concrete was reported by Ohama (14). Bean reported higher dynamic strength (30-35%) and energy transmission capacity of LMC (17).

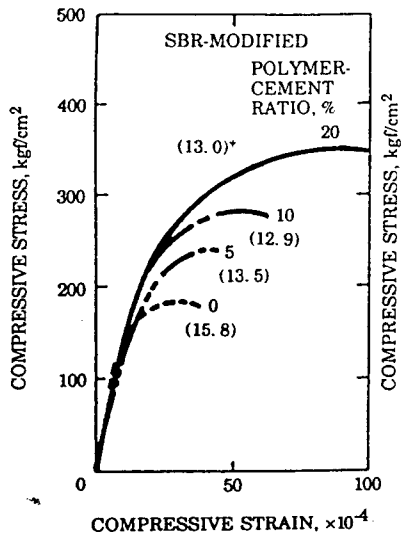

Figure 2.4 Change in compressive strength, LMC and normal concrete comparison (10)

As with normal concrete, moist curing is important in LMC for optimum strength development. Wet curing promotes hydration at early ages. Following the moist cure a dry cure period is necessary to allow an evaporation of excess water and the subsequent film formation in the comatrix system while the cement hydration process is in progress. This results in two or more times the strength, compared to the strength before dry curing (10).

LMC is more sensitive to high temperatures. The strength of LMC is rapidly reduced when temperatures are elevated, especially when they rise above the glass transition temperature of latex (80-100°C).

2. Ductility and toughness. The plastic film increases strain at maximum strength (4,13). This results in a 15 to 50 percent lower modulus of elasticity (19). The reduction increases with increased latex/cement ratio, especially when the ratio exceeds 10 percent. The increased strain, which is about two to three times higher than that of unmodified concrete (20,21), is believed to effectively reduce microcrack propagation.

3. Shrinkage and Creep. LMC is reportedly more sensitive to plastic shrinkage than conventional concrete (4). Total drying shrinkage may be either larger or smaller than that of normal concrete, depends on polymer type and polymer-cement ratio (10). The lower water-cement ratios of the mixture may contribute to the lower drying shrinkage. Estimates of drying shrinkage may be determined from the moisture retention capabilities of the polymer film (17).

For conventional concrete, shrinkage properties are a function of the curing period, humidity, thickness, slump, aggregate, cement content and air content (22). For LMC, shrinkage depends on w/c ratio, cement and polymer contents, and evaporation rate (23). The reported final shrinkage of LMC is of the order of 800×10^{-6} (4).

Compared to conventional concrete having the same slump, creep strain in LMC is much lower. The polymer effect may strengthen the binder and improve long term strength due to effective water retention (19).

4. Durability. The excellent durability properties of LMC are widely reported. These include resistance to chloride permeability, freeze and thaw resistance, abrasion resistance, and deicing chemical resistance. The reduction of porosity, the modified pore structure, and the pore sealing effect, each play an important role in these improvements.

Compared to normal concrete, reductions in chloride ion content (from 36-62%), as well as an increased carbonation resistance have been reported (10,24,25). These permeability reductions appear to increase with age (12). In terms of abrasion resistance, less weight loss compared to normal concrete (19-32%) is observed (19). An improved impermeability is reported as a function of latex content. In contrast, increased freeze and thaw resistance is not strictly dependent on an increase in polymer-cement ratio (14).

5. Thermal Properties. Similar or slightly higher coefficients of thermal expansion are generally reported for LMC compared to normal concrete (19). The coefficient of thermal expansion of LMC is about 9-10 $x10^{-6}$/°C (6). However as in normal concrete, this property depends on aggregate properties.

6. Toughness. There is no available information on toughness properties, fracture energy or energy absorption. These are key factors related to fracture performance. However, LMC and LMM are reported to have larger ductility than normal concrete which contributes to better performance (6,20,26).

2.3 Problem Development

Since the first LMC overlay was placed in 1957(16), many studies have been conducted on both properties and performance of the material. Despite the generally

satisfactory performance of LMC, some early age and later age distresses are reported (27). Therefore, the early age performance of LMC and the experiences from some agencies are reviewed in this section to provide an insight into the distress mechanisms and their possible causes.

Some transportation agencies that have significant experience with LMC e.g. the Ontario Ministry of Transport and the Virginia DOT, report that early age cracking is related to plastic shrinkage (27,29). A survey of 4 bridges in Virginia reported that the majority of wide cracks occurring in two bridges could be attributed to plastic shrinkage. In the other two, many random hairline cracks were attributed to drying shrinkage. Some cracks were thought to be caused by bridge movement or reflection from the substrate deck (29).

Survey reports of 9 overlays in South Dakota indicated some minor transverse cracking after construction (27). However, after filling the crack with epoxy, no major problems were reported.

The Missouri DOT, which has more than ten years experience with LMC, reported some shrinkage cracking as well as delamination (30). The Iowa DOT attributed some cracking to poor curing conditions. Random and alligator cracking were also observed, but no cause was identified.

In Washington, ten overlaid bridges constructed in 1985 were studied. Two bridges were located on the western side of the state, whereas the rest were situated on the east side. Serious cracking problems were reported in one bridge, but the rest had cracks typically oriented in the longitudinal direction and some in the transverse direction (7).

Cracks were observed 3-72 hours after placement of the overlay. The reported frequency was generally greater at the start of the placement and lesser toward the end. Crazing cracks (alligator cracks) were also reported in one bridge several months after construction.

In Oregon, construction reports from 1989-1992 mentioned 'after-construction' cracking in several projects although they were not considered serious (31). Cracks were noted after one month and after one winter in LMC overlays placed in 1994. These cracks are typically reported in both the longitudinal and transverse directions. Random crack and crazing cracks are also frequently mentioned.

Overlay cracks are likely common in many states experience (7,27). Most agencies do not consider early age shrinkage cracking a serious problem, provided the cracks are sealed. Other factors such as traffic-induced vibration are sometimes mentioned although no statistical significance is reported (4,27). However, to achieve better long term performance an understanding of the mechanisms involved as well as the contributing factors is necessary.

2.4 Cause of Distresses

Researchers hypothesized that cracks in LMC occur soon after construction (32). Several factors appear to be related to LMC distresses including construction procedures, structural behavior, thermal loading, and material factors such as shrinkage. This section provides an overall background of these factors. The details of the contributing factors considered in this study are provided in section 2.6.

2.4.1 Construction Procedure

The quality of the LMC overlay is sensitive to construction process. Petrographic analyses of the cored samples from some Oregon projects (33) indicated a possible relationship between cracking and delamination and the surface preparation method. Hydroblasting appears to provide fewer cracks on the substrate surface, compared to milling. Placement time may influence temperature differences between the new overlay and the existing deck. This was also mentioned as a cause of temperature-related cracking (34). Furthermore, delayed finishing may cause overlay surface tearing and cracking from crust formation.

2.4.2 Structural Loading

At early ages, there are no traffic loads on the overlaid deck, only loads from construction activities are applied directly to the bridge overlay. However, it is rarely possible to close the bridge to traffic in the adjacent lanes. This may affect the overlay performance particularly when high traffic volumes combine with heavy truck traffic. This effect has been reported (4,29,35), although not verified and has been considered a statistically insignificant factor by one researcher (23). Other studies indicated a possible effect from this factor (27,35,36,37).

The bridge type was also mentioned as a possible factor. More flexible structures, such as steel structures, have more reported cracking (27,29). Weakened substrates from scarified surfaces tend to have higher flexibility than the original structures. The induced flexing and vibration from the trafficked lane tends to widen existing cracks in the

substrates. This may induce higher stresses in the setting overlay than it can resist. As a result, cracks may propagate through the overlay. Transverse cracks may also form (36).

In addition, the presence of substrate distress from the uncorrected structural deficiencies may cause cracks later or at early ages when tensile strength is low. The deck movement caused by deflection or temperature change may result in reflective cracking through the overlay thickness (27).

2.4.3 Environment Impacts

The environment may impact overlays through evaporation rate and bridge temperatures. The low water content in LMC results in less bleed water, compared to conventional concrete. This increases its sensitivity to environmental conditions. The combination of wind, temperature and humidity affects evaporation rates. For overlays having high surface area to volume ratios, this factor has been reported as the single most significant contributor to early age cracking (4,36). The evaporation rate can be estimated from an American Concrete Institute (ACI) nomograph (36). A low rate, i.e., less than 0.15 $(lb/ft^2)/hr.$, is normally recommended. However, Kuhlman (34) suggested a lower rate of less than 0.10 $(lb/ft^2)/hr.$ to minimize plastic shrinkage cracking.

The combination of wind, temperature and solar radiation affects bridge temperatures. High temperature differential between deck and overlay is recognized as another contributor to cracking problem (7). To minimize this problem, the placement under some environmental conditions is normally restricted.

2.4.4 Shrinkage

Plastic and drying shrinkage are reported in LMC as in normal concrete. Several reports suggested the possibility of shrinkage as an important cause of cracking, especially during early ages (7,29).

Plastic Shrinkage. Plastic shrinkage occurs during the time when concrete is still plastic and the evaporation rate is higher than the bleeding rate. Capillary menisci at the air-water interface penetrate into the concrete matrix (32). Tensile capillary pressure develops, and plastic shrinkage cracking is a consequence. This action may occur in response to several individual, or a combination of, conditions, especially high air temperature, high concrete temperature, low humidity, and high wind velocity.

For LMC which has low w/c, low bleeding is normal. At very early ages when the latex film is not completely formed and protection is not sufficient, plastic shrinkage cracking is likely to occur. Under dry ambient conditions, the cracks commonly appear in the first 24 hours. High deck temperature and prolonged exposure are reportedly related to this crack type. Plastic shrinkage cracks are often reported in LMC construction (7,29).

Drying Shrinkage. Moisture loss to the environment after the concrete is hardened causes drying shrinkage in LMC, similar to conventional concrete. LMC shrinkage is reportedly lower than in conventional concrete due to the presence of the latex as shown in Figure 2.5 (4).

A concern about differential shrinkage in the new overlay compared to the relatively stable substrate is often mentioned (10,39). This differential movement may cause cracking, particularly in the first two to three weeks when the shrinkage rate is high. One study

identified this differential movement as a primary cause of cracking in the overlay (36). LaFraugh (7) suggests that thermal shock between the base concrete and overlay contributes to cracking, however, no details are available.

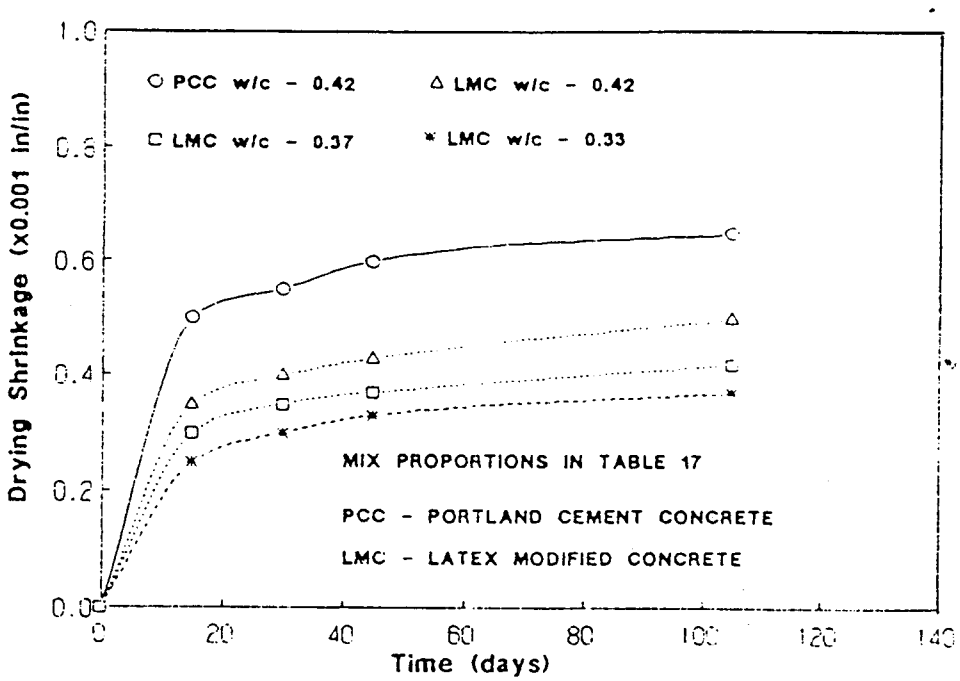

Figure 2.5 Comparison of shrinkage performance between LMC and conventional concrete (4)

Researchers have attempted to combine these factors. However, most research has been concerned with the mature properties of the material and long term performance. Very little information is available on early age modified concrete properties. In addition, no mechanistic approach has been found to relate these factors to modified concrete overlay performance.

2.5 Cracking Characteristics

The cracking information in this section provides some background about the characteristics of observed cracks and their possible causes.

2.5.1 Random Cracks

These cracks are generally 6 to 12.5 mm deep and 0.01 to 1 mm wide, usually appearing a short time after placement. The cracks normally appear in random patterns spaced 300 to 350 mm apart (27). Although initially shallow, repetitive thermal cycling may cause the crack to propagate through the overlay thickness.

Plastic shrinkage is the main cause of these cracks. The low w/c ratio, combined with improper curing, may result in insufficient bleed water to replace evaporation loss, followed by cracking. The relationship between bleed water and cracking was shown in Kuhlman's research (34).

Considerable evidence shows that random cracks usually occur in the first 24 hours following placement and may extend to 19 mm deep (40). The most frequently reported circumstances occurs are under construction conditions of high w/c ratio mixture, high air temperature (>29 °C), and high wind velocity (27).

Drying shrinkage is another cause of random cracking found in many LMC overlays. These cracks result from the continued loss of moisture in concrete after initial hydration. Although drying shrinkage occurs throughout the life of concrete, asymptotically approaching an ultimate value, the bulk of this shrinkage occurs within two years (27). However, the LMC shrinkage rate at early ages (first two weeks or three weeks after

construction) is higher than that of normal concrete (27,39). Oregon DOT noted additional cracking during the first year of monitoring (42). Normally this type of crack is finer and deeper than plastic shrinkage cracking (40,42). Several factors influence drying shrinkage cracks such as w/c ratios, cement contents and polymer contents (34).

Occasionally, tight map cracking is reported during the first several months after construction. This might be caused by differential shrinkage and deck creep. The Interstate 182 project in Washington is an example of this cracking pattern (40).

2.5.2 Transverse Cracks

These linear cracks occur transverse to the longitudinal axis of the bridge at 910-1520 mm spacings. Normally, these cracks penetrate through the overlay depth into the substrate and may be difficult to observe because they are partially hidden in the transverse tining.

In some cases, the bridge substrate deck is significantly fatigued and exhibits block cracking. Reflective cracking may appear on the overlay surface in a checkerboard pattern. This is usually followed by delamination (43). For new bridges, where the overlay is placed before form removal occurs, cracks can occur in the negative moment region as soon as the forms are removed. In addition, cracks may occur over existing joints due to delayed sawing and may be accompanied by debonding near the joint (34). Vibration and flexing from moving vehicles aggravate existing transverse cracks, resulting in a more severe situation.

Bishara (27) reported a significantly increased amount of random and transverse cracking in LMC after seven winters. The rate of increase was lower during the first three years. Differential shrinkage strain and the extension of substrate existing crack were identified as contributing factors.

2.5.3. Longitudinal Cracks

These cracks are found in a few cases. The cause is not clearly understood. Some researchers believe that they might relate to the type of structure. There is evidence that these cracks occur mostly at the ends and middle or edge of decks built in prestressed I beam bridge types (43). However, in the same project, longitudinal "pull cracks" were reported as the result of improper grooving after crust formation in the LMC overlay.

Although these cracks are sometimes not considered serious, the presence and degree of severity of all cracks, if not corrected, increases as time passes. Shallow surface cracks may propagate through the overlay into the substrate deck. After sufficient freeze and thaw cycles, the accumulated moisture content can lead to debonding and spalling due to either freezing water or intrusion of fines. Chloride intrusion can initiate steel corrosion, reducing deck service life as a consequence.

2.6 Contributing Factors to Early Age Cracking

Environmental factors and the physical properties of latex modified concrete (LMC) are often mentioned in the literature as cracking-related factors. These two

factors are hypothesized to contribute to early age cracking in this study and are discussed in detail in this section.

Since the overlays are constantly exposed to the environment, several variables were studied to predict the impact of the environment. Three factors were identified as critical to deck performance: solar radiation, shade temperature and wind velocity (36,38,44). Data for these variables are obtained from weather reports. To numerically study the cracking mechanism, these variables were related to the overlay performance through bridge temperatures in terms of temperature differential, using theoretical heat transfer models (38,44).

2.6.1 Temperature

Temperatures normally change with time, for both yearly and diurnal cycles (45). The yearly cycle, which depends on the relative position and distance between the earth and sun, is important in long term performance studies. However, in early age studies, the diurnal cycle is of prime concern. This cycle causes temperature fluctuations and thermal stresses in the bridge structure. The magnitude of these stresses may be sufficient to cause or exacerbate the distress of bridge decks (44).

To predict the temperature effect, the daily temperature variation must be known. In the daytime, particular during the summer, bridges normally have greater heat gain than loss and rising temperatures result. This pattern reverses and bridge temperatures drop at night. Minimum temperatures generally occur before sunrise and increase to maximum in mid-afternoon.

The difference between maximum and minimum air temperature affects bridge temperature distribution. Moreover, during clear days and nights, the variation in temperature through bridge sections is small about 2 hours after sunrise (38,44,46). Several researchers have assumed a thermal equilibrium state for bridges equivalent to the surrounding temperature (38,44,46).

The diurnal variation of air temperature with time is often assumed as a sinusoidal cycle between minimum and maximum temperature using the following equation (38,93).

$$air\ temp. = \frac{1}{2}(T_{max.} + T_{min.}) + \frac{1}{2}(T_{max.} - T_{min.})\sin(0.262(t-9))$$

where t = time, hours

$T_{max.}$ = maximum temperature in the day

$T_{min.}$ = minimum temperature in the day

In this study, satisfactory results were observed from the comparison between actual air temperatures from weather reports for a case study and the prediction. An initial condition of uniform temperature equal to the surrounding at about 2 hours after sunrise was assumed in the analyses.

2.6.2 Solar Radiation

Solar radiation is the most important mechanism for heat transfer in bridge structures (38,44). Similar to temperatures, solar radiation changes with time, and it is of

interest to note that maximum and minimum temperatures and solar radiation occur at different times.

Latitude and local conditions may affect the solar radiation intensity (44). Latitude affects solar day length. Local conditions such as wind velocity, cloud cover, and precipitation may affect the general trends. However, these factors are not directly included in this study. The absorb radiation also depends on the nature and color of the surface; dark and rough surfaces absorbed more radiation than light and smooth surfaces.

Solar radiation intensity, I (t), can be approximated from (38,44):

$$I(t) = \frac{2S}{T_{SL}} \sin^2\left(\frac{\pi t}{T_{SL}}\right)$$

Where t = time, hours

S = total daily solar radiation, Watt hr/m^2/hr

T_{SL} = length of the solar day

To provide an accurate prediction in this study, the following modified relationship is proposed for Willamette Valley conditions. This equation, based on Gloyne's model (38), Thepcahatri's model (44), and the weather reported data, is:

$$I(t) = \frac{1.6S}{T_{SL}} \frac{(\sin^2 \alpha + 2\sin \alpha)}{3}$$

Where $\alpha = \pi t/T_{SL}$

S = total daily solar radiation, Watt hr/m^2/hr

T_{SL} = length of the solar day

t = time, hours

2.6.3 Wind

Of the three mechanisms for heat transfer in bridges, wind speed has been found to have the greatest influence on the convection, an energy transfer mechanism between the solid surface and the air. Wind speed impacts the convection coefficient, h_c by increasing or lowering surface temperatures. The higher the wind speed, the closer the bridge surface temperature is to the air temperature. Under the same conditions of temperature and solar radiation, when wind speed is lower, large thermal stresses are produced.

Since the bridge deck is normally considered as a flat plate, several empirical convection coefficients (h_c) have been proposed as a function of wind velocity (v_v, mph) (47,48). In this study, the coefficient was estimated in the form of (48):

$$h_c = 0.665 + 0.133\ v_v$$

Generally, wind speed varies with topography. However, average values are normally used. A large temperature gradient probably occurs under conditions of high solar radiation, wide ranges of diurnal temperature (15-20 °C) and light wind (2.2-3.1 m/s) (38). Based on the variations in these three factors, temperature distributions in the bridge deck can be predicted. Consequently, the calculated stress level induced by the thermal distribution can be determined. Finally, assessment of the thermally-induced stress due to any considered condition can be achieved. Furthermore, crack propagation can be predicted using the known service temperature differential as the driving force.

2.6.4 Shrinkage

In conventional concrete, several empirical equations have been proposed to predict shrinkage with time, particularly drying shrinkage (49,50) The relationships are normally defined as functions of curing time, relative humidity, shrinkage-half-time, or ultimate shrinkage.

For LMC, Bishara (51) proposed two empirical models to predict shrinkage of LMM and LMC after the first 24 hrs. These expressions, shown in the following, agreed well with his test data, in which approximately 95 percent of total shrinkage at early age occurred within the first two months.

LMM: $$\varepsilon_{sh} = 1700 \times 10^{-6} \times [\frac{t^{0.55}}{3 + t^{0.55}}]$$ ----------eq.1

LMC $$\varepsilon_{sh} = 817 \times 10^{-6} \times [\frac{t}{5.13 + t}]$$ ----------eq.2

where ε_{sh} = shrinkage strain at time t

t = time, days

However, there are no prediction models for plastic shrinkage of either normal or latex modified concrete. Furthermore, a standardized test method is not available. Therefore, the estimated shrinkage in this study was based on the experimental data.

In summary, the effect of latex film formation incorporating the cement hydration process significantly improves LMC properties. Their beneficial qualities result in quality overlays, although early age cracking is reported. Among several related factors, environmental conditions and material properties are hypothesized as major causes of

overlay cracking. These two factors are analyzed to predict the overlay performance by incorporating fracture mechanics as detailed in the next chapter.

3. TOOLS AND MODELING TECHNIQUES

3.1 Introduction to Fracture Mechanics

Failure criteria are essential in estimating the capacity or studying the performance of any structure. Conventional strength criteria do not account for flaws or defects in the microstructure, and therefore, may not provide a reliable explanation for some materials. In 1898, using a strength criterion, Kirsch (54) showed that the existence of a hole could reduce the strength of an elastic, homogenous material by a factor of three. Later, Inglis's work (55) further demonstrated a stress concentration effect. The following equation suggested an infinite stress at the crack tip where an elliptical flaw, as shown in Figure 3.1, is degenerated into a sharp crack as $b \rightarrow 0$. Therefore, a fracture mechanics approach has been developed to study material behaviors in a more realistic way.

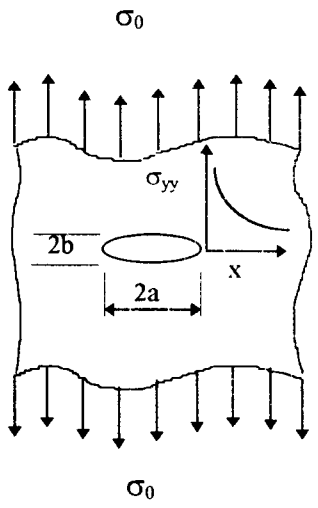

FIGURE 3.1 Stress distribution around an elliptical hole in an infinitely large plate

$$\frac{\sigma}{T_S} = 1 + 2\frac{a}{b}$$

where σ = stress at edge of ellipse
T_S = tensile stress in the far region
a = half length of ellipse along major axis
b = half length of ellipse along minor axis

Fracture mechanics is a method of characterizing the fracture behavior based on principles of released energy, flaw effect and material toughness. Therefore, it is considered a suitable tool to provide a fundamental understanding of the development and performance of crack propagation in a material.

In 1920, Griffith (56) first introduced the application of the fracture mechanics concept to a brittle material. This concept suggested that unstable crack growth occurred when the system received energy exceeding the energy needed to form a new crack surface. The modification of Griffith's concept for a metal, led to the development of standard testing techniques, fracture parameters and ultimately to design specifications which routinely incorporate these parameters. Recently, the most significant applications of fracture mechanics has been used to control brittle fracture and fatigue failure of metal structures.

The attempt to apply fracture mechanics to portland cement concrete material was pioneered by Kaplan in 1961 (57). A fracture mechanics-based model provides a better description of crack development in a composite material like concrete, compared to the conventional stress criteria which assumes an immediate drop to zero stress after the peak stress (5,52). However, in concrete, microcracking is not accompanied by any

substantial contraction corresponding to that which occurs in metallic materials, thus, no essential difference exists between plane stress and plane strain conditions (75). The width of the specimen or the length of a crack front cannot be expected to be of any major importance in concrete. In short, concrete behaves differently from metallic materials. Therefore, some theories may not be suitably applied to this material except under certain circumstances (for example, when extremely large specimens are tested for parameter determinations) or some theoretical modifications are applied (59).

To explain the failure behavior/performance of a structure, two approaches have been developed in fracture mechanics (60).

1. Failure occurs when the intensity of stress concentration at the macroflaw such as crack tip is higher than the cohesive strength of material (stress intensity approach).

2. Failure occurs when the stored energy during loading is higher than the energy required to create the new crack surface (energy balance approach).

During crack propagation, energy can be dissipated in three ways (59):

1. Surface energy dissipation due to the creation of new crack surfaces.

2. Energy dissipation due to the formation of microcracking or yielding ahead of a critical crack path.

3. Energy dissipation in the wake of a crack path.

The classical theory of fracture mechanics, Linear Elastic Fracture Mechanics (LEFM) is based on the assumption that energy is dissipated as new crack surfaces are formed. This approach can be applied appropriately to a material such as a metal. This

theory relates the energy to the stress intensity factor K_{IC} or the critical energy release rate G_{IC}.

For some materials, the second type of energy dissipation is important. The Dugdale Model can be applied (59). This model is categorized as the second approach and is based on the concept of a uniform stress distributed along a suitable cohesive zone to represent plastic yielding in ductile materials (61).

For concrete-like materials, while all of the above are important, the second and third types of energy dissipation are substantially more important due to strain softening and aggregate interlocking (ligament bridging). This leads to a model based on the second approach, using a similar idea for cohesive force as in the Dugdale model. However, the model development is different. Several models have been developed including the Fictitious Crack Model (FCM)(62) and the Blunt Crack Band Model (63). However, these two models have a common conceptual framework, that within a strain-softening region the dissipation energy is forced to attain a non-zero value (64).

The LEFM and FCM are the two basic, well developed approaches that are reviewed as the basis for this study. However, it is important to note that although the study of fracture mechanics of concrete is advancing at present, no unique set of material parameters are generally agreed to explain concrete fracture behavior. Similarly, no standard testing method is available for this material.

3.2 Linear Elastic Fracture Mechanics (LEFM)

The concept of LEFM is based on a high state of stress at the crack tip which leads to a reduced loading capacity for the body. Some parameters such as fracture toughness and critical stress intensity factor are assumed to be material properties.

Crack propagation and the material's ability to withstand a given load can be explained based on the energy change during crack extension. Assume that a large uncracked plate having a unit thickness is stretched (Figure 3.2(a)). Uniform stresses, σ, occur along the line m-m. The superposing of this stress condition with a uniform pressurized crack (Figure 3.2(b)) results in stress free surfaces from the canceled out stresses between the two points, c and d. Therefore, the energy loss required to change the uncracked plate (Figure 3.2(a)) to the cracked plate with crack length 2a (Figure 3.2(c)) can be represented by the strain energy shown in Figure 3.2 (b). This strain energy is equal to the work done by the applied pressure, σ, on the surface of the crack.

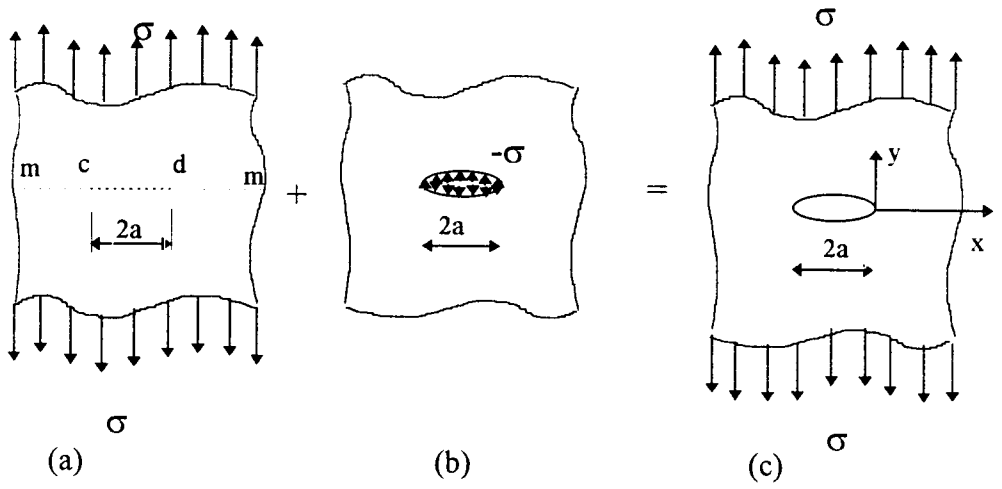

FIGURE 3.2 Energy change between crack and uncracked plate

$$U = \frac{1}{2}\int \sigma v dA \quad \text{.....eq.3.1}$$

where U = strain energy

σ = the applied uniform pressure which is equal to the uniform stress in Figure3.2 (a)

v= vertical opening of a crack length 2a

dA = area increment = 1(dx)

The vertical displacement can be expressed as:

$$v = \frac{\sigma}{\mu(1+\upsilon)}(\sqrt{a^2 - x^2}) \text{.....} eq.3.2$$

Substituting the expression for vertical displacement in equation 3.2 (65) yields equation 3.3

$$= \frac{1}{2}\int \sigma \frac{\sigma\sqrt{a^2 - x^2}}{\mu(1+\upsilon)} 1(dx) \text{.....} eq.3.3$$

dx = crack propagation increment

υ = Poisson ratio

μ = shear modulus

Integrating equation 3.3 over the upper surface and multiply the result by 2 to account for both surfaces yields:

$$= \int_{-a}^{a} \sigma \frac{\sigma\sqrt{a^2 - x^2}}{\mu(1+\upsilon)} 1.dx$$

$$= [\frac{\sigma^2}{\mu\ (1+\upsilon)}]\frac{1}{2}[x\sqrt{a^2 - x^2} + a^2 \sin^{-1}\frac{x}{a}]$$

$$= \frac{1}{2}[\frac{\sigma^2}{\mu\ (1+\upsilon)}][0 + a^2\frac{\pi}{2} - 0 - a^2(\frac{-\pi}{2})]$$

$$= [\frac{\sigma^2 \pi\ a^2}{2\mu\ (1+\upsilon)}] \text{.....} eq.3.4$$

Substituting the modulus of elasticity, E= 2μ (1+υ) yields:

$$= \frac{\sigma^2 \pi a^2}{E}$$

When the crack propagates a short distance, x = da, strain energy is released, dU. This strain energy should be at least equal to the energy required to break the atomic bonds of the material, dw.

$$dU \geq dw$$

$$\frac{dU}{da} \geq \frac{dw}{da}$$

where dU/da = Strain energy release rate = G

dw/da = crack resistance = R

If R = critical strain energy release rate = G_c

The critical condition occurs when G = G_c, the crack begins to propagate and the stress reaches σ_c, $\frac{dU}{da} = \frac{dw}{da} = G_c$. The critical strain energy is a property of the material. In the case when the crack length is 2a,

$$G_c = \frac{dU}{d(2a)}$$

$$G_c = \frac{1}{2}\frac{dU}{da}$$

$$G_c = \frac{1}{2}\frac{d(\frac{\sigma_c^2 \pi a^2}{E})}{da}$$

$$G_c = \frac{\sigma_c^2 \pi a}{E}$$

In general, in the vicinity of crack tip as shown in Figure 3.3, the expression for the stresses at any point are

$$\sigma_x = [\frac{K_I}{2\pi r}] cos\frac{\theta}{2}[1 - sin\frac{\theta}{2} sin\frac{3\theta}{2}]$$

$$\sigma_y = [\frac{K_I}{2\pi r}] cos\frac{\theta}{2}[1 + sin\frac{\theta}{2} sin\frac{3\theta}{2}]$$

$$\tau_{xy} = [\frac{K_I}{2\pi r}] sin\frac{\theta}{2} cos\frac{\theta}{2} sin\frac{3\theta}{2}$$

where r,θ = polar coordinates

$\sigma_x, \sigma_y, \tau_{xy}$ = stresses acting on the element

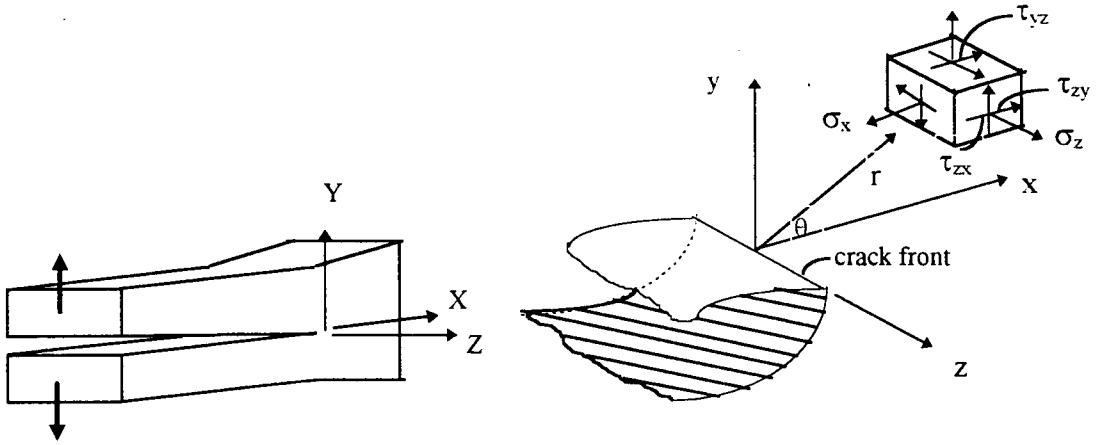

Figure 3.3 crack tip coordinates and stress system

$$K_I = \sigma\sqrt{\pi\ a}$$ ----------eq3.5

K_I, the stress intensity factor, defines the magnitude of the crack tip singularity. The relationship between K_I and σ (equation 3.5) leads to the expression for G in equation 3.6. If K_I is sufficiently large, or reaches the critical value $K_{I\,c} = \sigma_c\sqrt{\pi\ a}$, an unstable fracture occurs and the crack propagates. Similar to the critical strain energy G_c, the critical stress intensity factor, K_{Ic} is also a material property and specimen size independent.

$$G = \frac{K_I^2}{E}$$ ----------eq.3.6

or $K_I = \sqrt{GE}$

Therefore, a determination of crack propagation can be considered from a comparison of G and G_c or from K_I compared to K_{Ic}. This model was well developed for homogenous materials under three well defined loading modes. These modes are: mode I for opening, mode II for sliding, and, mode III for tearing as shown in Figure 3.4 (65).

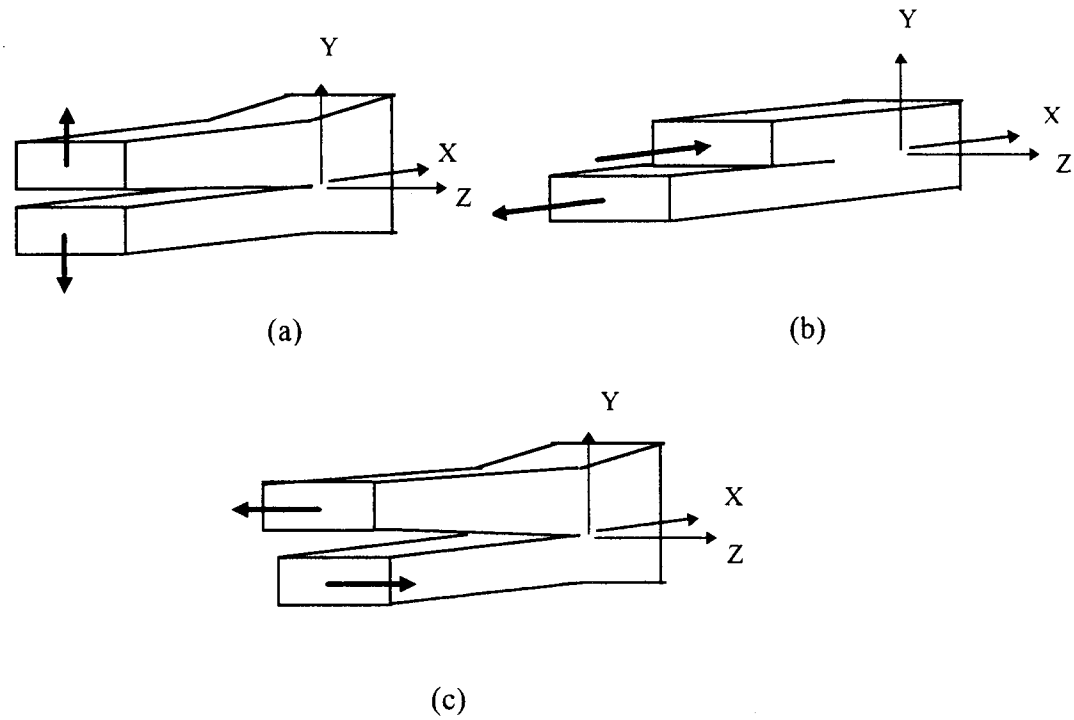

Figure 3.4 Three modes of fracture in a material (65)

However, concrete is not an elastic material and concrete fracture is preceded by microcrackings instead of yielding as in a metal. Concrete behavior differs from the homogenous material as explicitly shown in Figure 3.5 (66). The behavior of materials under applied forces are generally divided into three regions: linear elastic, prepeak and postpeak nonlinear regions which reflect strain hardening and strain softening behaviors,

respectively. Strain softening is a characteristic of an increasing deformation with decreasing stress capacity.

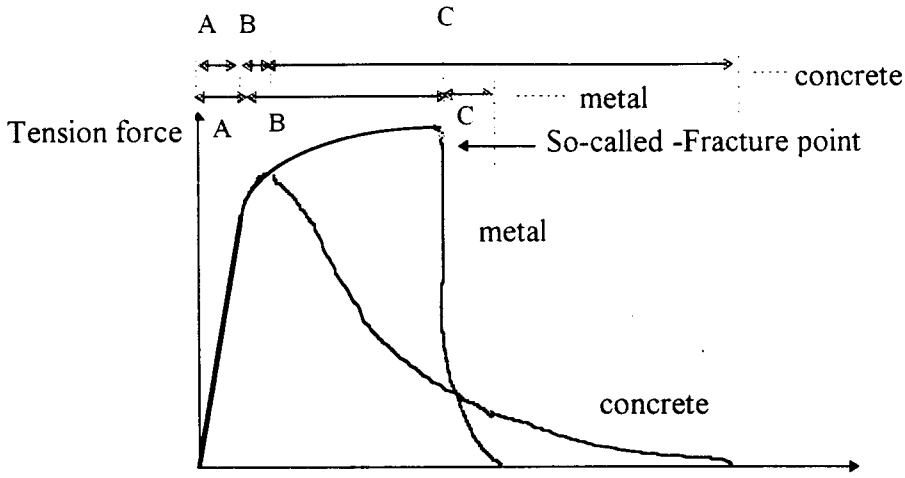

note: A : elastic region
B : strain hardening region
C : strain softening region

Figure 3.5 Behavior comparison between concrete and metal (66)

For concrete-like materials, microcracking, a large size process zone, substantial slow crack growth prior to peak load, and aggregate bridging influence the non-linear behavior of concrete. The strain softening region is significantly larger than that of strain hardening due to these effects, especially from coalesced cracks and aggregate bridging. This influences the process of decreasing stress carrying capability from tensile strength to zero stress. Therefore, the post-peak behavior is necessarily involved in the failure performance of concrete as well as the non-linear behavior of this material.

To properly apply the widely used approach LEFM to concrete, an extremely large size specimen is necessary to determine the correct fracture parameters (67) or some modifications are needed (5,68). The consideration of slow crack growth and crack tip nonlinearity effects are necessarily included in the modified LEFM as proposed in several models (5,68,69,60).

3.3 Fictitious Crack Model (FCM)

In concrete, a well-defined crack does not exist. Concrete failure does not result from a single crack formation, but rather from a complicated sequence of crack growth, crack arresting behavior and gradual degradation of the material (71). The concept of stress transfer ability in partially damaged zones leads to the development of the cohesive crack approach. The Fictitious Crack Model (FCM), proposed by Hillerborg and his coworkers to study the concrete crack development was the first developed model (67,72).

In the FCM, material at the crack extension path is assumed to be in one of three states, 1) elastic state, 2) fracture state or 3) state of no possible stress transfer (68). In the fractured state, microcracks cause softening but stresses are possibly transferred, so a fictitious crack is assumed. This fictitious cracked area or the Fracture Process Zone is defined as the region where tensile stress in the material is decreasing from the maximum value (f_t) to zero as the crack width reaches a defined critical separation distance. Stresses in this zone are defined by a special function of crack opening displacement or σ-w relationship. The behavior of all points outside this zone is assumed as an elastic state, and

the σ–ε relation is used to describe the stress state. The FCM does not consider the width of the fracture zone. This model differs from the later developed model, the Blunt Crack Band Model, in which the fixed width of a crack band is considered and the σ–ε relation is utilized for both pre- and post-peak performance (73).

The study of the structure of concrete can be conducted at three different levels: meso level, micro level and macro level as shown in Table 3.1 (74). However, it is important to note that for fracture studies, the fracture process zone is normally modeled at the macroscopic level. At this level, material properties may be assumed stochastically identical for all parts. Furthermore, single mode loadings, especially Mode I, are commonly investigated. Some research has been conducted on the other modes. A consistent nonlinear fracture mechanics has been developed for both mode I and mixed mode loadings of concrete (66).

3.3.1 Principles and Assumptions

The concept of FCM is demonstrated through a tension test, which is assumed stable deformation control (Figure 3.6)(75)

An assumed homogenous, prismatic specimen with two equal gauge lengths (l_0), identified as zone A and B, is subjected to tension loading to failure. A limited width of fracture zone is assumed in the stress direction. Three diagrams in Figure 3.7 explain the potential deformation behavior of the sample. The complete stress-elongation curve (Figure 3.5(7))is composed of three parts, A^*, B^* and C^*. As the specimen is loaded, the stress-

elongation behaviors of zones A and B are similar and explained by the first part A* until the maximum load is reached (Figure 3.7 (b)).

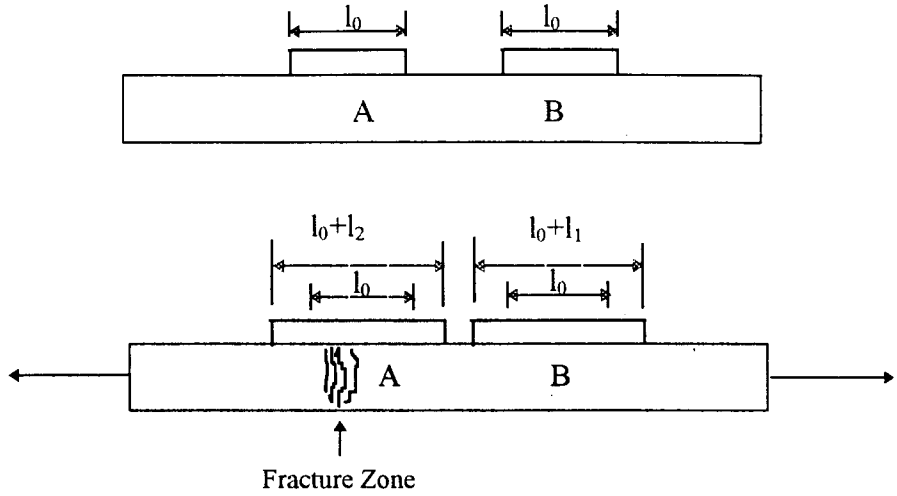

Figure 3.6 Principle of Fictitious Crack Model Concept applied to tension member

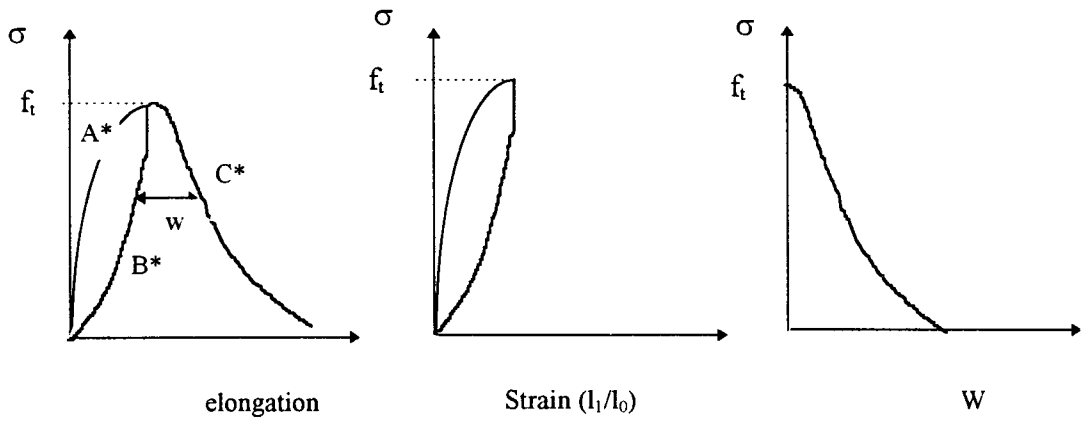

(a) complete stress elongation (b))σ-ε for uncracked part (c)σ-Δ for cracked part

Figure 3.7 Stress-elongation of cracked and uncracked portion

When the fracture zone is formed somewhere in the specimen, assumed in zone A, microcracks develop and the load begins to decrease. The elongation in fracture zone A is affected by the developing crack width as shown by part C^*. At the same time, the reduced load decreases the stress in zone B. The reducing stresses follow an unloading branch show by part B^* in Figure 3.7(b). The deformation outside fracture zone A decreases as a result of the decreasing load.

Strain softening behavior is dominant in the localized fracture zone A. The stress decreases while the deformation is increased. The deformation behavior of this cracked zone is shown by the difference between Figures 3.7 (a) and (b). This difference (Figure 3.7(c)) is key in FCM.

From Figure 3.6, after the specimen was subjected to the applied load and cracking formed in zone A:

for the uncracked zone, B, the total length $l_B = l_0 + l_1 = l_0 - \varepsilon l_0$

for the cracked zone, A, the total length $l_A = l_0 + l_2 = l_0 - \varepsilon l_0 + w$

Where: l_1 and l_2 = excess deformation of gauge lengths in zones B and A, respectively
l_0 = the gauge length,
ε = strain
w = additional deformation due to fracture zone.

Since the assumed width of the fracture zone is zero, the σ-w relationship describes the tied-crack performance and a gradual stress transfer reduction in the fracture zone A. This stress state is demonstrated in Figure 3.8. In short, stress transfer in the fracture zone is assumed to depend on the relative displacement of the fictitious crack face, $\sigma = f(w)$.

Tensile strength is assumed for the zero crack width, $f(0)= f_t$ and gradually decreased to zero stress when the specified crack distance is reached. $f(w) = 0$.

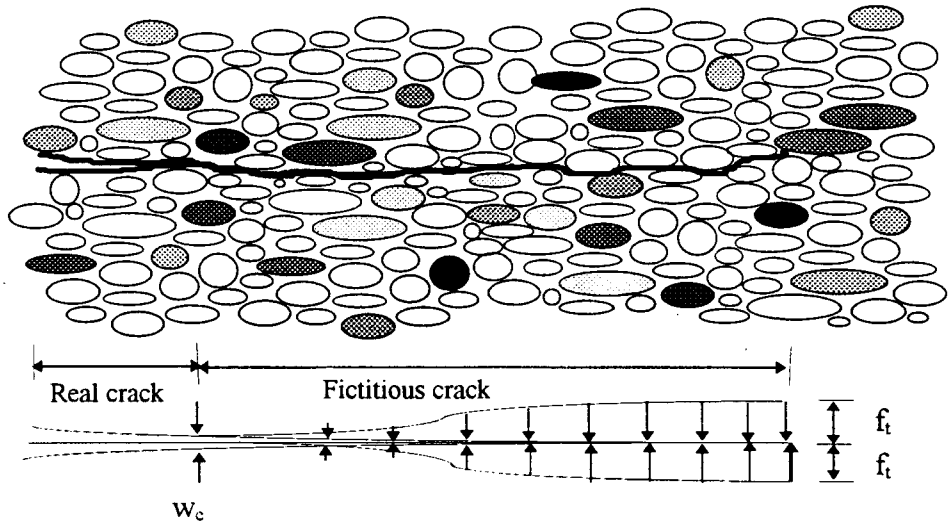

Figure 3.8 Stress state at cracking area by FCM

If G_F is defined as the absorbed energy required to completely separate a unit crack area, then the total energy absorbed in this simplified fictitious crack is

$$A\int_0^{w_c} \sigma dw = A\, G_f$$

Where A = cross sectional area
w = crack width
w_c= w-value for $\sigma = 0$,
G_f= area under σ-w curve $= \int \sigma(w)dw$

To apply the Fictitious Crack Model, several assumptions are made. These are: (72,75)

1. The fracture process zone develops initially when the maximum principal stress reaches the tensile strength. The direction of the process zone is perpendicular to the direction of the first principal stress.

2. The material in the process zone is partially damaged but still able to transfer stress. The stress transferring capability depends solely on the stress-separation relationship. The properties of the material outside the process zone are governed by the stress-strain relationship.

3. The width of the initial crack opening is zero.

Using these assumptions, the size of the process zone, the bridging stress and the applied load can be determined. These results allow the crack propagation to be tracked .

3.3.2 Methodology

A superposition technique was employed to calculate the peak load, deflection, and crack mouth opening displacement in this study. This technique is less time consuming than an iteration technique in which the global stiffness matrices of the structure are inverted in each calculation step (76).

The superposition technique incorporating a finite element method was employed to calculate the basic solutions of stresses and crack mouth opening displacements. The assumed strain softening of the fracture zone ahead of the real

crack tip and the stress criterion were incorporated after this step. The calculation steps are summarized in a flowchart in Figure 3.9.

In this section, the methodology is presented by examining a beam loaded at the third points and the assumed linear softening (Figure 3.10 (a) and Figure 3.11 (a)).

To control crack propagation, the nodes beyond the precracked tip are released one by one. Unit external and unit internal forces are applied at the loaded point and nodes along the crack path in the fracture process zone and solved for the basic solutions. Based on superposition, the first and second assumptions yield :

$$f_t = \alpha_0 \sigma_0(0) + \alpha_i \sigma_i(0)$$

$$\sigma(x) = f_t(1 - \frac{w(x)}{wc})$$

$$w(x) = \alpha_0 w_0(x) + \alpha_i w_i(x)$$

where f_t = tensile strength

x = measured distance from the fictitious crack tip (x=0), based on a moving coordinate system with the origin at the tip. x increases in the direction opposite to the direction of crack propagation

α_0, α_i = load multiplication factor for unit external and unit internal loads, respectively, applied at node i in the process zone

$\sigma_0(0)$ = normal stress at crack tip due to a unit external load

$\sigma_i(0)$ = normal stress at crack tip due to a unit internal load at node i in the process zone

w(x) = crack width at distance x

w_c = critical crack width

A small element size and a linear displacement between elements are assumed in manipulating these relationships. These provide satisfactory approximate results (77).

$$\alpha_i = t' L \sigma_i$$

Therefore, $$\alpha_i = t' L f_t [1 - \frac{w(x)}{wc}]$$

Where t' = thickness
L = element length

This system of equations is arranged in the following form and solved for unknowns α_0 to α_n

$$t'Lf_t\left\{\begin{bmatrix} w_0(x1) & w_1(x1) & .... & w_n(x1) \\ w_0(x2) & w_1(x2) & .... & w_n(x2) \\ .... & .... & .... & .... \\ w_0(xn) & w_1(xn) & .... & w_n(xn) \\ \frac{\sigma_0(0)}{f_t} & \frac{\sigma_1(0)}{f_t} & .... & \frac{\sigma_n(0)}{f_t} \end{bmatrix} + w_c \begin{bmatrix} 0 & 1 & 0 & .. & 0 \\ 0 & 0 & 1 & .. & 0 \\ .. & .. & .. & .. & .. \\ 0 & 0 & 0 & 0 & 1 \\ 0 & 0 & 0 & 0 & 0 \end{bmatrix}\right\}\begin{Bmatrix} \alpha_0 \\ \alpha_1 \\ .. \\ \alpha_{n-1} \\ \alpha_n \end{Bmatrix} = t'Lf_t \begin{bmatrix} w_c \\ w_c \\ .. \\ w_c \\ 1 \end{bmatrix}$$

This approach is employed due to its simplicity and compatibility with the available finite element program, ANSYS (91).

3.3.3 Strain Softening Diagram

The three key factors in FCM are fracture energy (G_f), crack width, and, tensile strength. However, it is generally agreed that the shape of the strain softening diagram or σ-ω curve dramatically influences the predicted failure mechanism of the material. The model accuracy is sensitive to the assumed shape of this relationship (66,75).

The σ-ω relationship was first proposed by Hillerborg and coworkers as a straight line (75). Several functional forms have been proposed subsequently, including bilinear, trilinear or exponential functions (Figure 3.11) (66,77). These forms provide better agreement with the test results than a simple straight line. A bilinear shape of the σ-ω relationship was reported to provide sufficient accuracy and realistic load-displacement curves for conventional concrete (78,79).

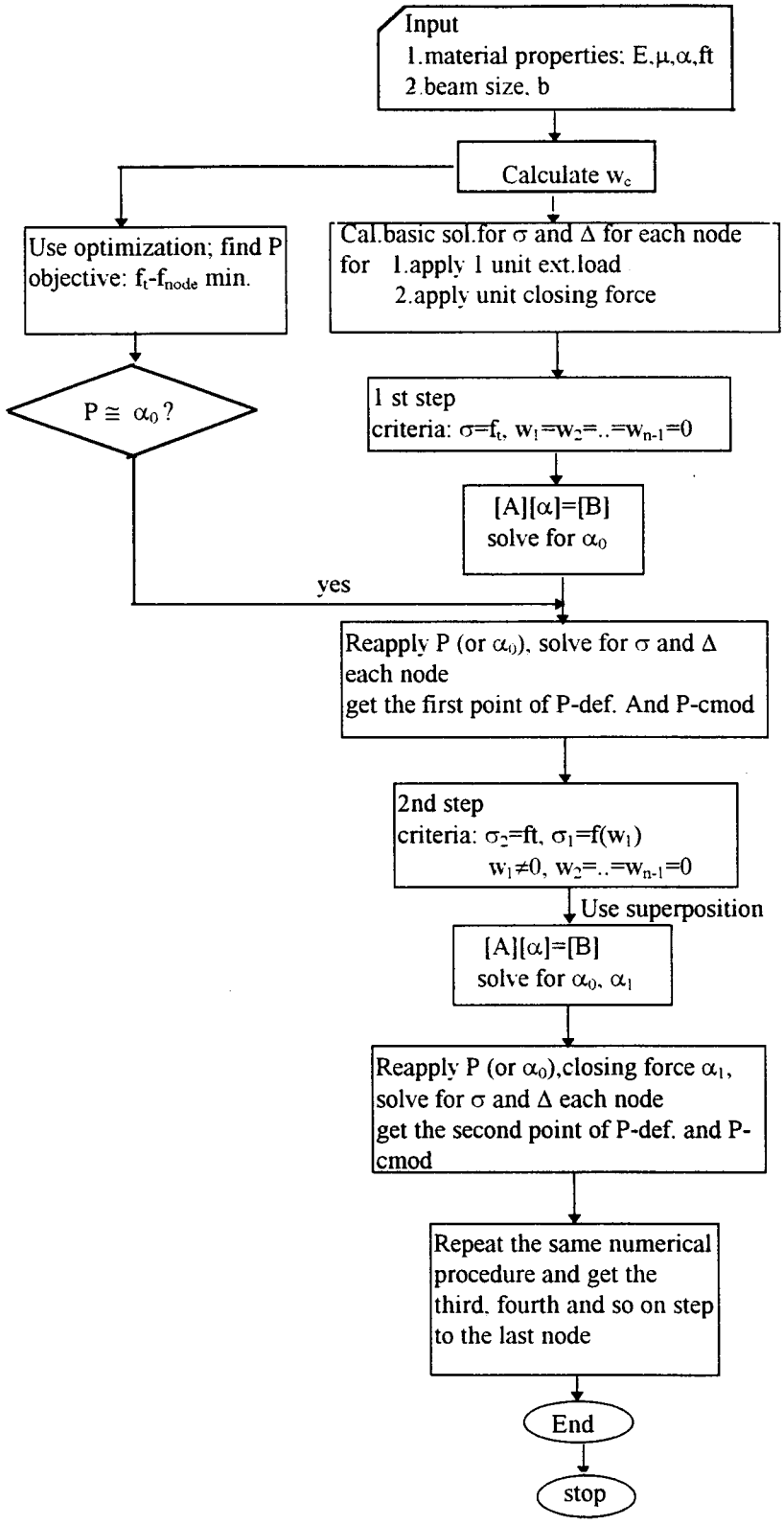

Figure 3.9 Flow chart for the calculation steps, using superposition technique and FCM

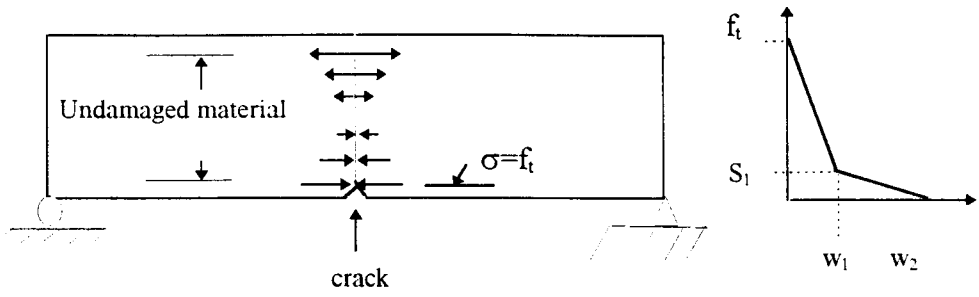

(a) beam subjected to external load and internal closing forces (*b)* bilinear diagram

Figure 3.10 Fictitious Crack Model Concept applied to a three point bending beam incoporating bilinear strain softening diagram

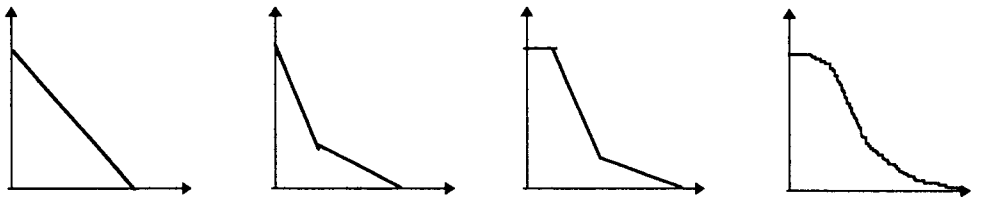

(a) Linear (b)Bilinear (c)Trilinear (d) Exponential

Figure 3.11 Proposed shapes of strain softening diagrams

To improve the prediction accuracy, several approaches have been proposed, sometimes in combination with particular techniques. For example, Du (66) modified the trilinear model, using an optimization procedure, accompanied by accurate measurements of crack length and crack opening displacement using the Moire Interferometry technique. This resulted in a good prediction compared to the experimental data.

Two approaches are used to obtain suitable strain softening diagrams, best fit and trial and error approaches. For the best fit approach (68,71,79), either load-deflection or load-crack mouth opening displacement (cmod) from each test is used to determine the diagram that best fits the experimental data. This approach provides the best fit strain softening diagram for each individual case.

For trial and error, several sets of the necessary points to establish the strain softening diagram are chosen and used as input to numerically analyze for the load-deflection curve. Only the set that provides the best agreement to the average from the tests was chosen as a suitable strain softening diagram.

For LMC, film formation appears to significantly affect the behavior; particularly ductility and post peak performance. Therefore, the proper strain softening diagram is necessary to provide a realistic prediction. Since the linear and bilinear relationships have provided satisfactory predictions for normal concrete, both were investigated in this study.

The area under the load-deflection curve determines G_f (64), and the values of f_t and E were calculated from the best fit of the tension and flexural test results. The critical crack width was determined from G_f and f_t for the linear strain softening diagram. For the bilinear case, the assumed s_1, w_1, and the calculated value of w_2 as defined in Figure 3.10 (b) were determined from f_t and the equivalent G_f, based on the trial and error approach.

3.4 Finite Element Model

The performance study of LMC is complicated due to diverse phenomena such as shrinkage strain, thermal strain, as well as formation and propagation of the crack. Therefore, a finite element (FE) method is used to model the crack formation and/or propagation. In the application phase of this study, crack propagation in the overlay is induced by the temperature gradient instead of the applied external load. However, the concept is similar.

To use FE to investigate the cohesive crack propagation, the element size and meshing are also of interest. Too coarse a mesh will result in a model that cannot accurately simulate the cohesive force and crack propagation, and the numerical representation will be irregular. Too fine a mesh requires too much computing time. To achieve a regular and reproducible result, Carpinteri (92) suggested a nondimensional parameter, brittleness number to determine a lower bound for the mesh size. This parameter is in the form of $S_E=G_f/(mhf_t)$; where G_f is fracture energy, m is the number of nodes along the depth and f_t is the tensile strength. The chosen mesh size in this study was based on this limitation and available computing time.

3.5 Heat Flow Conditions

Since environmental factors influence bridge deck cracking, the temperature distribution through the deck depth was first calculated using heat transfer models. Three mechanisms; convection, radiation and conduction result in the flow of heat. The

first two mechanisms affect the heat flow between the bridge and the surroundings while conduction is responsible for the heat flow within the deck.

When the material properties are assumed to be temperature independent, the transient heat conduction is linear and the basic equation for three dimensional heat flow is (80):

$$\frac{k}{\rho\, c}\left(\frac{\partial^2 T}{\partial^2 x}+\frac{\partial^2 T}{\partial^2 y}+\frac{\partial^2 T}{\partial^2 z}\right)=\frac{\partial\, T}{\partial\, t} \qquad \text{--------- (eq.3.7)}$$

where k = conductivity of the medium =1.4w/m°C for concrete(46)
T = temperature
t = time
ρ = density of the medium = 2400 kg/m^2 for concrete
c = specific heat = 960J/kg°C (46)
x,y,z = Cartesian coordinates

One dimensional heat flow in a vertical direction is sufficiently accurate for bridge superstructures (38,47,81). Equation 3.7, simplified for one dimensional flow, is shown in equation 3.8. The temperature distribution can be predicted using the finite difference technique.

$$\frac{k}{\rho\, c}\frac{\partial^2 T}{\partial\, x^2}=\frac{\partial\, T}{\partial\, t} \qquad \text{----------eq.3.8}$$

At a boundary such as the top or bottom surface of the deck, energy is normally transferred between the surrounding air and the surface. The boundary condition associated with the above equation is (80):

$$k(\partial T/\partial x) = q \qquad \text{----------eq.3.9}$$

where q = boundary heat input(lost)/unit area which is equal to the summation of heat lost from the effects of solar radiation, convection and irradiation (the effect of rainfall and evaporation are ignored)
$= q_s + q_c + q_r$

For the top surface, convection, radiation and irradiation are important, whereas the last two factors are ignored for the bottom surface. The boundary equations are illustrated as follows (36).

Top surface: $$k(\frac{\partial T}{\partial x_{x=0}}) = \alpha\ I + h_1(T_A - T_{x=0}) - \varepsilon\sigma_{SB}(R_s^4 - R_*^4)$$ -----eq.3.10

Bottom surface: $$k(\frac{\partial T}{\partial x_{x=L'}}) = h_2(T_A - T_{x=L'})$$ -------eq.3.11

where α = absorptivity coefficient of top surface
h_1 = heat transfer coefficient including convective and radiative heat losses
h_2 = heat transfer coefficient at bottom surface
σ_{SB} = Stefan-Boltzman's constant
R_S = bridge temperature on absolute scale
R_* = air temperature on absolute scale
L' = total thickness of the medium

The boundary and initial conditions were used as input for the analysis. The initial condition generally is chosen from the condition when the temperature gradient is a minimum (38,47). Since there is no experimental data available, an assumed uniform temperature at a value equal to the minimum air temperature will be used in this study.

4.EXPERIMENTS AND RESULTS

A two stage study was conducted to fulfill the objectives of this research. The first stage included material testing and model setup. The second stage was an application of the proposed model to predict the environmental effects on the overlay performance.

Little information was available in the literature on early age properties of modified concrete. Some properties of LMC have never been studied, particularly fracture energy and flexural curvature at initial cracking. However, to apply fracture mechanics to failure behavior, it is necessary to know these parameters.

Laboratory testing generated strength and fracture parameters in addition to providing some information on the development of LMC properties with time. The results of load vs deflection from the second phase analysis were also compared to the test data to verify the proposed σ-ω relationship. These parameters were used as input to predict the outcome of crack propagation and crack mouth opening displacement (cmod) in the application phase.

Since there are no standard tests available for early age concrete, especially for modified concrete, conventional concrete test methods and specimen preparation techniques were used whenever possible. Specimen sizes differed slightly from ASTM standards or RILEM recommendations due to the characteristics of the material and the limitations of the available equipment.

4.1 Material and Test Setup

LMC mixes, similar to those used by the Oregon Department of Transportation (31) were used in this study. Portland cement ASTM C-150 type I, siliceous sand and gravel, and a styrene-butadiene polymeric emulsion were used for specimen preparation. This latex type (approximate density 1018.5 kg/m^3) contains a polymer content of 47-49 percent of total emulsion. The mix proportions and material properties are shown in Tables 4.1 and 4.2.

The three point bending test of beams 10.2 by 10.2 by 43.2 cm., loading upwardly (Figures 4.1 and 4.2), was used to investigate flexure properties and fracture energy. This size was selected to reduce the dead weight, to allow molds to be used for both flexure and fracture energy tests and to compare the results with other work (74,83). The test data were directly collected through the Validyne data acquisition system: "Easy Sense version 2.01" (84).

The specimens were cast in two lifts, and the tension side was designated as the top side to facilitate notch casting and crack width measurement during early ages. A tamping rod and modified table vibrator were used as the means for compaction. The slump test (ASTM C143) was performed to check the workability for each mix. After finishing, the specimens were covered with a plastic sheet and wet burlap for 24 hr. before demolding. The demolded specimens were left for an additional 24 hr. before being uncovered and placed in an ambient environment (approximately 17-21°C and 70±10 %RH) until tested, similar to the field curing method for LMC.

Table 4.1. Mix proportions of latex modified concrete (31)

Material	Amount (kg/m^3)
cement	391.5
sand	963.5
gravel	824.6
latex emulsion	122.1
water (w/c = 0.32)	63.8

Table 4.2. Mechanical properties of coarse and fine aggregates

Sieve Size	sample 1			sample 2		
	mass retained (gm.)	percent retained (%)	cum. percent retained	mass retained (gm.)	percent retained (%)	cum. percent retained
Fine						
# 4	4.3	0.69	0.69	3.5	0.62	0.62
# 8	109.4	17.72	18.41	93.6	16.50	17.12
#16	86.1	13.95	32.36	81.2	14.32	31.44
#30	79.4	12.86	45.22	69.4	12.24	43.68
#50	221.0	35.80	81.02	192.3	33.90	77.58
#100	95.4	15.45	96.47	104.7	18.46	96.04
pan	21.8	3.53	-	22.5	3.97	-
total	617.4		274.17	567.2		266.48
fineness modulus			2.74			2.66
moisture content			4.02%			4.44%
Coarse						
1"	0.0	-	-	0.0	-	-
3/4"	0.0	-	-	0.0	-	-
1/2"	515.0	46.31	46.31	575.0	40.69	40.69
3/8"	326.0	29.32	75.63	467.0	33.05	73.74
pan	271.0			371.0		
total	1112.0			1413.0		
moisture content			2.74 %			2.76%

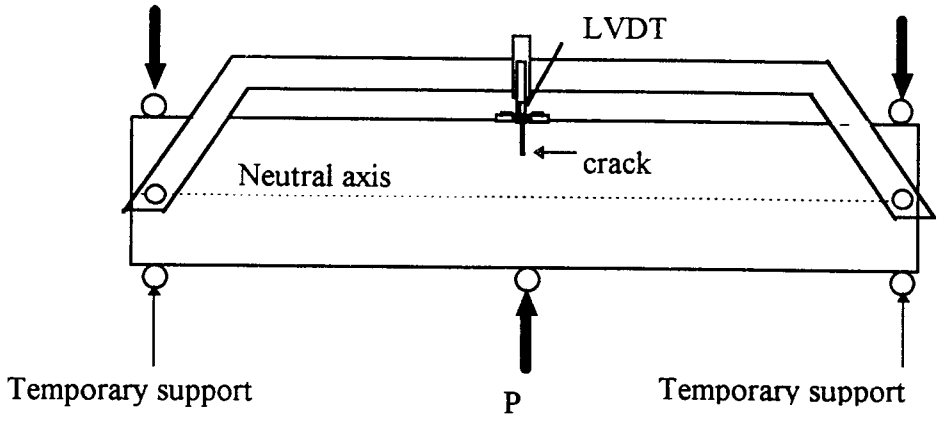

(a) Schematic diagram of test setup

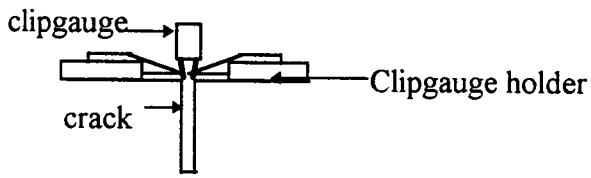

(b) detail of accessories to measure crack mouth opening

Figure 4.1 Test setup for fracture test

For the very early age LMC, the test was conducted with the specimen in a special Plexiglas mold to prevent material disturbance from demolding or handling (Figure 4.3). The mold design allowed longitudinal sliding in the laminated sides to insure flexibility of the mold thus minimizing the mold effect during testing. The empty molds were tested for flexure before and after each specimen was tested, to allow the influence of the mold to be factored out (Figure 4.4). The early age test setup is shown in Figure 4.5.

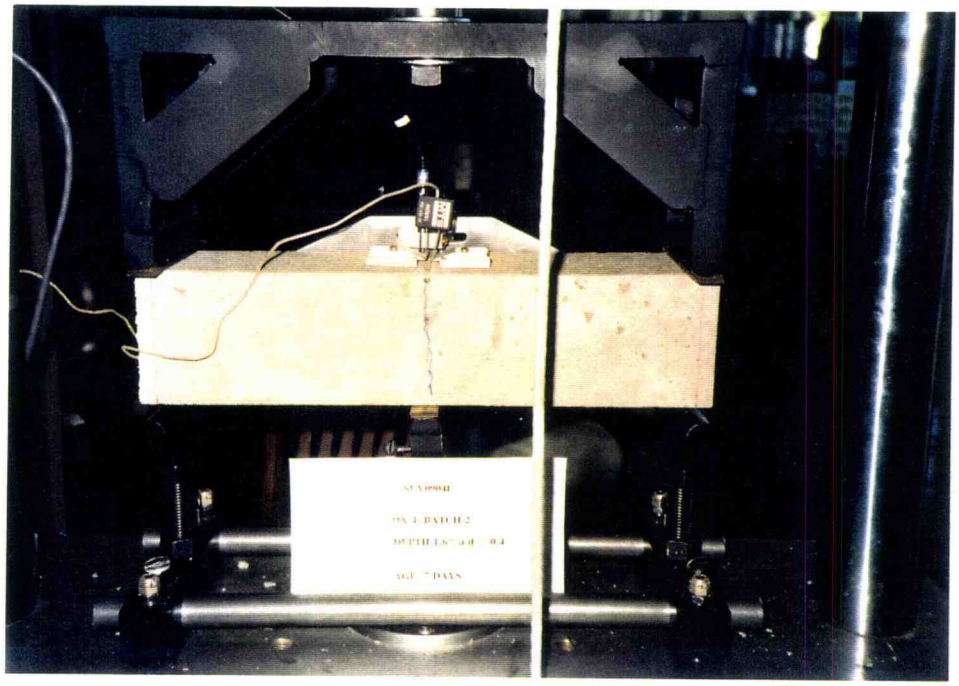

Figure 4.2 Three point bending set up for flexure and fracture energy test

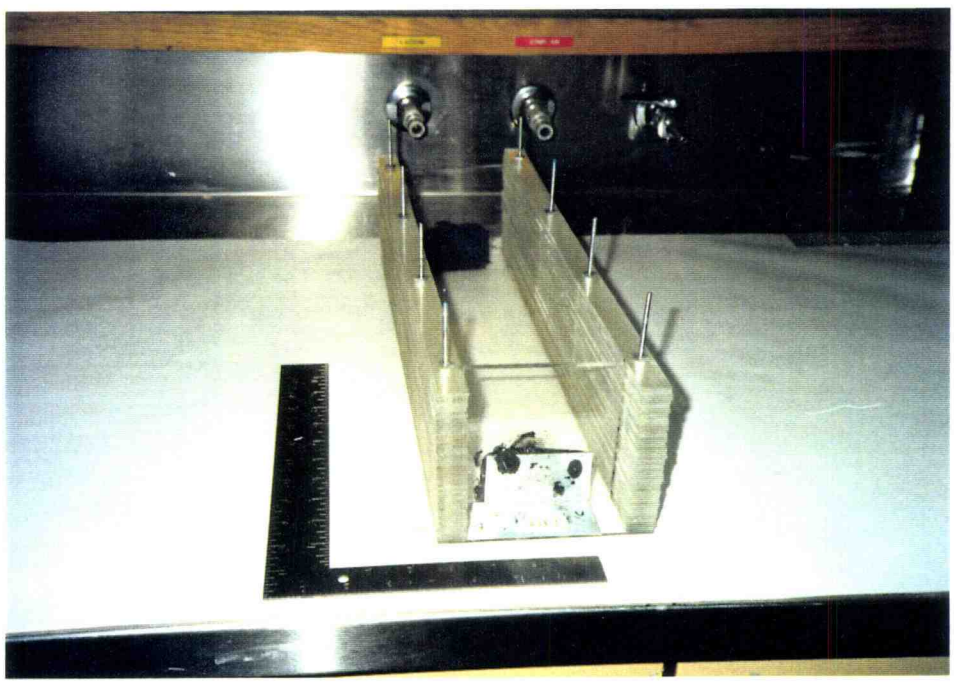

Figure 4.3 Special Plexiglas mold for flexure and fracture test at early age

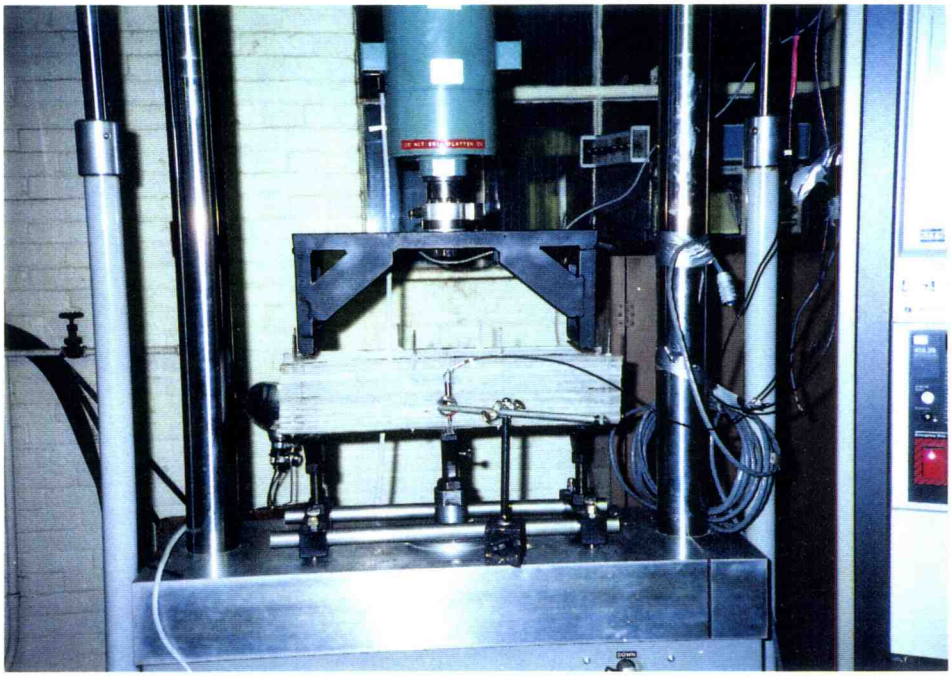

Figure 4.4 Test setup for Plexiglas mold calibration

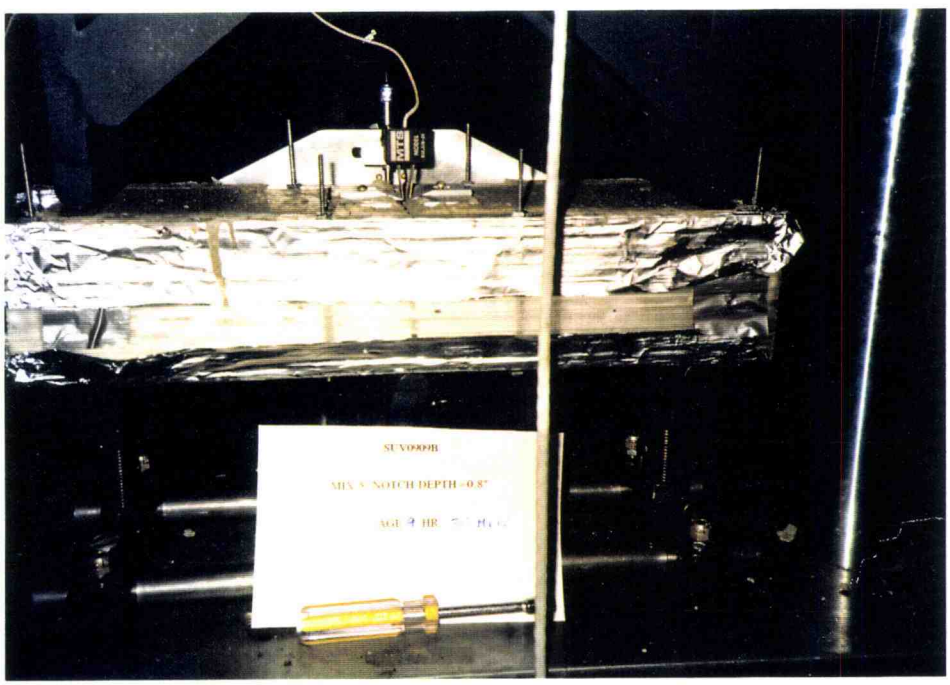

Figure 4.5 LMC early age test setup

4.1.1 Compressive Strength

Standard cylinders, 15.2 by 30.5 mm. were tested for compressive strength at ages 0.5, 1,2, 3, 7 and 28 days. The loading rate recommended by ASTM C39-1991 (85) was used as a guideline. For very young ages (< 24 hrs.), the loading rate was adjusted slightly to prevent sudden failure and to extend the test duration.

4.1.2 Tensile Strength

Although when properly conducted, the uniaxial tensile test provides results that can be characterized as the true tensile strength for concrete (86), the characteristics of concrete at early age limits the use of this test method. The low tensile strength of the material becomes a problem because the specimen must carry its own weight for the vertical test, unless some special arrangements are made or a horizontal uniaxial tensile test is used as an alternative.

Therefore, a simple test, the Splitting Test was chosen for this study. The 15.2 by 30.5 cm. cylindrical specimens were tested according to ASTM C-496-91 (85) at the same age as the flexure test. As with the compression test, the suggested ASTM loading rate was used as a guideline and the range was adjusted slightly (from 15 MPa/min to 1.5 MPa/min) for very young concrete.

4.1.3 Modulus of Elasticity

The bending tests were conducted on unnotched beams at ages of 0.5, 1, 3, 7 and 28 days to determine a modulus of elasticity and fracture energy. A constant

deflection rate was used to control the test. Cyclic loading using 10-20 cycles was conducted to prevent sudden failure and to achieve a stable failure mechanism for the entire load-deflection curve. The peak load and midspan deflection were used to calculate the modulus of elasticity.

The effect of shear deflection on the measured total deflection is recognized, particularly for the large span to depth ratio used in this study. Therefore, Seewald's equation for center point loading was used to correct the modulus calculated from the maximum load and deflection (87)

4.1.4 Fracture Energy

Although a direct tension test has been recommended by many researchers to determine an unambiguous value of fracture energy, the three point bending notched beam, recommended by RILEM (64) was chosen for this investigation. The decision was based on procedural simplicity, equipment availability, and the limitations of the early age concrete.

A tapered aluminum plate 2 mm. thick was temporarily fixed at the top of the mold to form the notch. This plate was removed as soon as possible to avoid premature cracking. Notch depth/beam depth ratios of 0.2 and 0.4 were used. Clip gauge holders were glued on the surface adjacent to the casting notch prior to the testing.

4.1.4.1 *Specimen Loading*

4.1.4.1.1 Notched beam

To study the fracture behavior for concrete-like materials, postpeak behavior is of particular interest as well as the influence of loading rate. In this study, crack mouth opening displacement control or strain control were used to achieve a stable test and to study the strain softening in the post peak region. This choice also avoided the potential effect from localized crushing at the loading point as well as the potential for change in internal microstructure from crack intensity near the crack tip.

A closed-loop, servo-controlled hydraulic testing machine (MTS) was used. A clip gauge, MTS model 632.02B-20, measured the crack opening displacement and sent feedback signals to control machine operations at two selected rates of 0.0003175 and 0.000127 cm/sec.

The loading rates have been reported to influence fracture energy; the higher the loading rate, the larger the fracture energy (64,88). Kormeling's study showed that although the loading rate increased by a factor of 2000, the corresponding fracture energy increased only by 48 to 82 percent (89). For this study, therefore, loading rates were chosen approximately equal to those used in Kormeling's study. The selected rate allowed the maximum load to be reached in about 50-120 seconds. The test also provided the complete pre- and post-peak load-displacement relationship in a short time compared to the test age of the specimen.

The effect of applying two loading rates in a single test is also of interest although no reports have been found in literature. To investigate this effect, three point bending tests were conducted on specimens of similar age from the same batch. The results indicated that only a small difference (6.2%) occurred in measured fracture energy. As a result, the testing program was conducted using the two selected rates.

Mid-span deflection was recorded through an LVDT (Linear Variable Differential Transducer) referenced to the neutral axis to avoid any error from support-localized crushing. This potential error would result in a difference in the calculated area of the load-deflection curve (up to 7%). It may also cause a significant shifting in reported mid span deflection (25-300%) (53). Before testing, beam dimensions and span were carefully measured.

4.1.4.1.2 Unnotched beam

For unnotched beams, the cyclic load under deflection control was used to prevent unstable failures. It was assumed that there was no significant difference between the calculated G_f from static bending and the cyclic tests (90). An x-y recorder was used to plot the load-midspan deflection in real time. This gave a visual means to monitor and control the test. The area under a boundary of the load-deflection curve was determined, using planimeter, and used to calculated G_f.

4.1.4.2 *Mold calibration*

Since the very early age specimens were tested within the special flexible mold, mold calibration was necessary to account for the mold effect. Each empty mold was tested in three point bending, using displacement control at a rate of 0.00127 cm/sec. A load cell, capacity 4450 N was used for load measurement. All tests were conducted to reach the approximate midspan deflection of 0.5 cm, which exceeded the midspan deflection at failure for all LMC specimens. Regression of the test results resulted in the load-midspan deflection relationship for each mold. A typical calibration curve and regressions are shown in Figure 4.6 and Table 4.3 . These relationships were used to adjust measured load-deflection relationships for the effect of the mold.

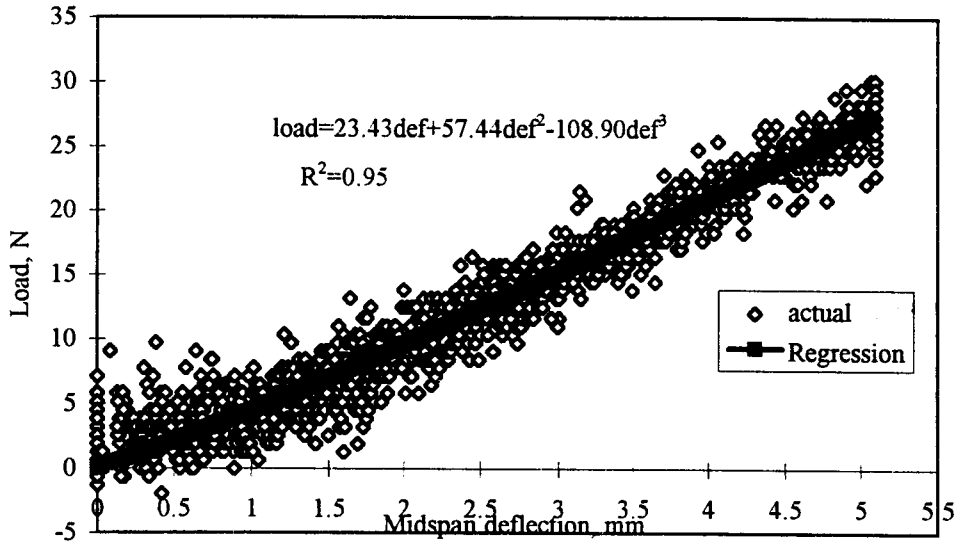

Figure 4.6 Typical load vs mid span deflection for mold calibration

Table 4.3 Load-Deflection relationship for early-age test molds

Mold identification	Load deflection relationship	R^2
A	load=0.3821def+135.4258def^2-243.2280def^3	0.9236
B	load=6.4273def+86.2309def^2-114.6107def^3	0.9339
C	load=23.42667def+57.4380def^2-108.8960def^3	0.9499
D	load=-6.5712def+155.3728def^2-252.4630def^3	0.9202

The test results indicated an insignificant effect of the mold. Under the ultimate midspan deflection for all test specimens (0.2-0.4 cm.), the load resistant effect from the mold was less than 13 N.

4.1.5 Shrinkage

Since there is no standard test available for early age concrete-like materials, shrinkage strain measurements in this study were conducted, using an embedded waterproof electronic strain gauge, KM200A: KE4881-884. This 20 cm.-long-embedded waterproof strain gauge is manufactured with a relatively low elastic modulus of about 39.2 MPa, and provides a suitable means for measuring strain in young concrete.

Shrinkage specimens were cast in wooden molds, 15.2 by 15.2 by 50.8 cm., covered with waxpaper on each side and the base to prevent the LMC from sticking to the mold and also to prevent water loss from absorption. The mold sides could be removed after the sample was sufficiently stiff to maintain the original shape. This minimizes specimen restraint. Before casting, the strain gauge and thermocouple were

carefully installed in the middle of the mold (Figure 4.7).An embedded thermocouple at the middle of the specimen recorded the temperature.

After finishing the surface, the specimens were kept in a controlled-temperature chamber, throughout the test period of 7 to14 days (Figure 4.8). An Environmental Control System (ECS), Despatch Industries 16000 Series, has the capability to control both temperature and humidity. The analog sensor input is converted to a digital signal in this microprocessor-based system, and performed the internal calculation with real temperature values. This provides a precision control system throughout the studied temperature range.

Two temperatures (12.7±1.6 and 29.4±1.6°C) and one relative humidity (50±4%RH) were used. The higher temperature (29.4±1.6°C) is a temperature specified by many agencies as the maximum temperature during which an overlay can be placed. The lower temperature enabled the difference in shrinkage strain of the specimens to be explicitly observed for both test conditions.

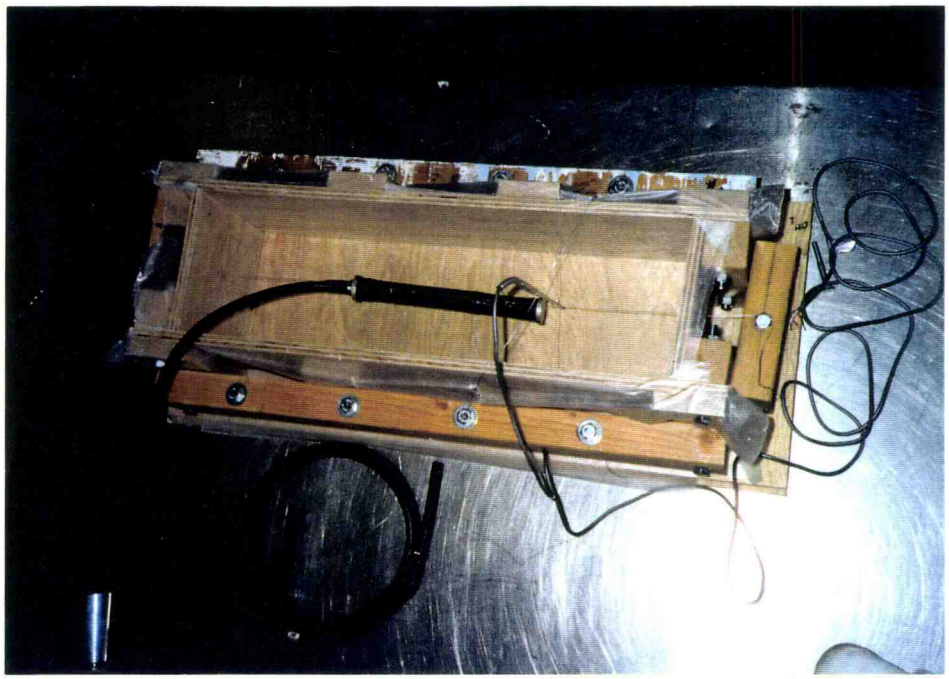

Figure 4.7 Wood mold for shrinkage testing

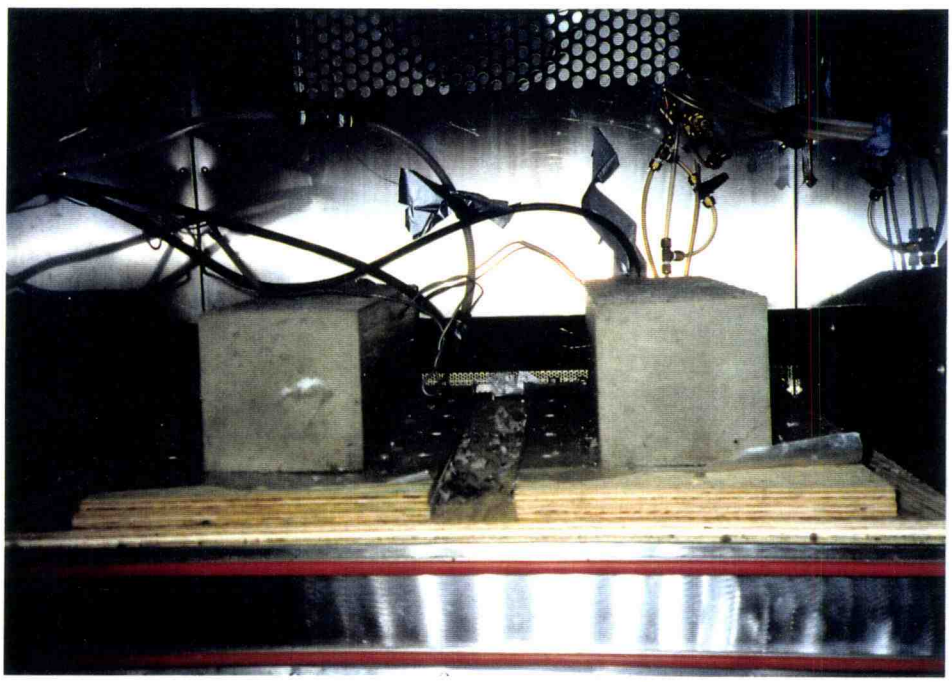

Figure 4.8 Shrinkage test specimens in controlled environmental chamber

4.2 Test Results and Discussions

The properties of LMC include the general strength and fracture properties from bending beam tests and shrinkage test are reported in this section.

4.2.1 General Strength Properties

The development of compressive strength, modulus of elasticity, tensile strength and flexural strength with time are shown in Figure 4.9. Regression analysis yielded the equations shown in Table 4.4.

The development of modulus of elasticity, E is much more rapid than that of compressive strength, f_c at early ages. Between the ages of 7 and 12 hours, the ratio of f_c to f_t decreases from 12.3 to 6.8 in the first 12 hours, and then increases again. This trend (Figure 4.10) is similar to normal concrete (83), and shows that a minimum ratio was reached at about 12 hours. This time period was greater than the initial setting time but close to the final setting time as reported by Ohama (4).

The calculated flexural strength versus time based on the uncracked section and the peak load for both notched and unnotched beams are plotted in Figure 4.11. It is recognized that the computed stress at the critical section of the notched beam cannot be accurately evaluated by conventional methods due to the effect of induced flexural stress, shear stress and the notch effect itself. However, these curves show the same trend of increasing strength with time.

The correction for shear deflection effect increases E by about 15 percent The regression analyses provided the satisfactorily predicted value at any age (R^2=0.979).

The difference between the estimate and the actual values are only noticeble for ages up to 8 hours.

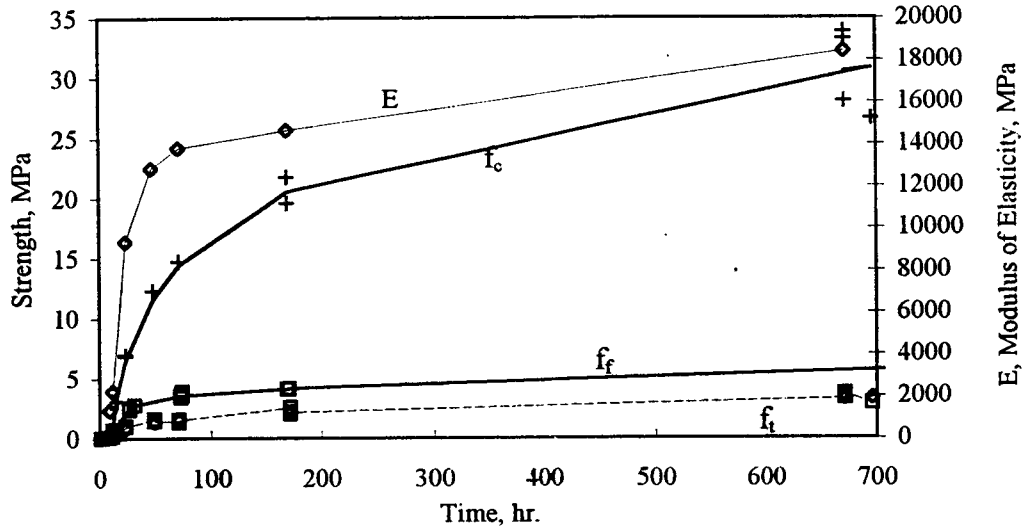

Figure 4.9 Strength and modulus development of LMC

Table 4.4 Regression equations for LMC mechanical properties

Mechanical Properties of LMC	Regression Equations	R^2
Modulus of Elasticity, E MPa	$E = -43319 + 33845\ln(hr) - 6690\ln(hr)^2 + 466\ln(hr)^3$	0.9890
flexural strength, f_f KPa	$f_f = -9450 + 7001\ln(hr) - 1361\ln(hr)^2 + 97\ln(hr)^3$	0.9345
compressive strength, f_c MPa	$f_c = \frac{e^{(-18.958+7.919\ln(hr)-1.404\ln(hr)2-0.085\ln(hr)3)}}{1+e^{(-18.958+7.919\ln(hr)-1.404\ln(hr)2-0.085\ln(hr)3)}}$	0.9850
Tensile strength, f_t KPa	$f_t = \frac{e^{(-27.626+19.163\ln(hr)-5.364\ln(hr)2+0.672\ln(hr)3-0.031\ln(hr)^4)}}{1+e^{(-27.626+19.163\ln(hr)-5.364\ln(hr)2+0.672\ln(hr)3-0.031\ln(hr)^4)}}$	0.9812

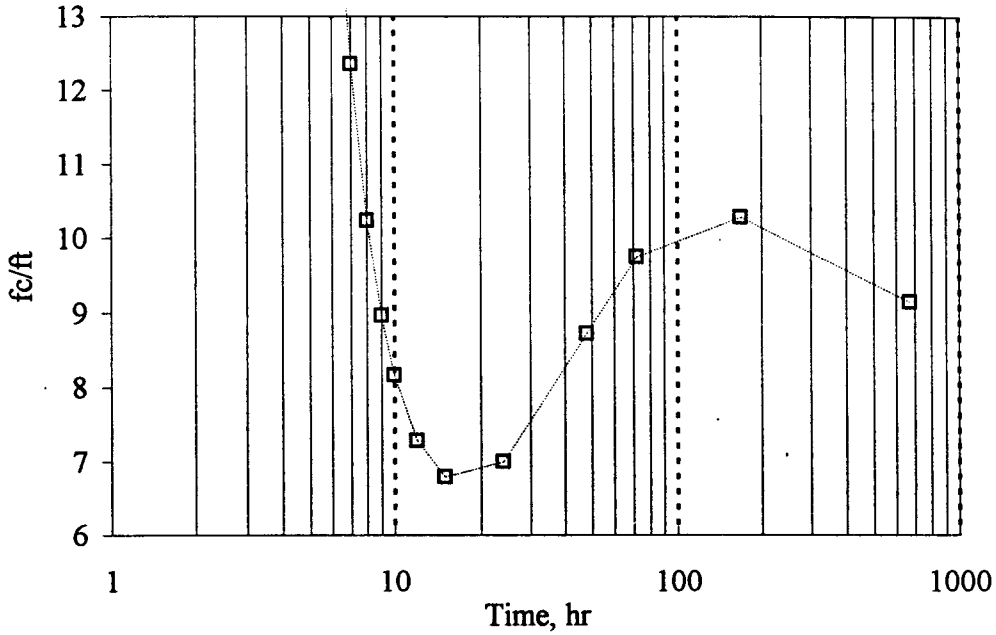

Figure 4.10 The development of f_c/f_t vs time

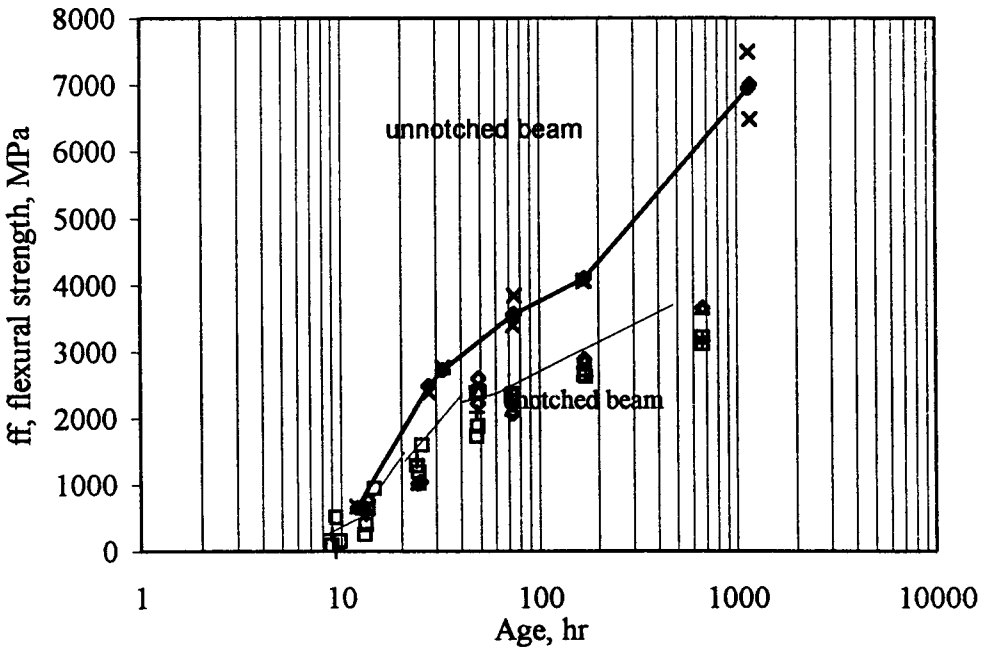

Figure 4.11 Development of LMC flexural stress with time

4.2.2 Fracture Properties

Notch sensitivity, defined by the ratio of flexural strength for notched specimens to the flexural strength for unnotched specimens, is likely to increase at ages up to 3 days, then decrease for all notch depth ratios (Figure 4.12). The notch depth ratios did not show any explicit relationship with LMC notch sensitivity (Figure 4.13) . The plot of midspan deflection at peak load over time (Figure 4.14) indicated the changing deformability with age of LMC. This pattern differed slightly from normal concrete in which the deformability after 12 hours, appeared unaffected by age (83). With early age LMC the deformability decreased and reached a minimum at about 24 hours (a/d=0.2), then increased again with time and continued to change for 28 days. Variation in test results for early age specimens may be due to material sensitivity to the test methodology as well as the limited number of test specimens.

A typical load vs cmod and midspan deflection plot (Figure 4.15) shows stable crack growth and three types of LMC behavior. The curve exhibited linearity up to a certain point (A), followed by nonlinear performance to peak load. The point A defines the "elastic limit" according to ACI 544.1R-82 (28). Increasing load produced increasing deformation which indicated some strain hardening effect. Beyond the peak load, increasing deformation with decreasing load indicated post-peak softening in the same manner as for conventional concrete (41). No information has been found to uniquely identify the transition point from linear to nonlinear behavior. In this study, the " elastic limit" was chosen in the following manner.

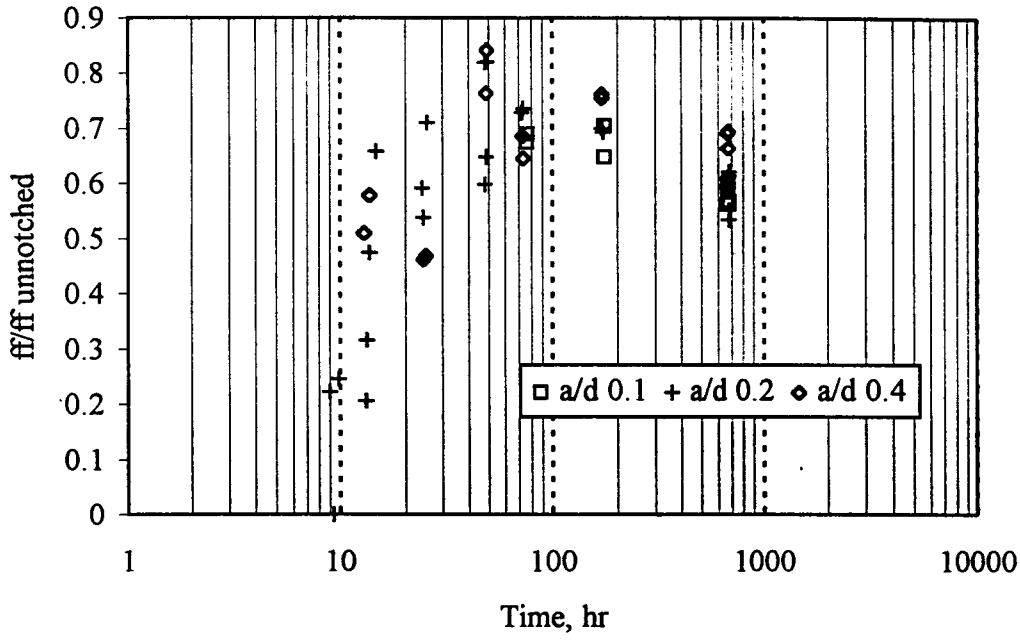

Figure 4.12 Development of notch sensivity with time

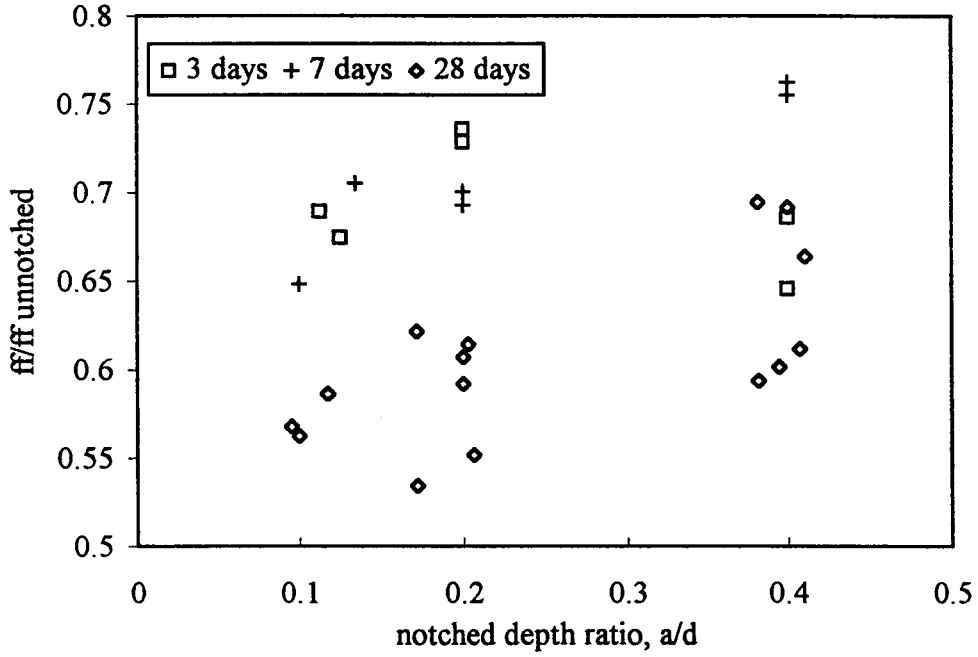

Figure 4.13 The effect of notch depth ratio on notch sensitivity

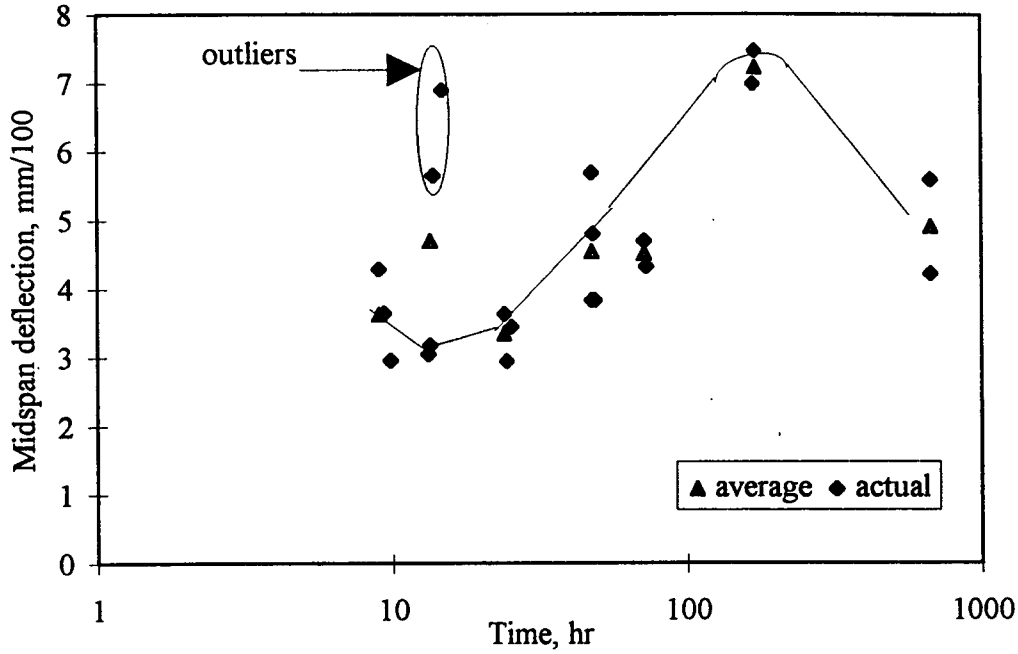

Figure 4.14 Development of deformability with time

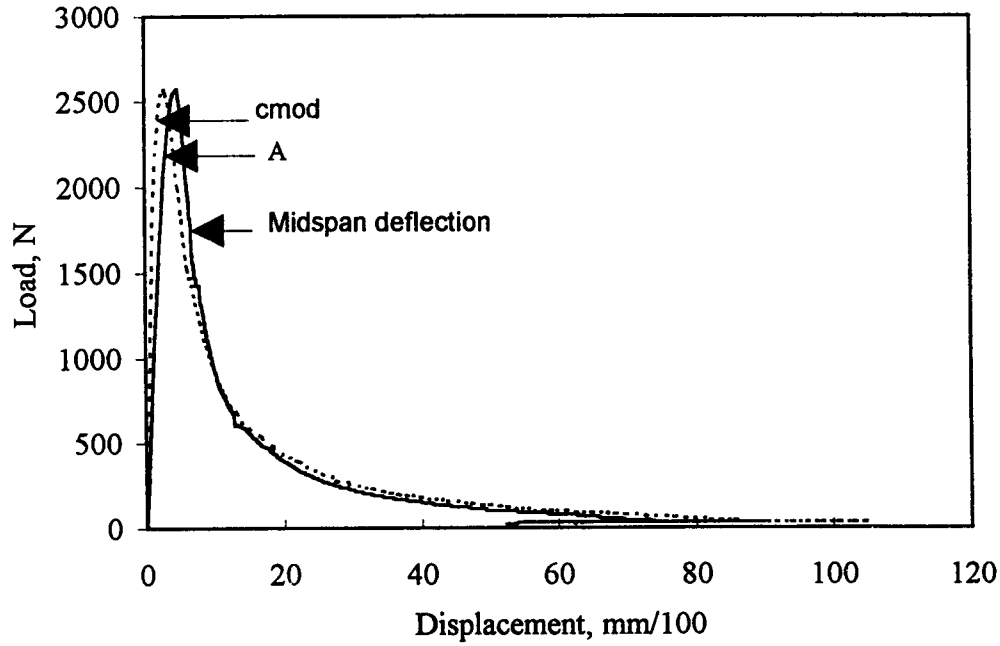

Figure 4.15 Typical load vs midspan deflection and load vs crack mouth opening displacement (cmod) relationships for notched beams

A third degree polynomial regression was fit to the data up to 95% of the maximum load in the post peak region. The fitted curve provided R-square values not less than 0.99. Another regression line was used to fit the linear part of the curve. Zaitzev's study (62) showed that conventional concrete was linear up to 65% of peak load. However, from the trial regressions in this study, linearity was found up to as high as 90% of the peak load, predominantly 85% of peak load (R^2=0.98-0.99). Therefore, the linear regression line up to 85% of peak load is chosen as a reference line (Figure 4.16). The elastic point chosen for this study is justified when the difference in load between the two regression lines at the same deformation is equal to or slightly greater than 5 percent of the peak load. From this criteria, the load associated with the elastic limit, Pe, and the ratio of Pe/Pmax are determined.

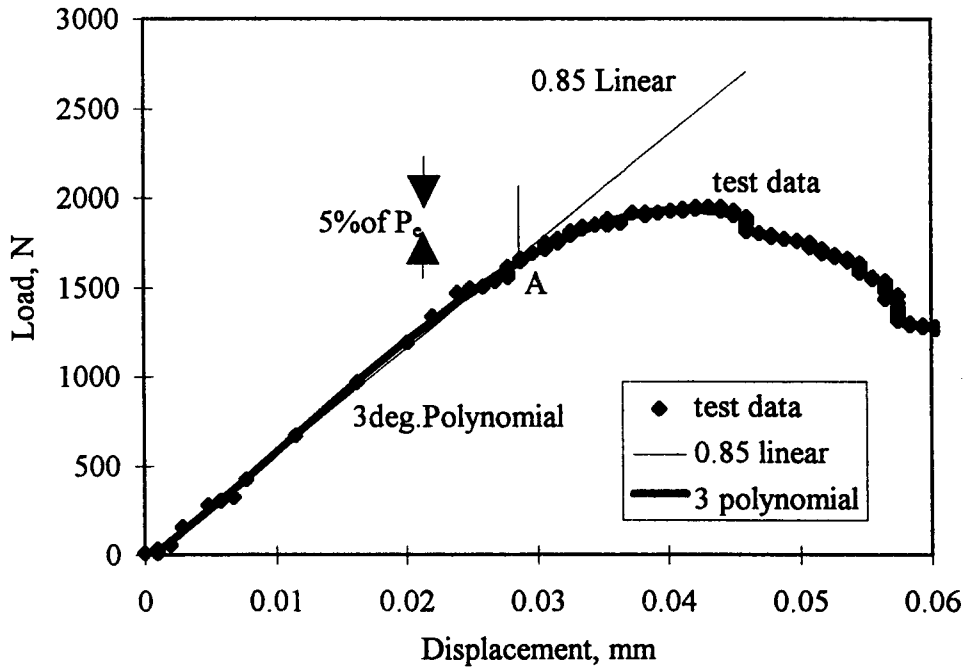

Figure 4.16 Determination of the elastic limit, Pe

From the calculated ratio Pe/Pmax., using the 5 percent criteria, there is no significant evidence of change in this parameter with time (p =0.5355) (Figure 4.17). However, when considering the notch depth ratio effect, there is a statistically significant difference between the mean values of Pe/Pmax (p =0.0005) (Figure 4.18).

The ratio of Pe/Pmax is higher than for conventional concrete (0.893 and 0.936 compared to 0.3 and 0.82 for notch depth ratios of 0.2 and 0.4, respectively) (53). These results agree with the general concept of modified pore structure due to the latex film formation, which is believed to have a pronounced effect especially at the interface zone. Reduced or bridged microcracks in this zone affect the transition from linear to nonlinear response.

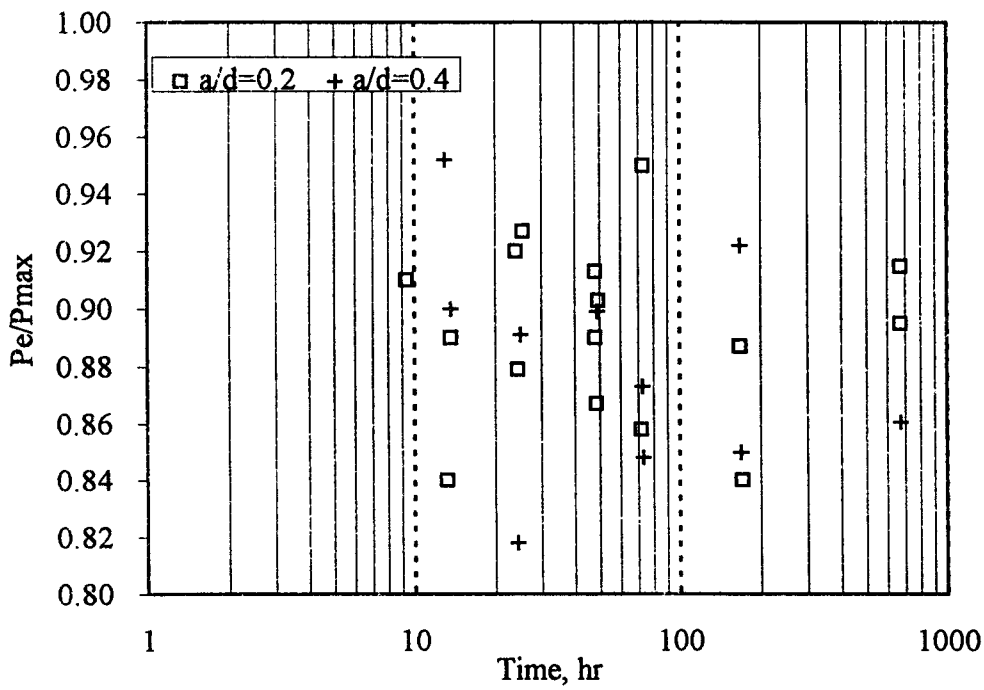

Figure 4.17 Relationship of Pe/Pmax. with time

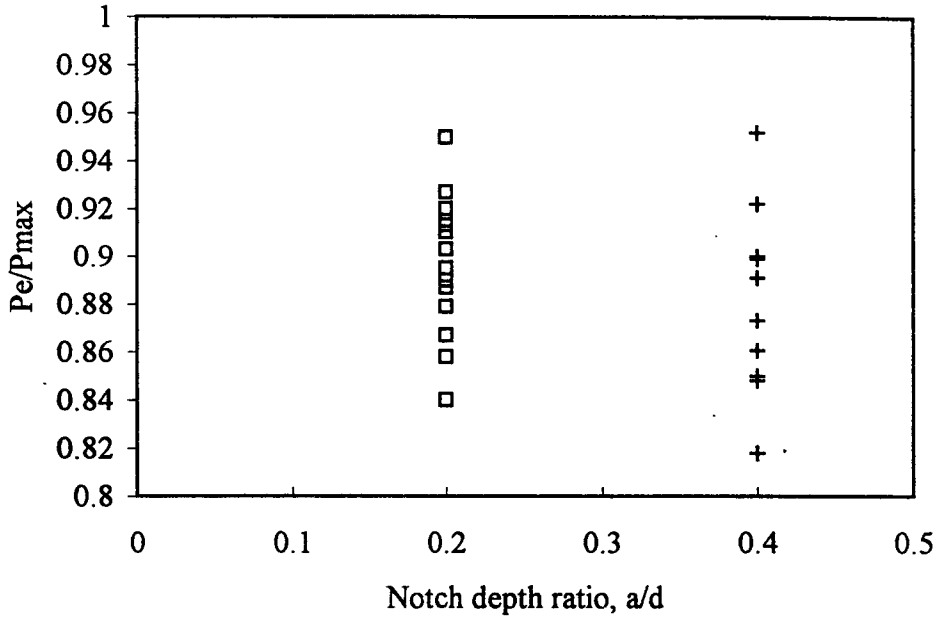

Figure 4.18 Relationship of Pe/Pmax. with notch depth ratio

From the test results, all specimens showed a bilinear relationship between the mid span deflection and cmod, similar to normal concrete (53). The slope S1 in the first portion of the curve reflects the non-systematic variation when taking age and notch depth effects into consideration.

However, the performance of the beam after cracking indicates the strong relationship between midspan deflection and cmod as shown in the typical curve (Figure 4.19). From the statistical analysis, there is no evidence of the relationship between the slope, S2, and time ($p = 0.5155$). Furthermore, there is no significant difference between means values from different notch depth ratios ($p = 0.0595$)(Figure 4.20). Therefore, this parameter is assumed to be constant. This assumption agreed

with conventional concrete study in which this parameter has been proposed as a material constant (53).

The load-deflection curve of an unnotched beam (curve c, Figure 4.21) is slightly different from that for a notched beam. Although the cyclic load was manually applied after the peak load was reached to restrain the suddenly increasing fracture energy, all unnotched beams showed a trend of decreasing both load and displacement.

The fracture energy (G_f), determined from the area under the load-midspan deflection curve (64), varied from 2.3 to 133.1 N/m, depending on age and, to some degree, on notch depth ratio. From statistical analyses, there is strong evidence of a linear relationship of fracture energy and time for both notch depth ratios, 0.2 and 0.4 ($p = 0.0000$ and 0.0000, respectively) as shown in Figure 4.22.

From Figure 4.23 (a) and (b), the comparison of load-deflection and load-cmod curves at different ages (f_c=0.8-29.8 MPa) show a similar trend. The fracture energy and strength increases with age and the higher strength, higher fracture energy results in larger peak load, however, the softening branch in the post peak region shows similar ductile responses. This slightly differs from normal concrete in which the higher strength concrete generally exhibits a more brittle response (64). However, the effect of notch depth is noticeable. The shorter notch depth is likely to be more brittle (Figure 4.24 (a) and (b)).

The calculated value of G_f from the deflection is very close to the value from cmod. Dead weight is likely to have a strong effect on calculated fracture energy, particularly at early ages (Figure 4.25). At ages up to 24 hours, the dead weight effect

varies from 35-350%. This effect decreases with time. After 24 hours, the effect of dead weight is in the range of 15-20%.

The relationship between fracture energy and time is fitted in the form:

$$G_f = -0.2041 + 0.0799\,ln(t) + 0.0686\,ln(t)^2 + 0.1083(\frac{a}{d}) \qquad (R^2 = .891)$$

Where t = time, hours

a/d = notch depth ratio

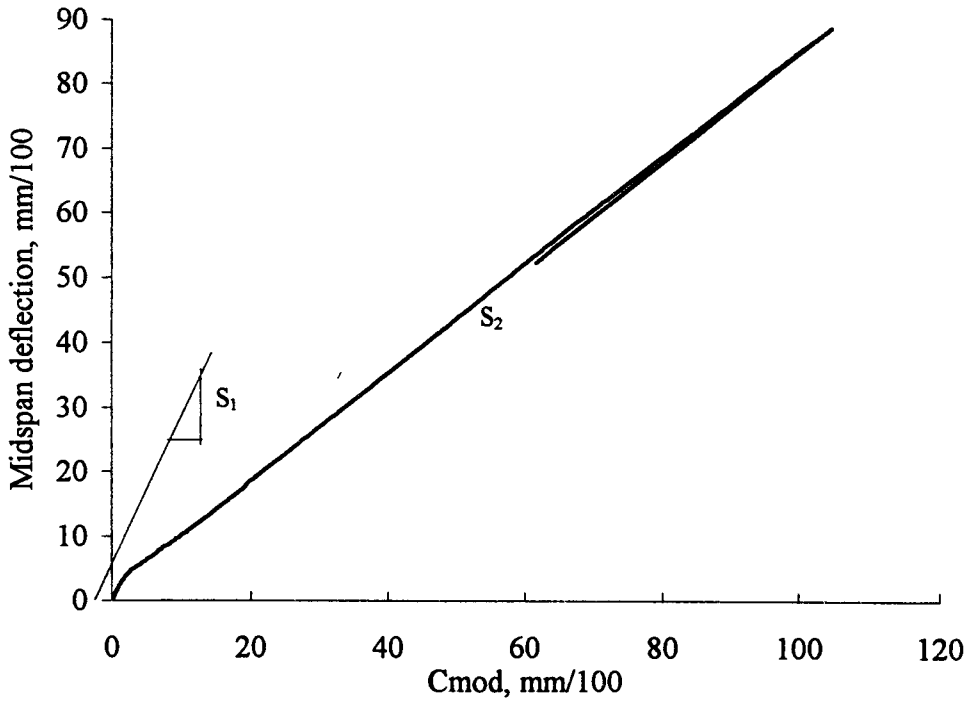

Figure 4.19 Typical bilinear relationship between mid span deflection and crack mouth opening

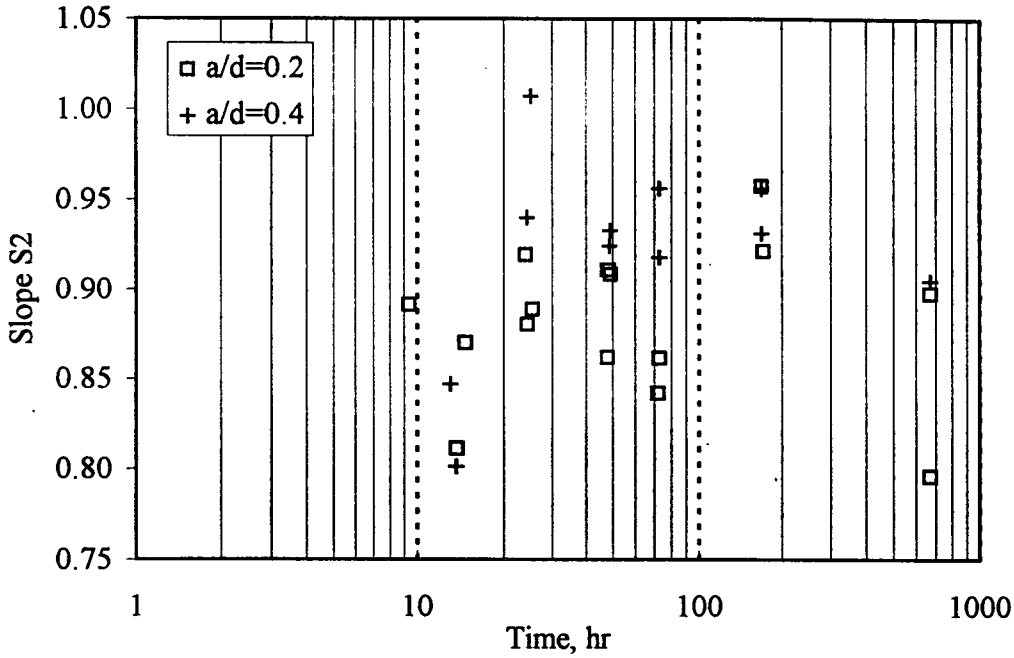

Figure 4.20 The relationship between slope S2 and time

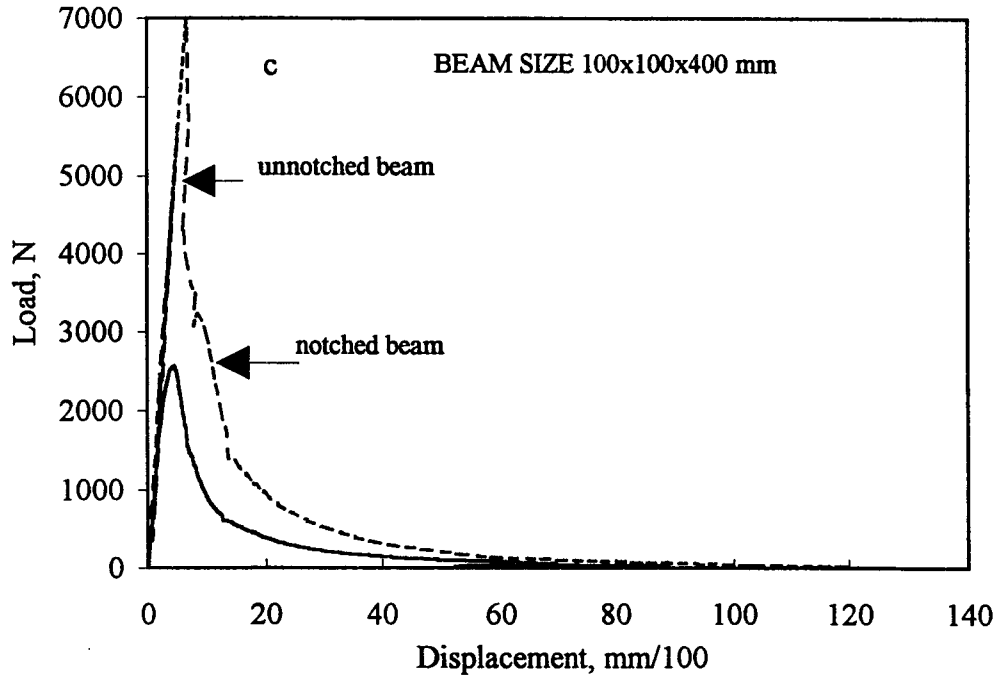

Figure 4.21 Typical load vs mid span for notched and unnotched beams

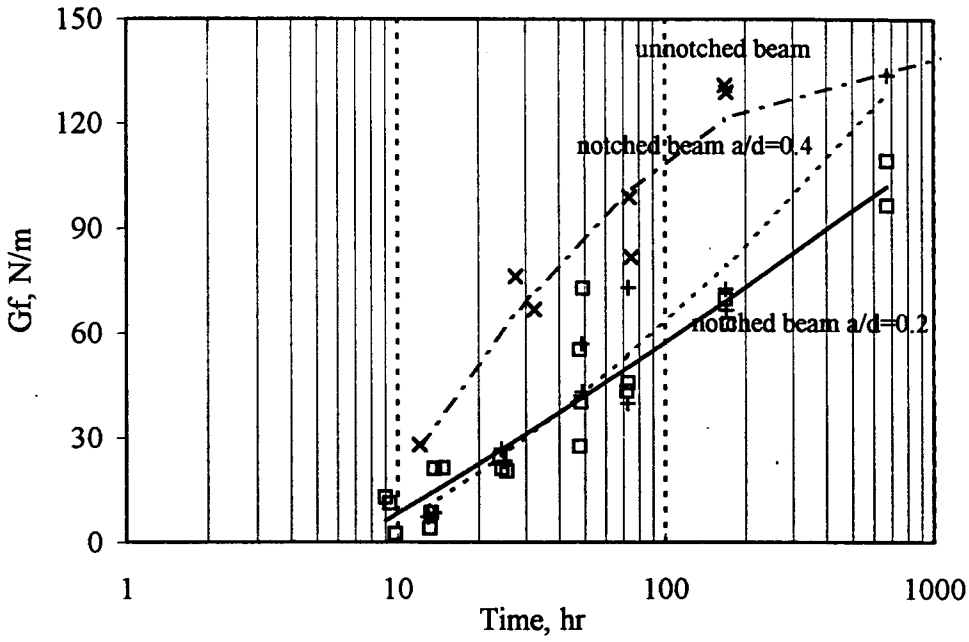

Figure 4.22 Development of LMC fracture energy with time

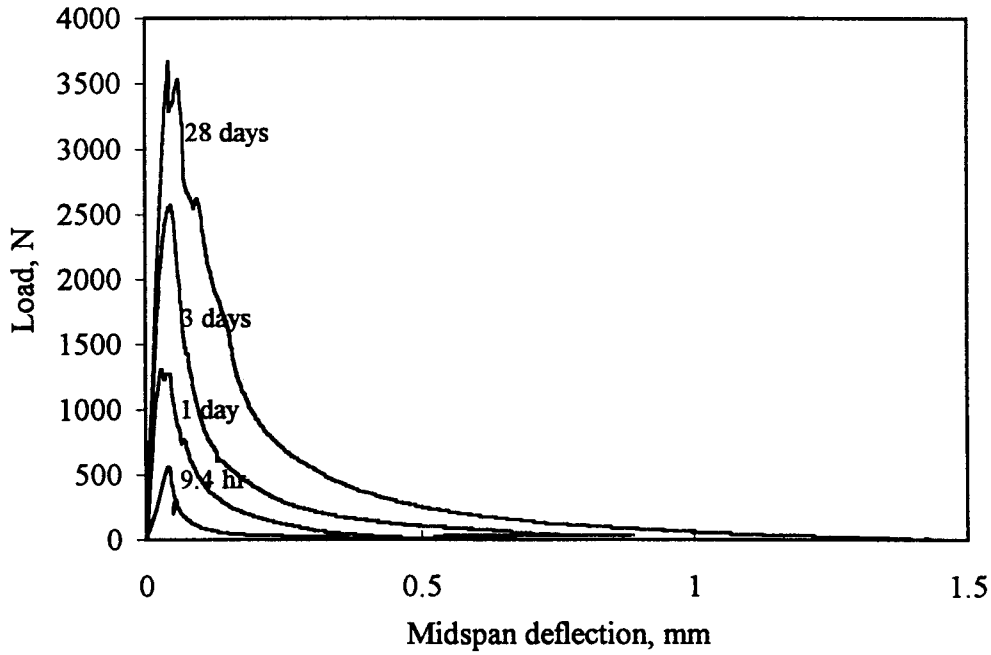

Figure 4.23 Relationship between load and displacement at different ages
*(a)*Load vs mid span deflection

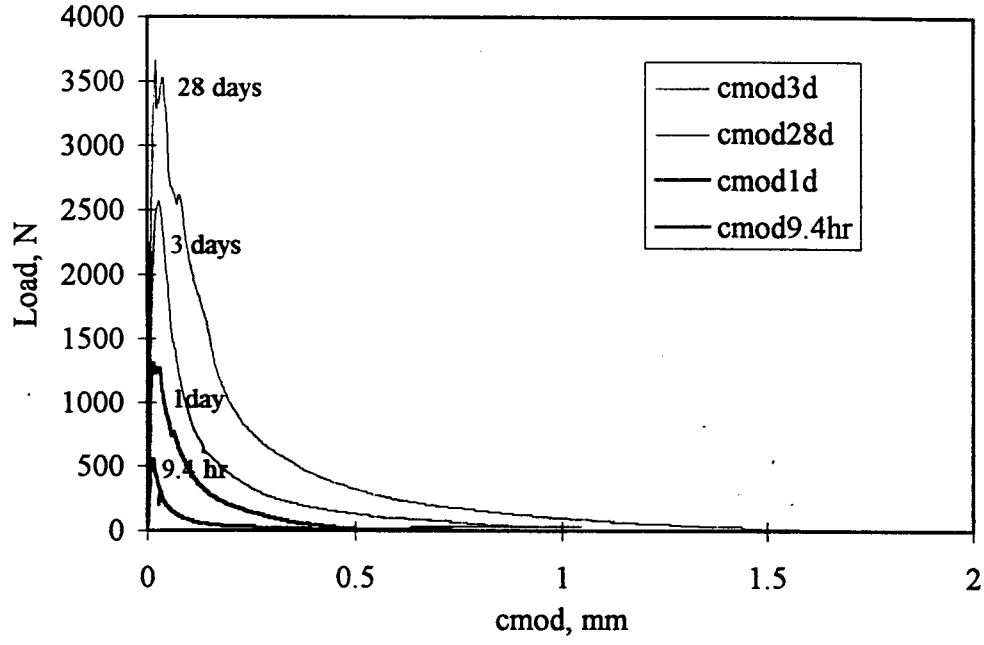

Figure 4.23 (continued)Relationship between load and displacement at different ages *(b)* Load vs cmod

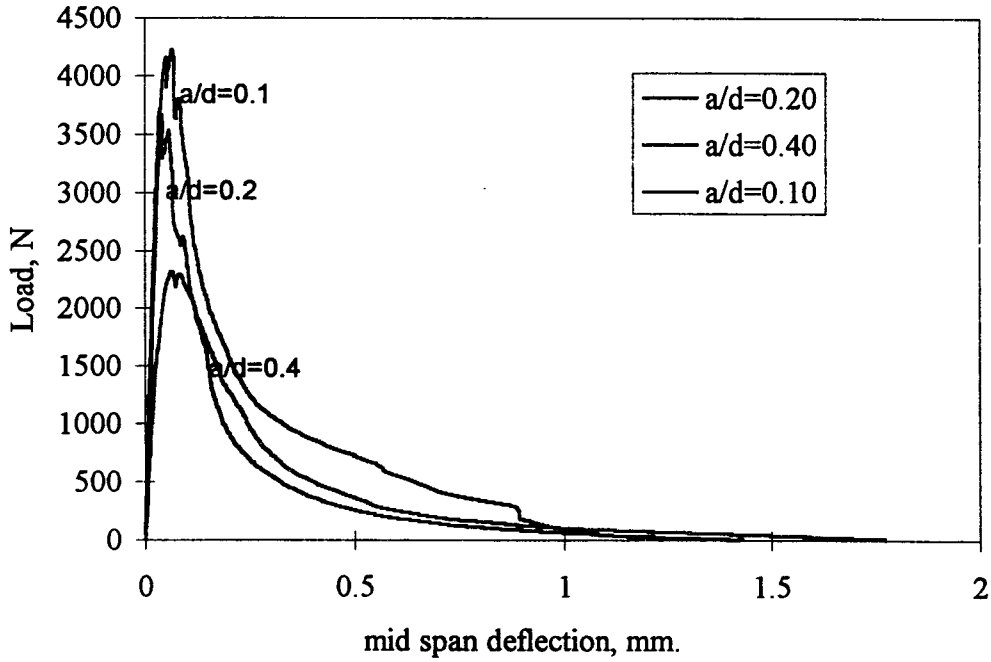

Figure 4.24 Relationship between load and displacement at different notch depth ratios *(a)*Load vs midspan deflection

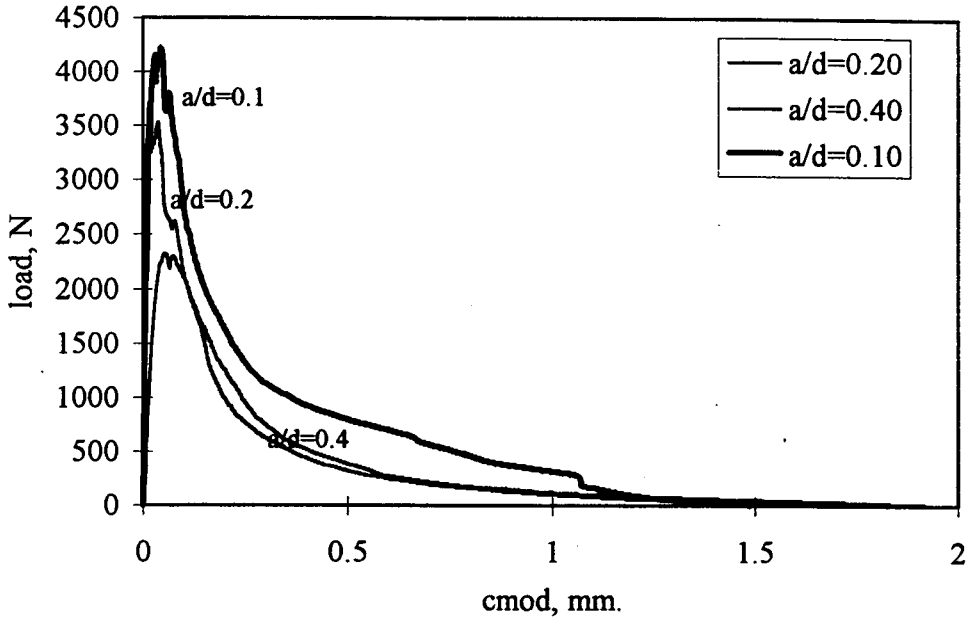

Figure 4.24 (continued) Relationship between load and displacement at different notch depth ratios *(b)* Load vs cmod

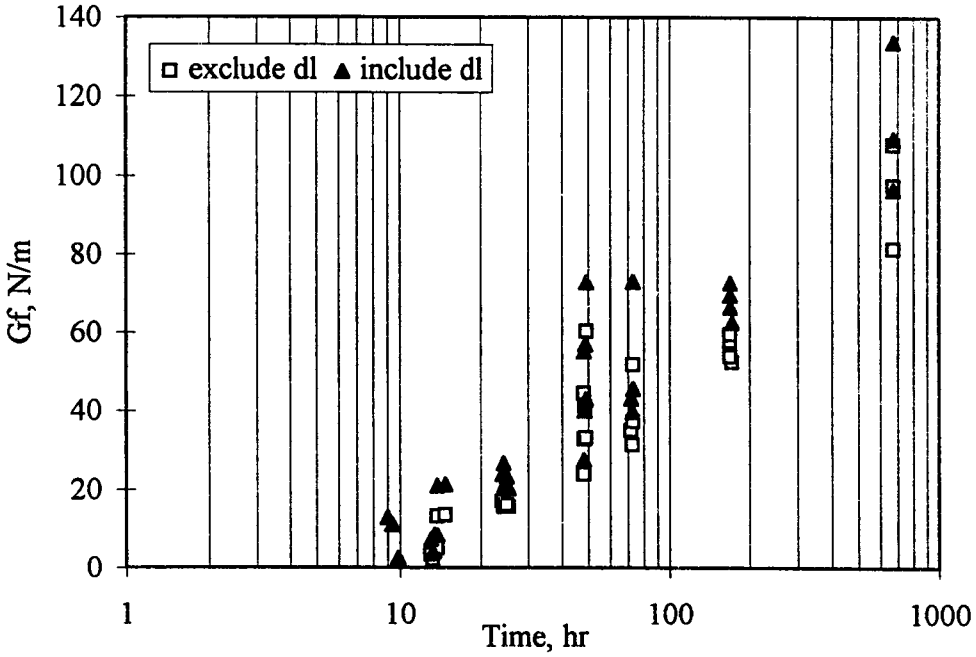

Figure 4.25 Effect of dead weight on fracture energy development

A limited number of later age beams (3, 7 and, 28 days) with smaller notch depth ratio (a/d=0.10) were also tested to compare the pre- and post-peak performance. From the plots of fracture energy versus notch depth at different ages (between 3 and 28 days in Figure 4.26), G_f tends to decrease with increasing notch depth ratio, from 0 to 0.1. The ratios greater than 0.10 appear to have a small influence on fracture energy. This differs from normal concrete where the notch depth ratio in this range strongly affects the fracture energy (71).

The test results from a limited number of cut notched specimens showed a trend of slightly increased fracture energy, compared to the typical cast notched specimens. This may indicate better simulation of real cracks in which the aggregate arrangement was not disturbed by notch casting. However, for early age testing, cutting notches is not practical.

The typical load vs midspan deflection of an unnotched beam is shown in Figure 4.27. The fracture energy is clearly higher than for the notched beam regardless of the notch depth ratio (Figure 4.22). This is due to the larger amounts of microcracks produced before the fracture process zone was fully developed. The ratios of G_f for unnotched beam to those for notched beam varied from 3.2 to 1.2, but the pattern influence from age was not shown in this study. The same trend was also observed for the relationship between G_f and compressive strength (Figure 4.28).

Characteristic length (l_{ch}), which indicates material brittleness, was another parameter of interest. Larger values suggest less brittle material behavior than for smaller values. This parameter, defined by fracture energy, modulus of elasticity and

tensile strength, ranged between 160-2400 mm depending on the specimen age. The value of l_{ch} may be used to estimate the size of FPZ, which is in the range of 0.3-0.5 l_{ch} for concrete like material.

LMC showed larger values of l_{ch}; about 3-8 times larger compared to conventional early age concrete at ages up to 1 day (83). However, this parameter dramatically decreased with time and reached the range for conventional concrete (200-400 mm.) at about 28 days (Figure 4.29). This trend was similar for both notched and unnotched beams. No significant difference in l_{ch} between two notched depth ratios was observed. However, the value of l_{ch} for unnotched beams was consistently higher than that for notched beams.

From the test observations, critical crack formations in notched beams were always confined to the area of notch, extending from the notch tip. However, in the unnotched specimens, the location of the critical crack could not be predicted (Figure 4.30 (a) and (b)). The assumption of coalesced cracks forming a single major crack may not always occur. In some unnotched tests, the adjacent cracks may curve, thus avoiding each other as is sometimes reported in normal concrete (41).

In addition, the failure surfaces indicated different failure mechanism for LMC, depending on age. Young LMC specimens up to 24 hours always failed at the aggregate-paste interface, while both bond failure and broken aggregates were found at later ages (Figure 4.31 (a), (b)). For the aged LMC (49 days), the excellent bond between matrices and aggregates was shown by a majority of broken aggregates (Figure 4.31 (c)).

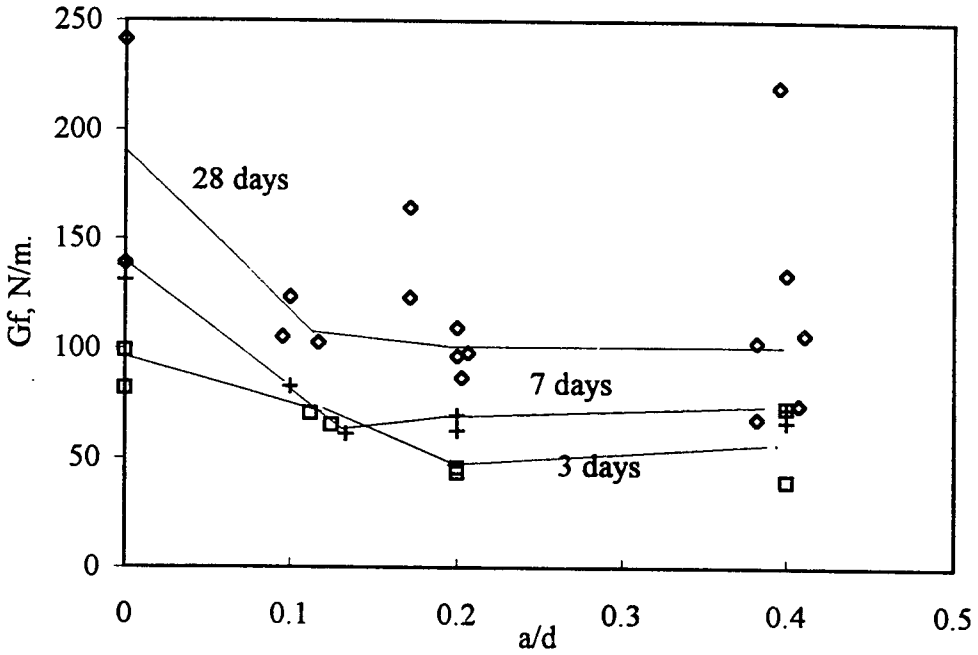

Figure 4.26 Effect of age and notch depth ratio on LMC fracture energy

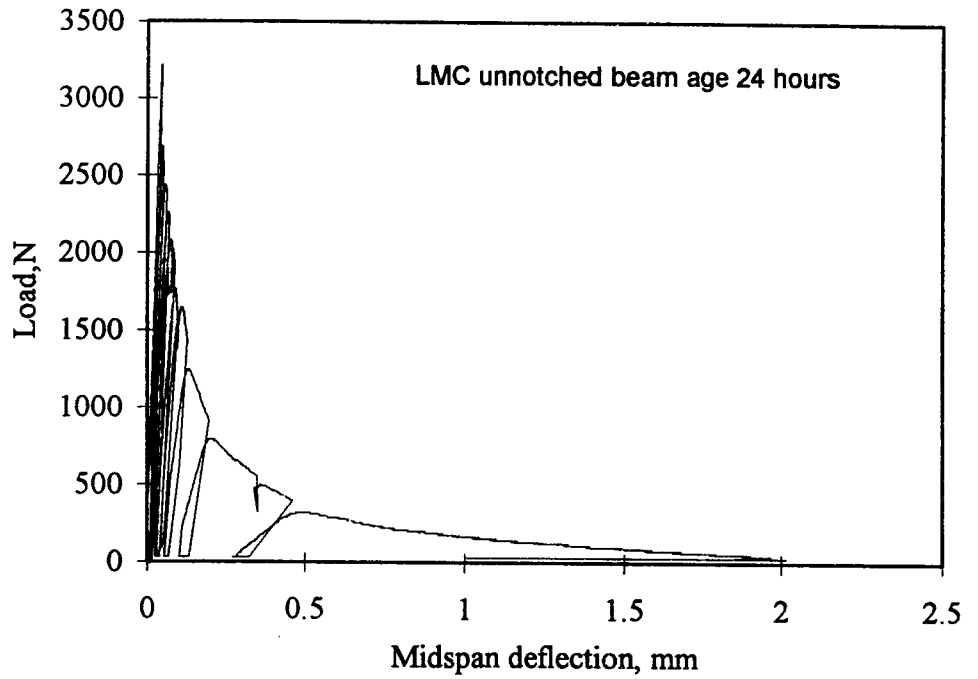

Figure 4.27 Typical load vs midspan deflection of unnotched beam

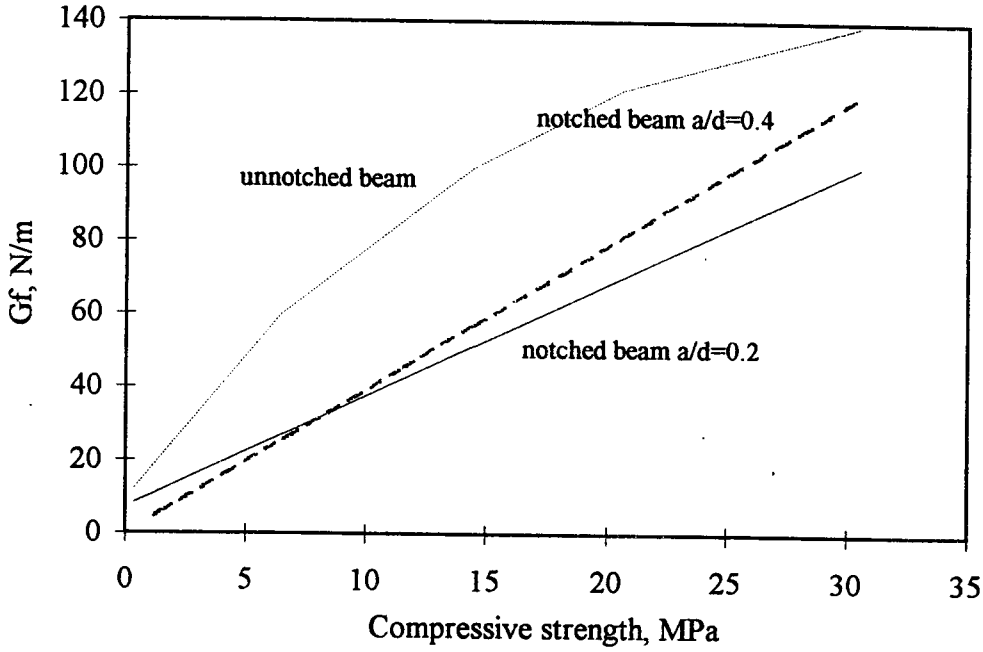

Figure 4.28 Relationship of LMC fracture energy with compressive strength

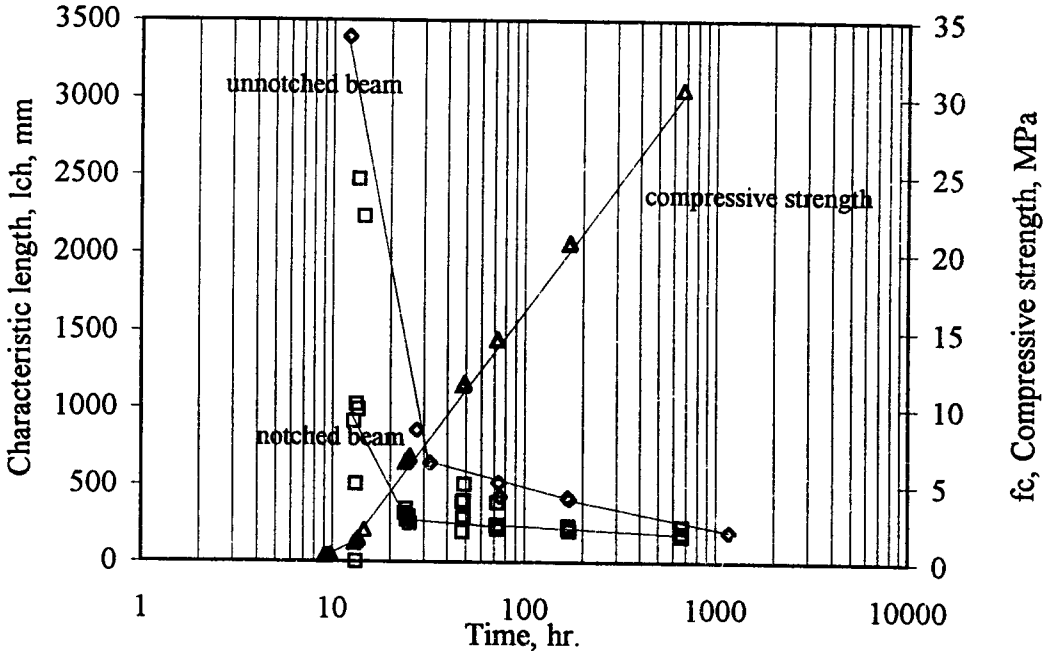

Figure 4.29 Development of LMC characteristic length with time

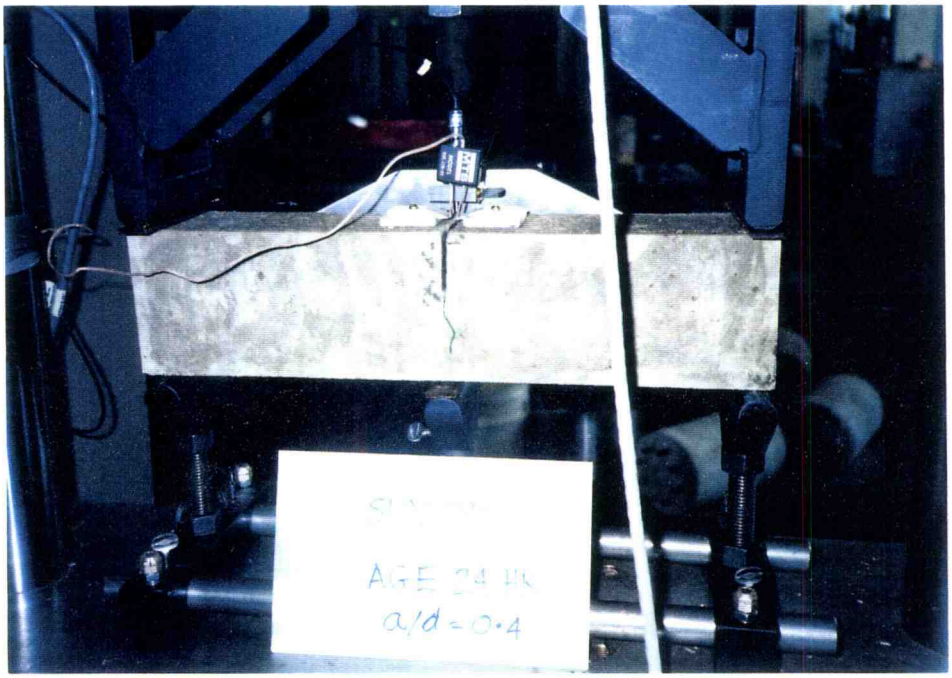

(a) notched beam

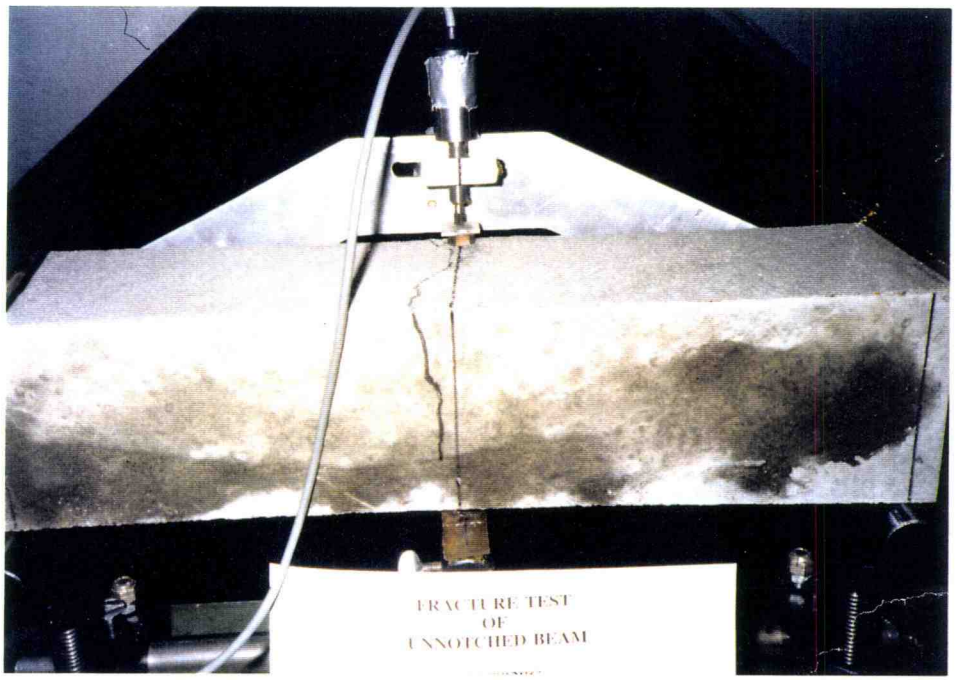

(b) unnotched beam

Figure 4.30 Difference crack pattern of test specimen

(a) bond failure, 24 hr

(b) bond failure and broken aggregates, 2 days

Figure 4.31 Difference failure mechanism at different ages

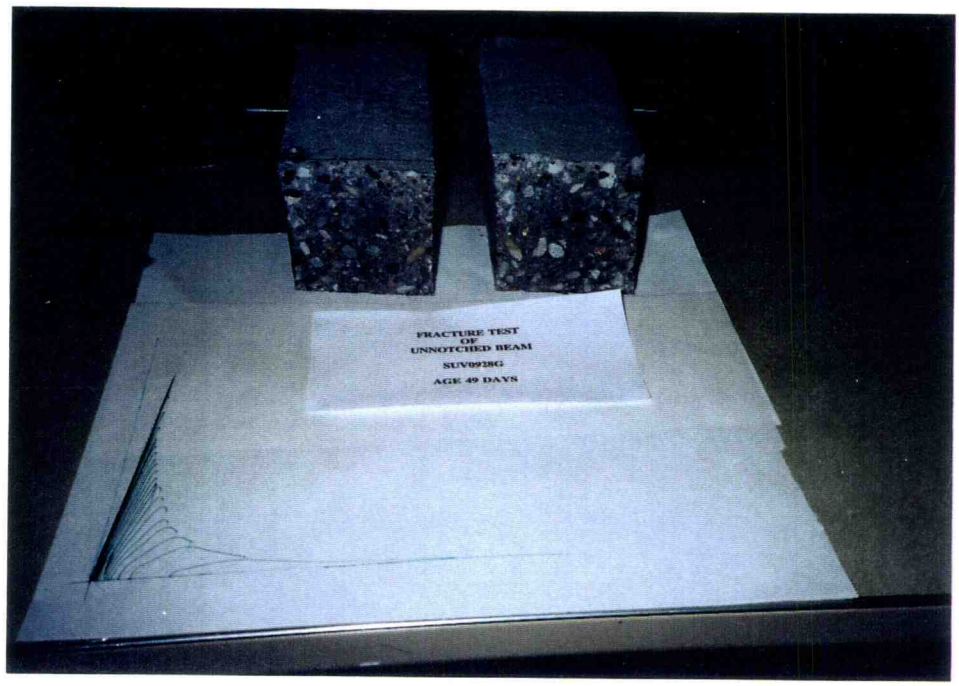

Figure 4.31 (continued) Difference failure mechanism at different ages
(c) broken aggregates, 49 days

4.2.3 Shrinkage Properties

The development of LMC shrinkage under two controlled conditions is shown in Figure 4.32. For both 12.7 and 29.4 °C 50%RH conditions, the specimens exhibited swelling during the first 5-6 hrs. followed by an increased shrinkage strain similar to normal concrete (58).

Shrinkage begins as soon as the water surface layer evaporates, about 4-6 hrs after placing. This time period closely approximates the setting time. Secondary shrinkage begins at about 12-16 hrs., just after the final setting time. The shrinkage rate at this stage is much smaller than for the first stage.

The controlled conditions are likely to have a pronounced effect on the performance and magnitude of shrinkage strain. During the first trial experiment under low temperature and humidity (12.7 °C, 50% RH), two specimens exhibited several severe cracks during the first 4 hours (Figure 4.33). Therefore, the modified 12.7 °C, 100% RH for two days and 50%RH for 5 days were utilized to avoid specimen cracking.

The severe cracking under low temperature/humidity conditions suggests that early age cracking is possible with delayed curing during cool night construction conditions. This may occur when LMC strength is not sufficiently developed to resist the tensile stress.

For both conditions, three cycles of temperature change (12.7 to 29.4 °C) were employed following 7 days of constant temperature/humidity. The shrinkage correlated to the temperature change as shown in Figures 4.34 and 4.35. Under the controlled condition of 50% RH, the capillary or pore water may evaporate. Therefore, this complicated phenomenon is possibly explained in terms of water loss (18).

In normal concrete, the difference between the temperature of the concrete and the surroundings affects the loss of water. The higher the temperature difference, the higher the water loss (Figure 4.36). The higher water loss also relates to the higher shrinkage (Figure 4.37). Under temperature fluctuation conditions, LMC behaviors may relate to water loss in a similar way.

When the air temperature rose from 12.7 °C to 29.4 °C in 1 hour (point A to B), the specimens took a longer time to adjust the interior temperature to the outside

air temperature (point C). A short time after point A, the air temperature was higher than the LMC temperature and the difference continued to increase. This resulted in continuing shrinkage at a decreasing rate until the minimum was reached when the temperature difference was a maximum (point B). After this point, even though the air temperature was held constant, the LMC temperatures were continuously increased at a lower rate. This reduced the temperature difference between the air and LMC. Therefore, shrinkage was increased.

At point C, when both temperatures were equal, shrinkage strain was close to the value before the temperature fluctuated. After passing point C, LMC shrinkage continued to increase due to an increasing temperature difference between the LMC and air. When the air temperature began to drop again for the last part of the first cycle (point D), LMC temperatures also began to drop at the lower rate. The simutaneously increasing differences until point E was reached (maximum temperature difference between LMC and the air), resulted in higher water loss and higher shrinkage. After point E, the air temperature became constant, the temperature differences began to reduce and reduced shrinkage was a consequence. When the air temperature began to increase at point F, the LMC began to behave in the same manner for the second and third cycles.

The test results of the 10 day study indicated that the majority of strain occurred during the first 48 hrs. Particularly, there was a dramatic increase in shrinkage strain during the first 5-15 hours.. The maximum values range between 0.0003 and 0.0005 for low and high temperature conditions. The earlier stiffening concrete (high

temperature condition) shows greater early shrinkage as in normal concrete (70). The lower strain was clearly shown with a lower temperature condition.

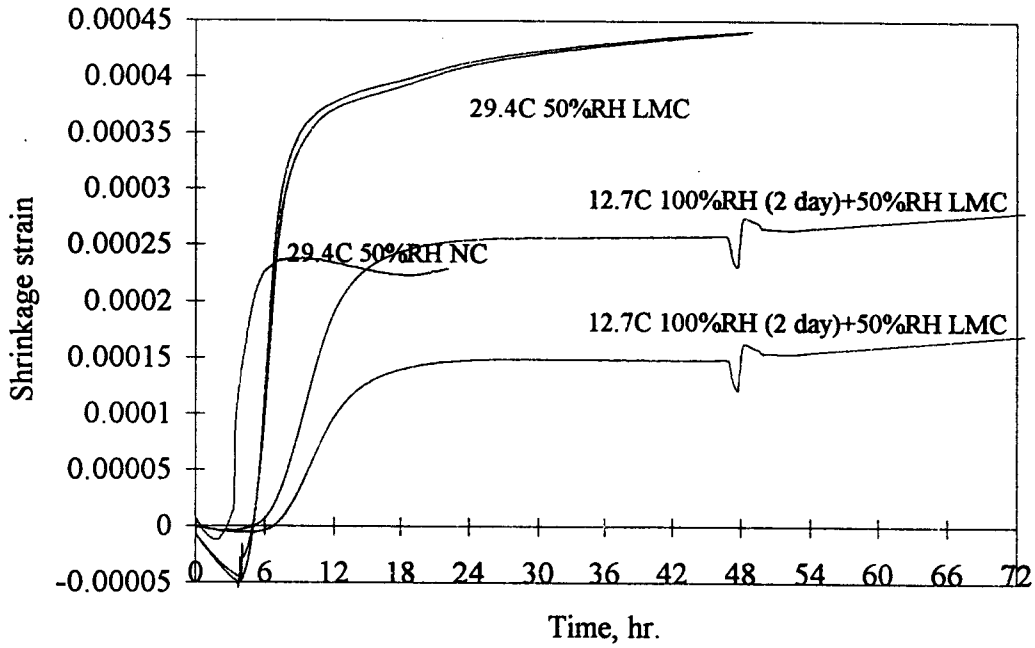

Figure 4.32 Development of LMC and normal concrete shrinkage with time for two temperatures

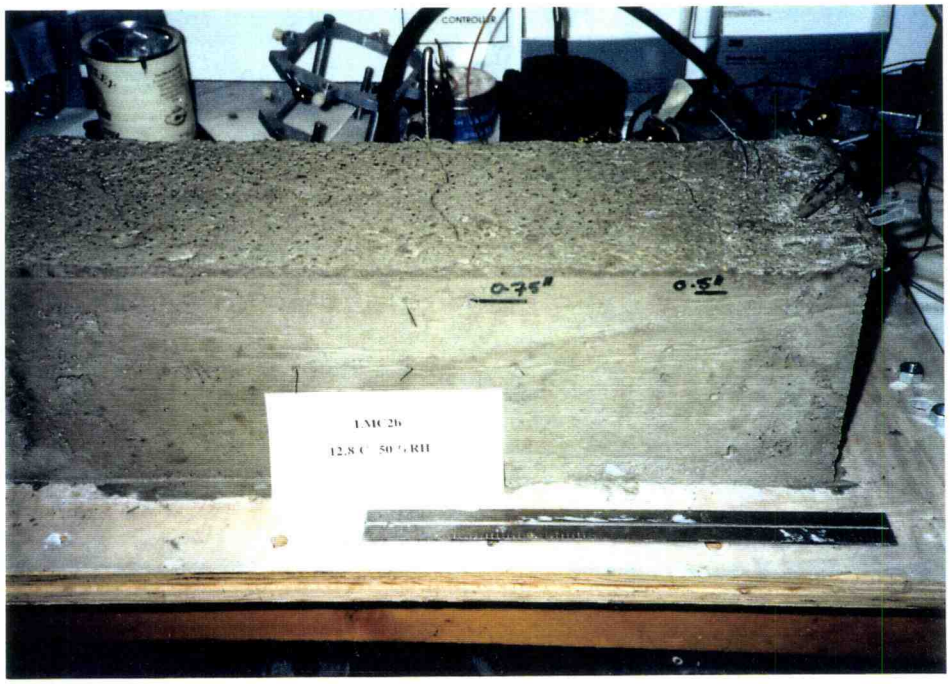

Figure 4.33 Severe cracking under low temperature/humidity condition

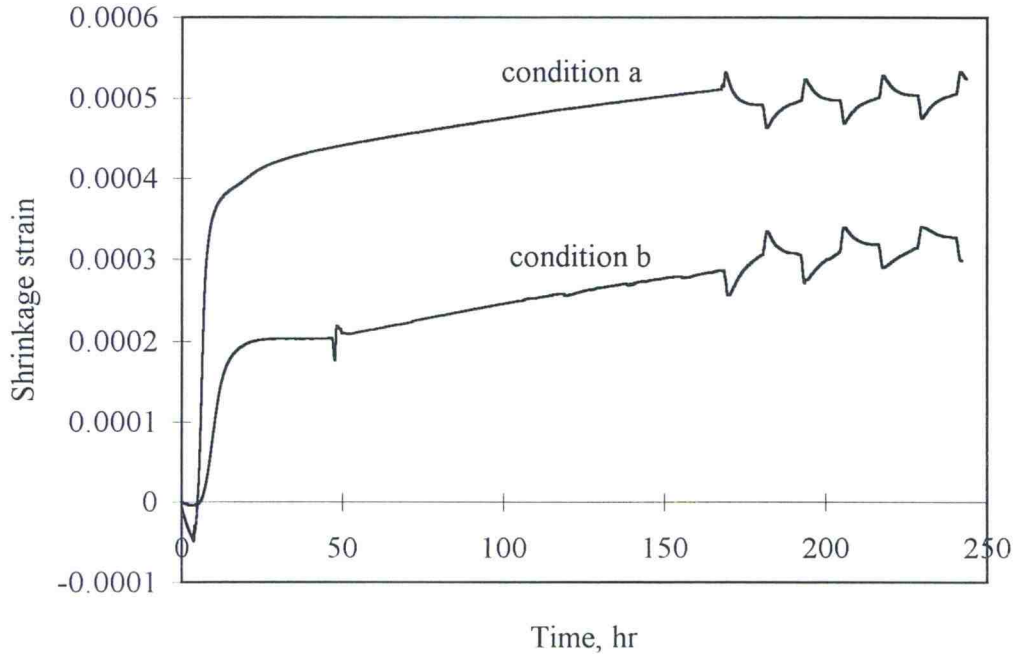

Figure 4.34 Shrinkage performance under control condition for 10days
Note: condition a: 29.4 °C 50%RH 7days + 3cycles of 12.7-29.4 °C
condition b: 12.7 °C 100%RH 2days + 12.7 °C 50%RH 5days + 3cycles of 12.7-29.4 °C

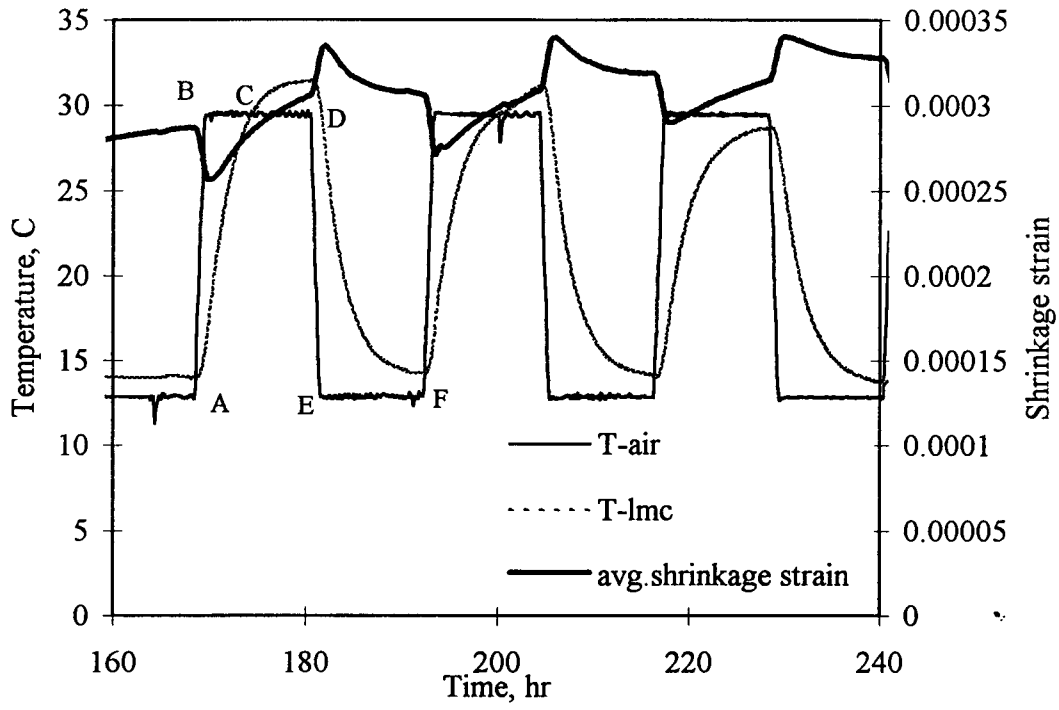

Figure 4.35 Shrinkage performance under cyclic temperature change between 160-250 hours

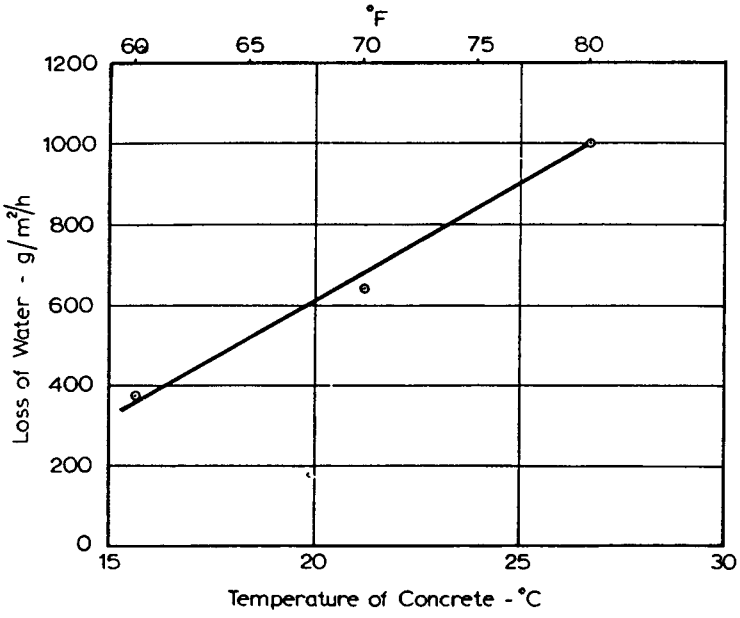

Figure 4.36 Influence of temperature of concrete(at an air temperature of 4.5 °C on the loss of water from concretein the early stages after placing (relative humidity of air 100 per cent, wind velocity 4.5 m/s)(18)

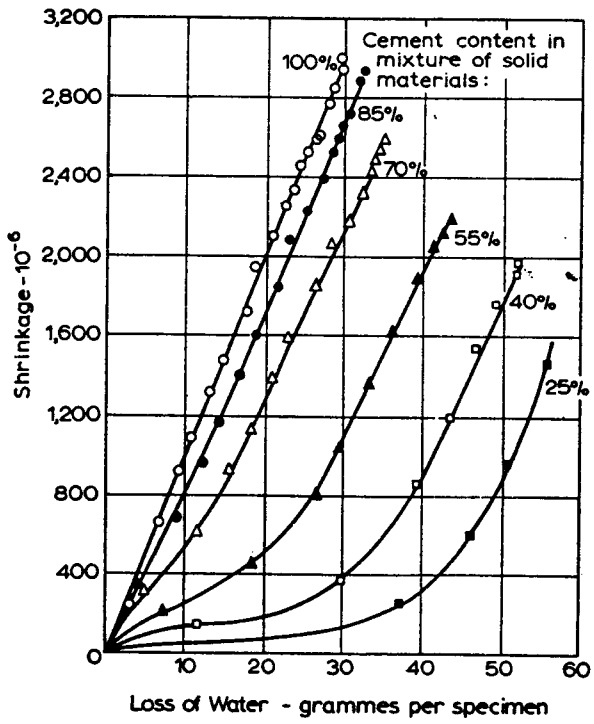

Figure 4.37 Relation between shrinkage and loss of water from specimens, cured for 7 days at 21 °C and then dried (18)

4.3 Summary

1. According to the test results, the critical time when early age cracking in LMC is of particular concern, may be based on two criteria. The first criterion involves the period when LMC has low tensile strength, and consequently high f_c/f_t. The second criterion involves the period when the material has low deformability. From these criteria, the particular duration of interest may range from slightly less than 12 hours to slightly greater than 24 hours.

2. The addition of latex modified the microstructure and affected several material properties including strength, deformability, and fracture behaviors. The contribution of latex film in bridging microcracks and improving bond strength in the interface zone probably affected stress transferring capacity, adding to the effects of strength and stiffness of aggregates, mortar matrix and the bond capacity between matrix and aggregate in normal concrete.

High Pe/Pmax ratios and ductility improvement were observed. Although the post-peak behavior showed a similar trend to that of normal concrete, the film formation possibly altered the continued microdamage mechanism. The increasing toughness and ductility improvement, either at peak load or at failure load indicated the higher consumed energy. Greater ratios of midspan deflection at failure to midspan deflection at peak load, compared to normal concrete (10-33 compared to 5-6) (53) was observed.

3. LMC's development of fracture energy (G_f) with time continued for 28 days. G_f values for unnotched beams were higher than for notched beam. However, the effect of notch depth ratio on fracture energy is less, compared to normal concrete, where G_f decreased as notch depth ratio increased (53,60). Generally lower values of the notch depth ratio provides a higher probability of available coarse aggregate in the cross section. At the macro level of concrete, coarse aggregates act as inclusion or crack arrestor. The increased length of a possible crack path results in a higher resistance for crack propagation and the higher G_f.

However in the LMC case, both pore structure in the matrix and interface zone are improved from film formation. This may provide a more pronounced effect than the

inclusion effect from aggregate as shown in normal concrete. In short, the effect of notch depth ratio is not clearly shown as in conventional concrete.

4. The effect of the latex film is particularly noticeable for large deformation. The modulus of elasticity in tension is about 1/2 the modulus of elasticity in compression which differs from normal concrete (10). When considering the single fracture parameter ($l_{ch}=EG_f/f_t^2$), the modulus of elasticity should be derived from either a tension, or flexure test. The higher of these values indicates the more ductile behavior. In this sense, the brittleness of LMC increased with time as well as with compressive strength, as for conventional concrete. However, the decreasing with time of l_{ch} (reached values in the same range as for conventional concrete at about 28 days) did not imply the same brittleness for the two materials. The deformability of LMC was clearly higher than normal concrete, due to the effect of film formation. Therefore, it should be noted that this parameter may not be accurately used for comparing the two different materials.

5. LMC shrinkage strain at 10 days ranges between 0.0003 and 0.0005, depending on the test conditions. Environmental conditions strongly affect both shrinkage magnitude and performance. Severe cracking may be qualitatively explained in terms of resulting tensile stress from capillary loss during the time that LMC is insufficiently developed stress.

5. ANALYSIS AND MODELLING

The LMC properties from the first stage of the study were used in the application phase which is detailed in this chapter. First verification of the modelling /technique and the selected strain softening diagram were completed. The model was then used to predict material and environmental impacts on early-age LMC.

5.1 Approaches Verification

Two approaches, a superposition technique and a finite difference method solution were first verified with the available information from the literature to determine the feasibility and accuracy of the predicted model.

Superposition. The load-deflection curve for a three-point bending notched beam from Wittman's study (79), based on an assumed linear strain softening diagram was simulated using the superposition approach. The beam size and material properties are shown in the Figure 5.1 (a).

Crack propagation was traced by releasing one supported node along the crack path at a time. During this step, a finite element program, ANSYS version 5.0A (91), was employed to calculate stresses and displacements. The results were automatically combined to solve for the equivalent external force, the closing forces, the final stresses and the displacements for each step.

Due to the symmetrical beam and loading conditions, only half of the beam was analyzed. The mesh was composed of quadrilateral elements which were gradually finer

near the crack path. The elements were collapsed to form triangular elements at the transition zone (Figure 5.1 (b)).

To determine the load required to propagate the existing crack, a vertical unit load was first externally applied at the middle span (Figure 5.1 (b) node 25). The existing crack was assumed to have zero width. Based on the criteria of stress is equal to tensile strength at the notch tip (node 13), the load multiplication factor (α_0), as defined in section 3.3.2, was calculated. The result was verified by an optimization approach, setting the tensile strength at the prenotched tip as an objective criteria and varying the applied load, P (shown in Figure 5.1), to minimize the difference between the calculated stress and tensile strength. The comparison yielded a satisfactory result, with a difference of about 1.1 %.

To calculate the next required load step to propagate the crack for a distance of one-element length, the first support at the crack tip (node 13) was released. A unit external load and a unit internal closing force were applied at midspan and at the first released node (node 25 and node 13), respectively. Stress at the next node (node 14) and displacement at the first released node (node 13) were calculated and input as defined variables (section 3.3.2).

$\sigma_0(0)$: stress at node 14 due to the unit external load

$\sigma_1(0)$: stress at node 14 due to the unit internal load

$w_0(1)$: displacement at node 13 due to the unit external load

$w_1(1)$: displacement at node 13 due to the unit internal load

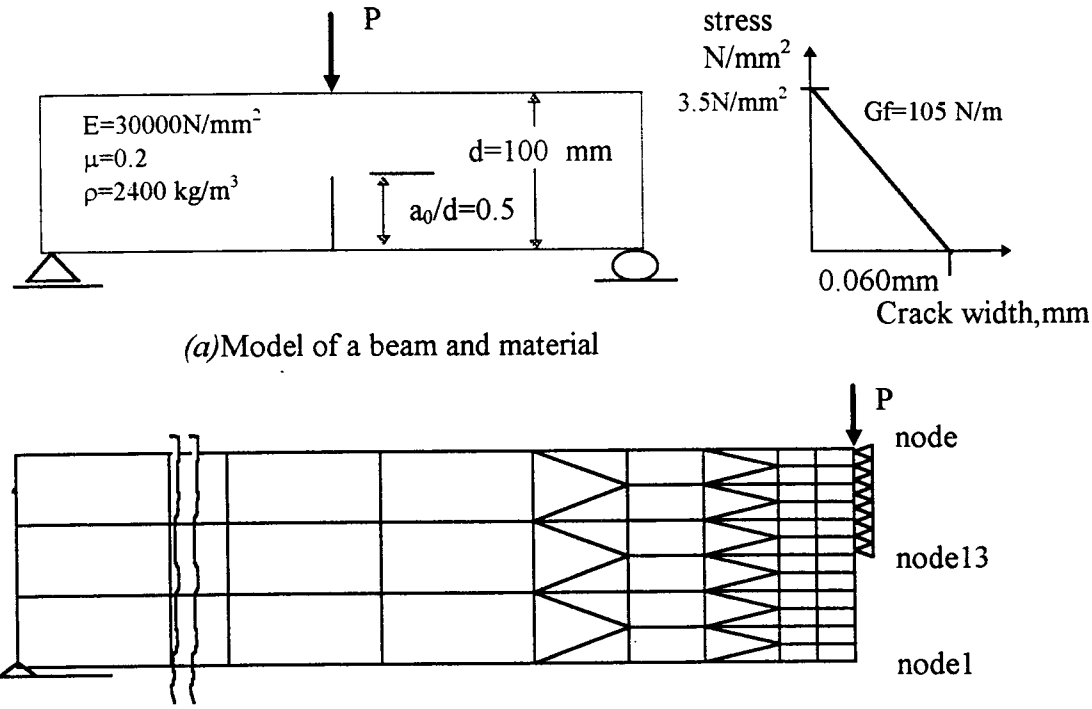

*(a)*Model of a beam and material

(b) Model of left-half of the beam

Figure 5.1 Superposition model verification

The calculated load multiplication factors α_0 and α_1 were equivalent to the external load P and the equivalent cohesive force at nodes 25 and 13, respectively. The program was rerun to obtain stresses and displacements from these applied loads. Load and displacements in the x- and y- directions were plotted as the second point in the load-crack opening displacement and load-deflection relationships.

The same procedure was used to calculate the values for other steps, by releasing supports along the assumed crack path one node at a time (the calculation steps are shown by a flow chart in Figure 3.9). A sufficient length ahead of the crack tip, the ligament length, is necessary for an accurate structural analysis. This limits the

analysis of advanced crack nodes through the cross section depth to obtain the final collapse. A critical ligament length of about 10% of the beam depth (as suggested by Carpinteri (92)) was used as the length before the collapse of the structure. Therefore, the supports along the crack path were released to node 23. Only the fictitious compressive closing forces affect the stress transfer ability in the fracture process zone, therefore the assumed closing stress must be non-negative. Zero or negative load multiplication factors were ignored in the next calculation step (77)

The effect of large deflections was also checked. The total load was broken into smaller steps and the program was rerun, using a large deflection analysis option. The results indicated an insignificant difference, compared to the result from a small deflection theory analysis (0.1%).

The result for load vs midspan deflection agreed well with the curve shown in Wittmann 's study (79). A slightly higher peak load using superposition (2.3%) was observed as shown in Figure 5.2.

Finite Difference The available information on temperature, wind speed and solar radiation from Thepchatri's study (44) was analyzed based on a one dimensional heat flow equation using the finite difference technique. Figure 5.3 (a) shows a satisfactory agreement between the predicted temperatures at the top and bottom surfaces and the field measurements. The calculated temperature distribution through the 432 mm thick slab is plotted in Figure 5.3 (b).

Thepchatri mentioned the dependency of the error on the chosen interval size (44). The proper dimension for the spatial increment is necessary to provide a positive

result for the coefficient and avoid oscillation. To minimize the solution error, the space interval, Δx, was chosen under the limit of $\Delta x \geq \sqrt{2K\Delta t}$; where K=diffusivity, Δt=time increment.

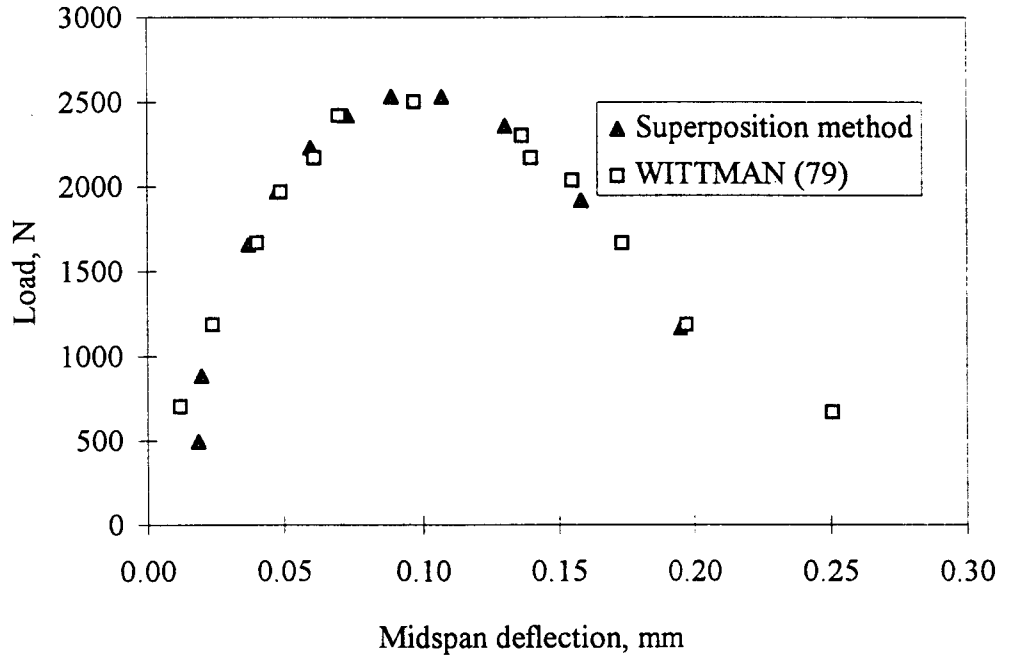

Figure 5.2 The comparison of load-deflection curves between Wittman's data (79) and predictions using the superposition method (Maximum load: 2473 N vs 2530 N)

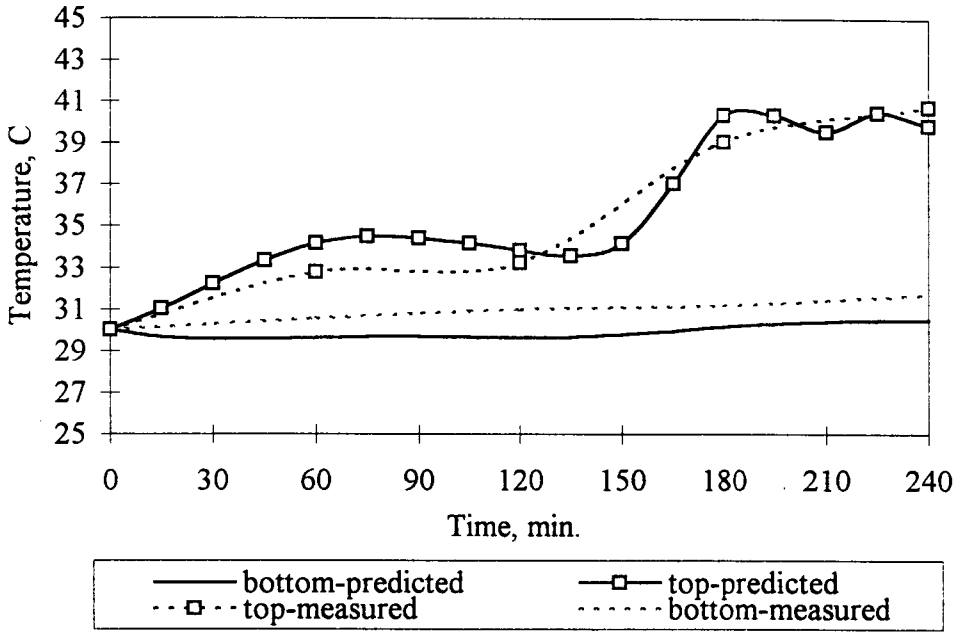

(a) The comparison between the predicted temperature and the field measurement

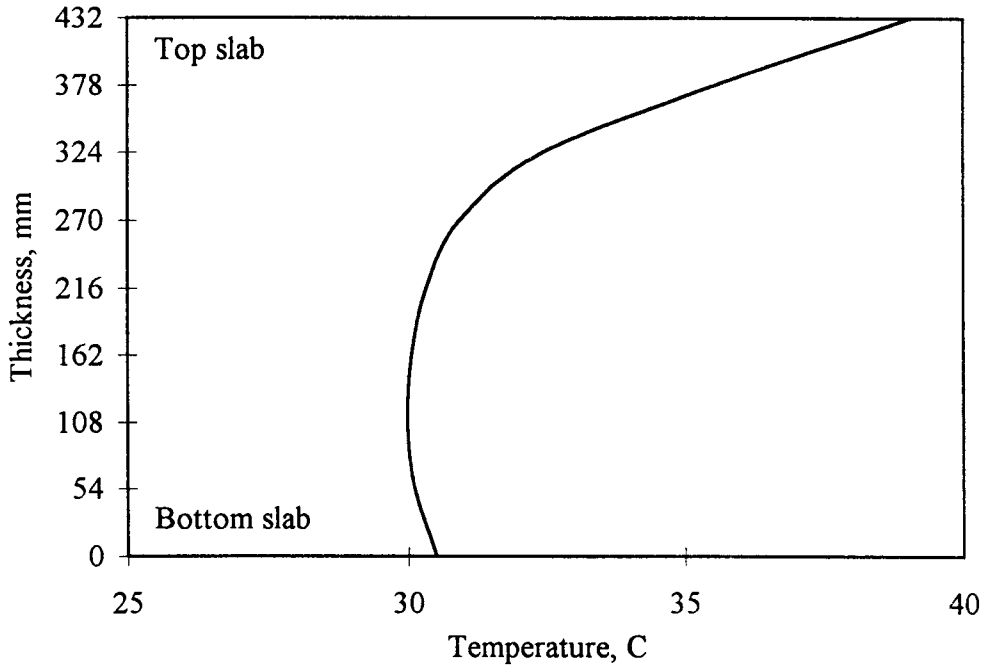

(b) Temperature distribution through a 432 mm deck

Figure 5.3 Prediction of temperature effect for bridge deck

5.2 The Chosen Strain Softening Diagram

The shape of the strain softening diagram is another factor that affects the accuracy of the model. Both linear and bilinear relationships were first verified before application. The load-displacement curve from the numerical analyses were compared to experimental results at different ages to determine the most suitable parameter set.

In this study, although the linear strain softening diagram provides a satisfactory prediction in the prepeak region; a higher peak load and inaccurate post peak performance were observed for all ages (Figure 5.4). The bilinear relationship which depends on f_t, w_1,s_1 and w_2 (as defined in Figure 3.10 (b)) provided better results. The parameters w_1 and s_1 were determined on a trial and error basis.

For conventional concrete, only one set of w_1,s_1 and w_2 values among several trial sets provided a predicted load-deflection curve which agreed well with the test results (92). The reported strain softening diagrams for normal concrete were used as a guideline for LMC. Numerical analyses indicated the sensitivity of the load-deflection curve to changes in these parameters (Figure 5.5 (a)). Since age affects LMC property development, the analyses of several sets of parameters for LMC were conducted at various ages. The comparisons between the predicted load-deflection curve and those from the test results at 9.4 hr, 1 day and 28 days are shown in Figure 5.5 (b), (c) and (d).

From the selected value $s_1=f_t/6$, w_1 and w_2 were determined from the equivalent G_f and the critical crack width, w_c. The values of w_1 appear to depend on LMC age

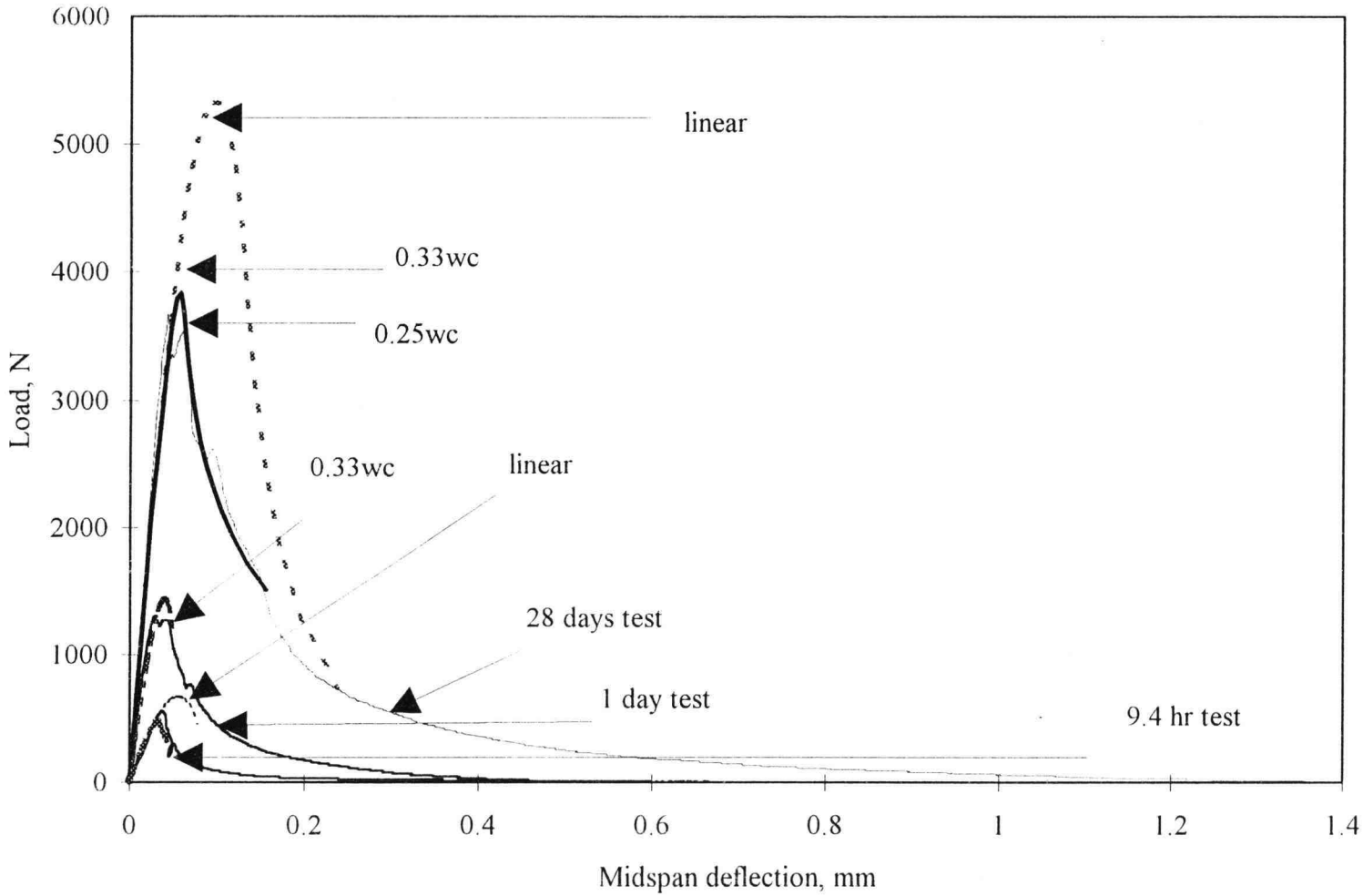

Figure 5.4 Comparison of load vs midspan deflection for linear and bilinear relationships at various ages

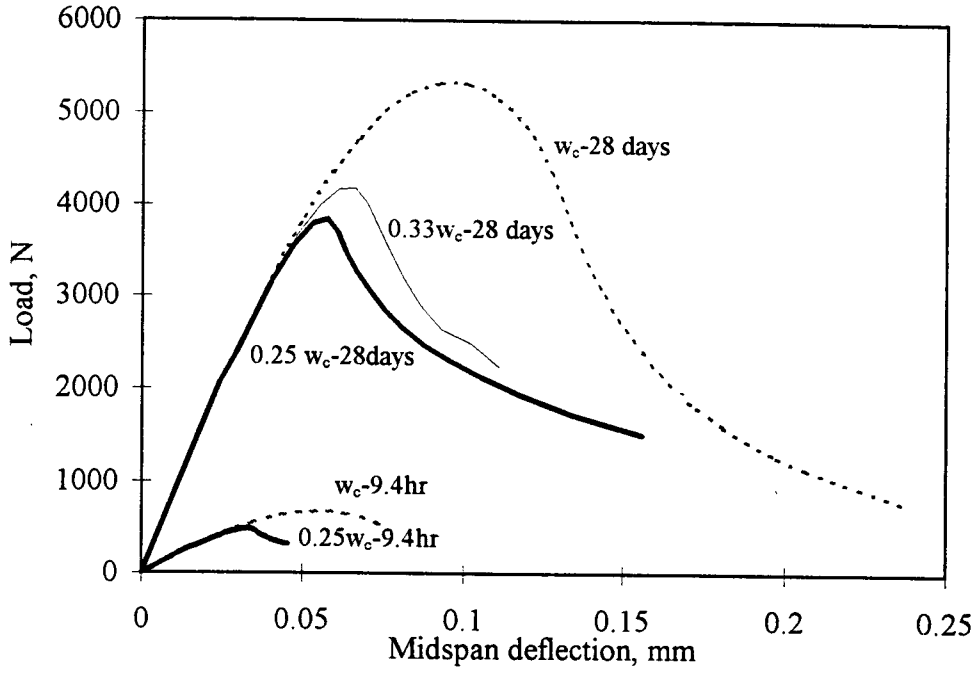

(a) Sensitivity of strain softening diagram on load-midspan deflection curve

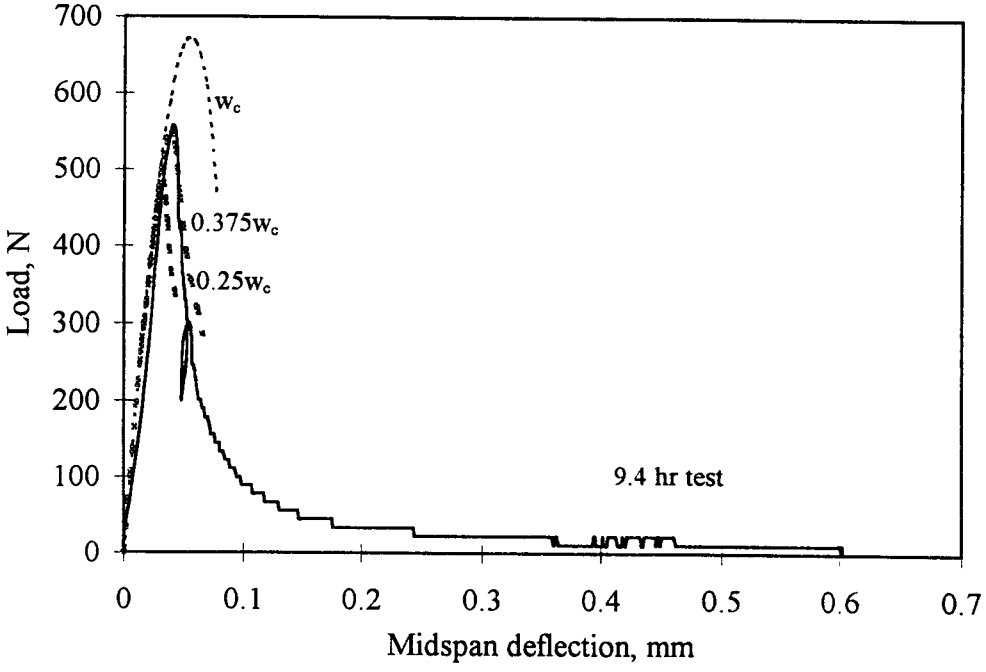

(b) Comparison of load vs midspan deflection at age 9.4 hr.

Figure5.5 Effect of strain softening diagram on load-deflection curve

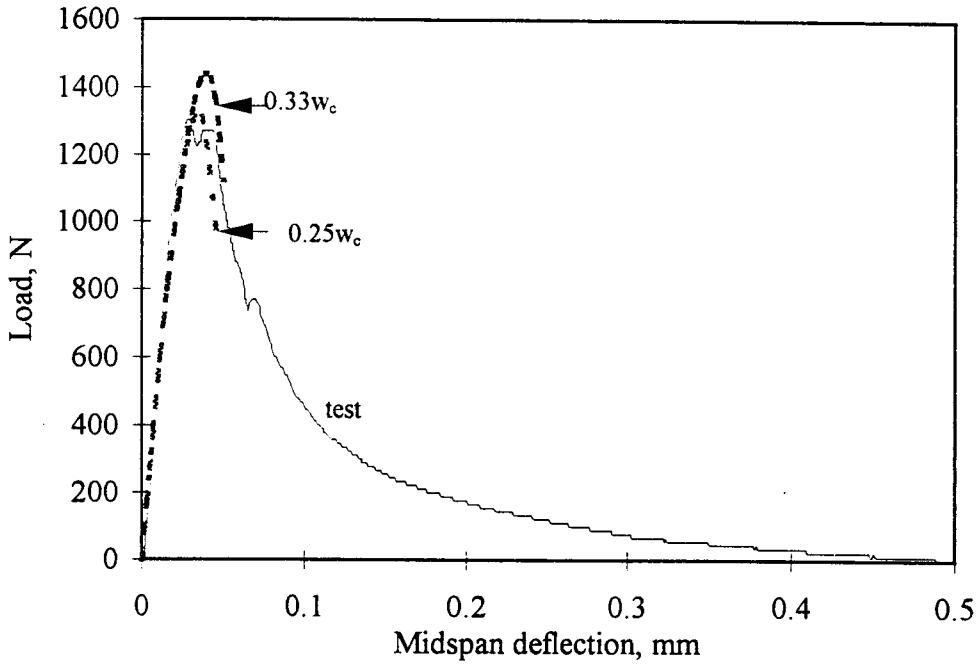

(c) Comparison of load vs midspan deflection at age 1 day.

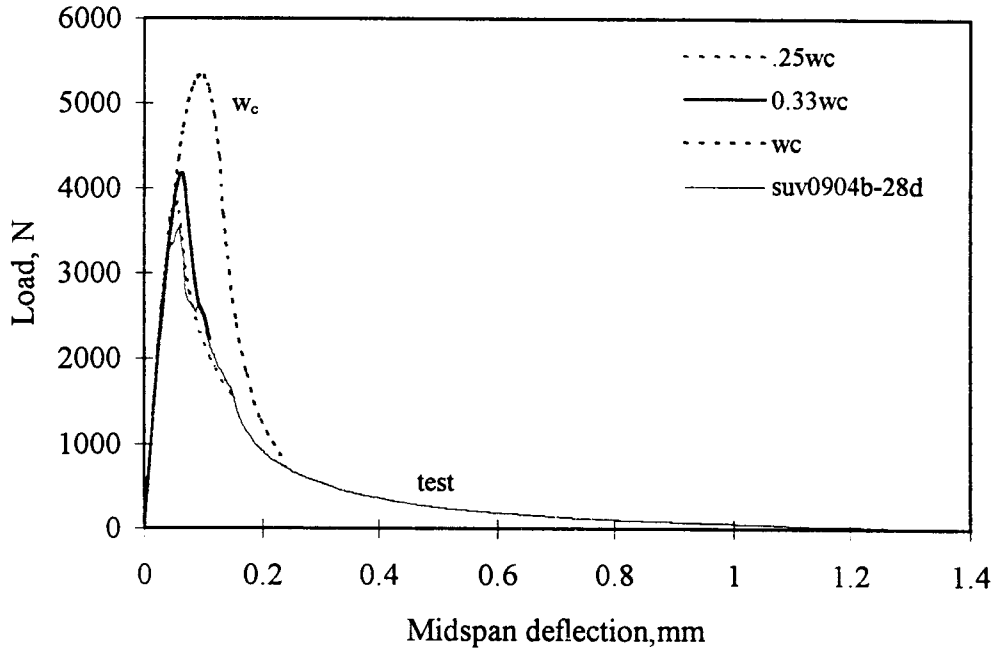

(d) Comparison of load vs midspan deflection at age 28d

Figure5.5 (continued) Effect of strain softening diagram on load-deflection curve

with w_1 slightly decreasing from $0.375w_c$ (9.4 hr.) to $0.333w_c$ (13.5 to 24 hr.) and finally reaching $0.250w_c$ (28 days).

It is important to note that while the values of f_t and E from regression provide good results for later age (1 to 28 days), the predicted results are lower for very early age. Therefore, a modified f_t is necessary. The modified f_t ($0.65\ f_f$ for 9.4 hr. and $0.3f_f$ for 13.7 hr.) is based on the flexural stress which provided a better fit of load-deflections compared to the test results. The flexure test possibly captured a more realistic deformability behavior than the splitting test, especially when rapid changes were occurring during early ages, before 24 hr.

In addition, different test procedures and test environments may affect property development. For the early age splitting test, specimens were kept in steel molds and wet cure conditions applied until testing time. This differs from the flexure and fracture test that were both similar in test setup. Even though the specimens were covered with wet burlap during curing, the specimens were unavoidably exposed during the test set up and the lengthy test, about 15-30min. This may result in different curing conditions, and therefore affect the property development at early ages. These factors may be significant and result in erroneous predictions if the splitting tensile strength was used.

In this study, the bilinear strain softening relationships with the knee point: $w_1=0.375w_c$ and $s_1= f_t/6$ was chosen to analyze the early age performance, less than 12 hr., $w_1=0.333w_c$ and $s_1= f_t/6$ for ages between 12 to 48 hr. and $w_1=0.250w_c$ and $s_1= f_t/6$ for ages longer than 48 hr. Load-deflection curves show reasonable agreement

between the predicted and the actual test results as shown by the dotted and solid lines in Figure 5.6.

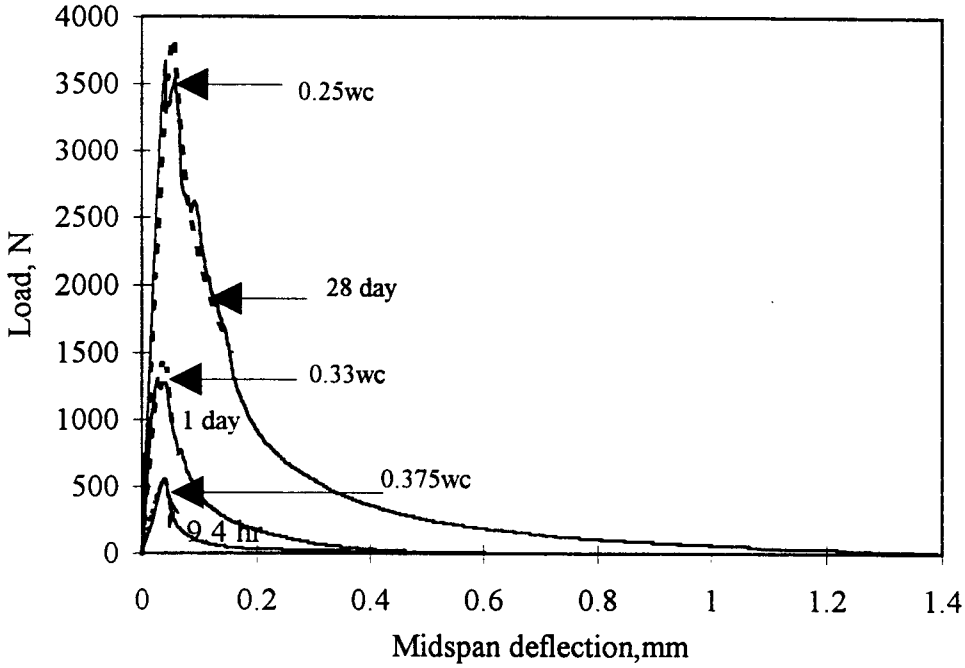

Figure 5.6 Comparison of load-deflection curves between tests and the predicted results from the chosen strain softening diagram

5.3 Environmental Effect

5.3.1 Case Study

Oregon weather reports were chosen to evaluate environmental effects. Normally temperature and solar radiation vary with location and local conditions. The variation for four different places is shown in Figures 5.7, 5.8 (a) and (b). In Figure 5.7, the effects of cloud cover and high humidity that often occur west of the Cascades might be

a key to the difference in the Portland and Eugene patterns, compared those for Burns and Bend, which are located in the semi-desert area east of the Cascades.

For this study a 10 year weather data set from the Willamette Valley was used. Severe conditions, under a combination of high temperature, high solar radiation and low wind speed, produces the largest temperature gradient in the bridge. Therefore, the maximum, minimum and average temperatures were first analyzed to select the most severe month. Subsequently, the daily weather data for that particular month of the chosen year (which was assumed to represent an average environmental condition) were studied, in conjunction with the three factors. As a result of this step, a set of data that showed the potential for the largest temperature gradient was used to analyze the temperature and stress distribution in the bridge deck. The results of the analysis demonstrate the most severe environmental effects on bridge decks.

The environmental conditions for the chosen location show that the ranges in temperature and wind velocity in the most severe month of the study period fall in the same range. Temperature differences range from 20.5 to 24.4° C and wind velocity ranges from 0.54 to 4.20 m/s. These ranges indicate a strong possibility that wide temperature gradients develop in bridge deck overlays which are normally placed during the summer or fall (38). This supports the hypothesis of the study that the thermal effect is a significant factor for cracking performance of early age LMC bridge deck overlay (Eugene weather station: 1985 -1993).

The changes in temperature with time for three consecutive days with the same repeated diurnal climatological cycle were analyzed. This selected period governed the time

of maximum and minimum temperature, and the critical time when the curing concrete had not yet fully developed its strength. The calculated temperature gradient was used as temperature input data for the stress analysis. The maximum temperature gradient was also compared to the temperature differential that would initiate cracks or exacerbate the existing cracks.

5.3.2 Unit Temperature Differential

Imposed temperature differentials were used to relate crack propagation in bridge decks to changes in the environment. A unit negative temperature differential, incorporated with the equivalent nodal forces, was applied to trace the crack growth from temperature influence. A 305 mm thick deck having a uniform initial temperature equal to the surrounding temperature, was subjected to a unit negative temperature at the top and bottom slab. Due to the low thermal conductivity of concrete like material, the nonlinear temperature distribution was normally reported. A parabolic temperature distribution across the deck was predicted in this study (Figure 5.9). The detailed derivation can be found elsewhere (82)

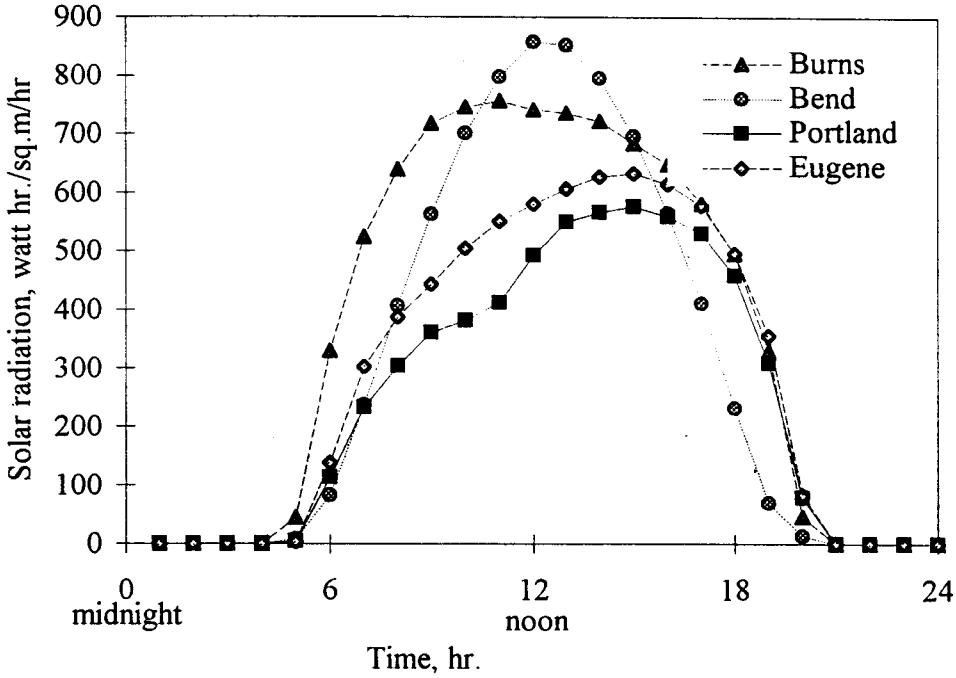

Figure 5.7 Variation of solar radiation from case study in Oregon

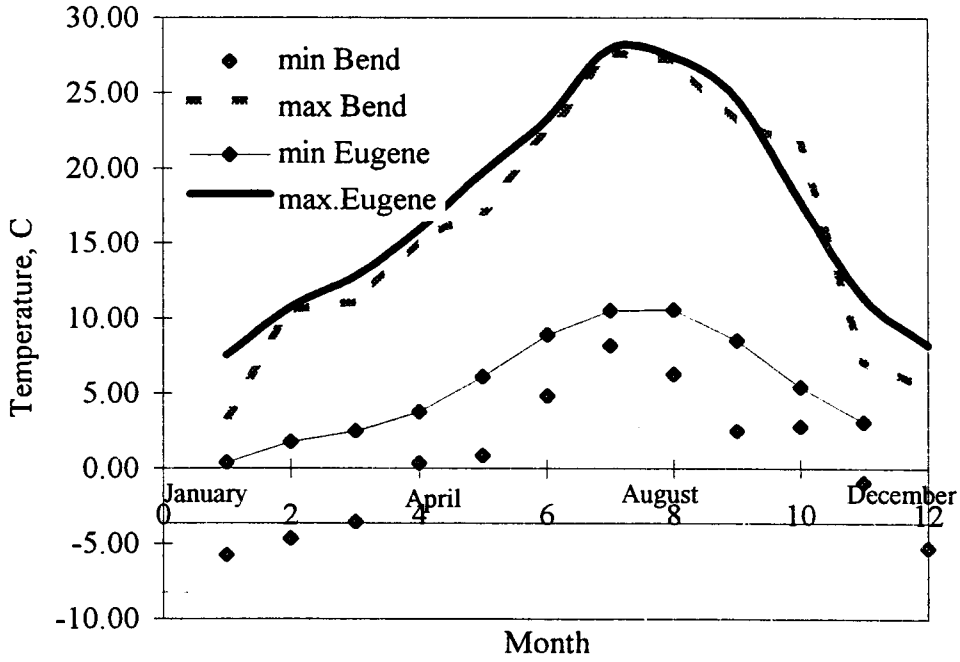

(a) Maximum and minimum temperature in each month from the study case

Figure 5.8 Temperature variations from the study case

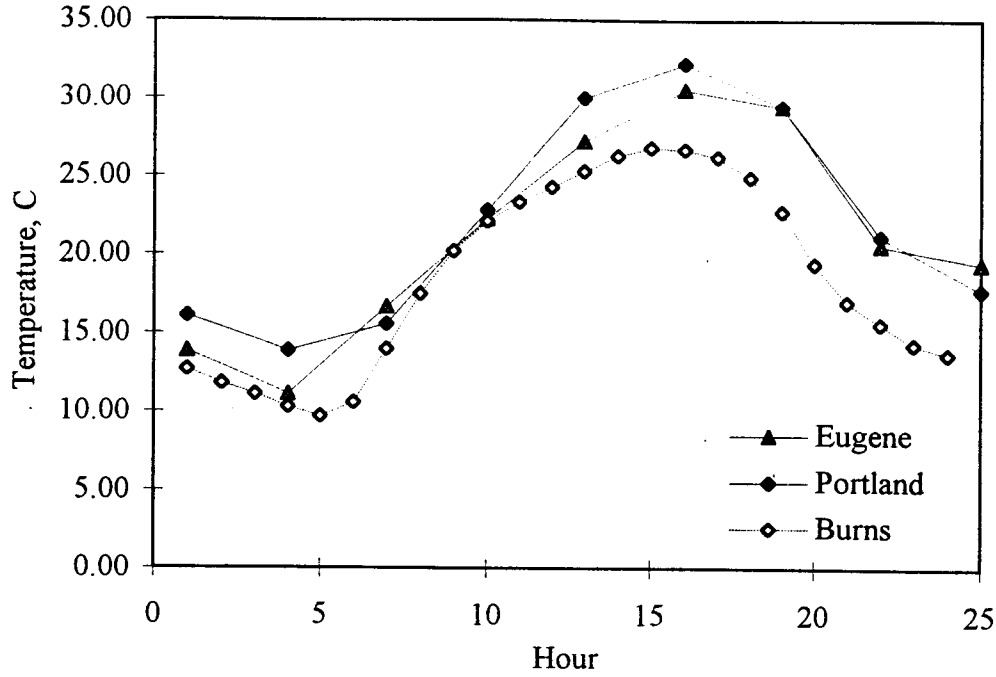

(b) Hourly temperature variation from the study case

Figure 5.8 (Continued)Temperature variations from the study case

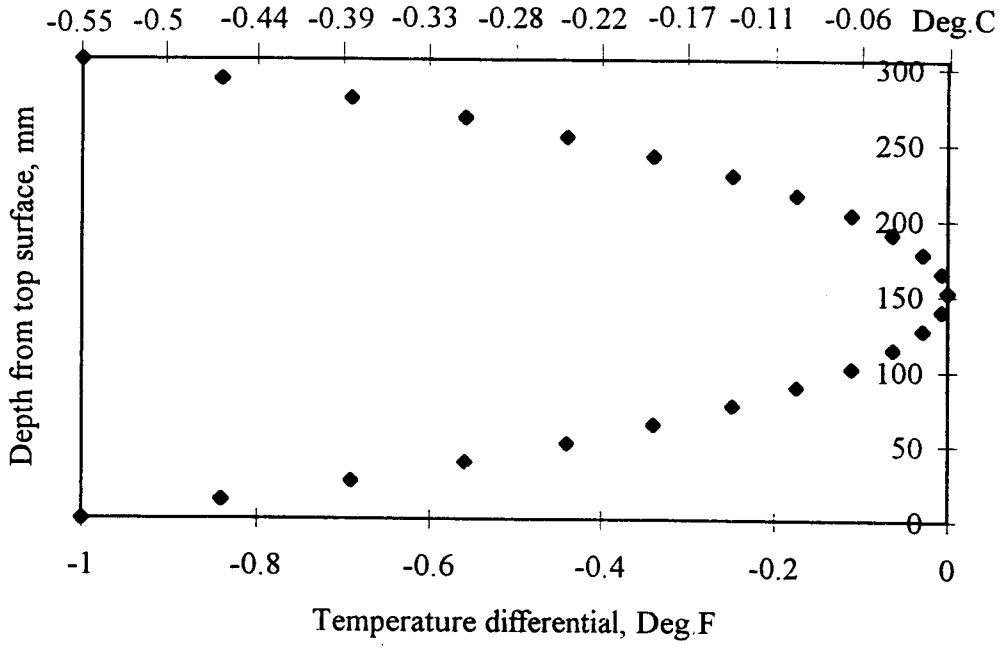

Figure 5.9 Unit temperature distribution

5.3.3 Temperature Distribution

To demonstrate the environmental effect, the actual temperature variation for a 72 hour period from the weather report (18-21 July 1985) was analyzed. The selection was based on the highest measured solar radiation, although the maximum range of air temperature occurred in August. This variation incorporates the predicted variation of solar radiation with time (Figure 5.10, 5.11 (a) and (b)), and the average wind speed were used to analyze temperature distribution. These data were assumed as a typical severe Willamette Valley environment during summer.

The temperature distribution analysis was conducted for each time increment of 1 hour for the first 24 hr., and then, at the critical times of minimum and maximum air temperature. The effects of solar radiation and air temperature on the top and bottom surfaces and the variation of temperature distribution through the deck depth with time are shown in Figure 5.10, and Figure 5.12 (a). From Figure 5.12 (a), thermal equilibrium was assumed on the first day at 8:00 am and the analyses were conducted for the following three consecutive days. The results indicated that the maximum negative temperature differential probably occurred during the second and third nights. These conditions would result in tensile stresses of 1.49-1.73 MPa on the top surface of the slab, which exceedes the tensile strength at 24 hr age (0.97 MPa).

Moreover, since the temperature distribution in bridge decks is affected by wind, a comparable study was also conducted on the effect of wind speed. The analyses of the light wind case (1.3 m/s) showed a small effect on the negative temperature distribution. The distributions from the two conditions, light and normal wind, in this

study (3.6-4.5 m/s) at two critical times, are compared using the dotted and solid lines in Figure 5.12 (b).

The results of crack propagation analyses at various ages is detailed in the next section, combined with the environmental information, may provide a guideline for the magnitude of the temperature differential which may initiate cracking or exacerbate existing cracking.

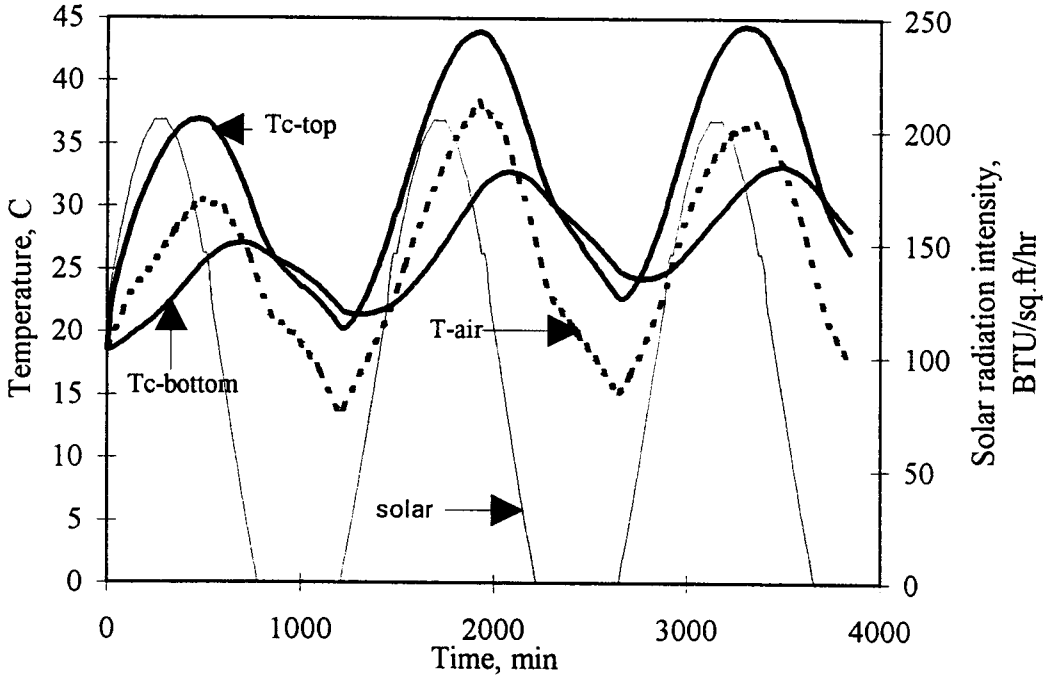

Figure 5.10 Variation of solar radiation, air and deck temperature with time

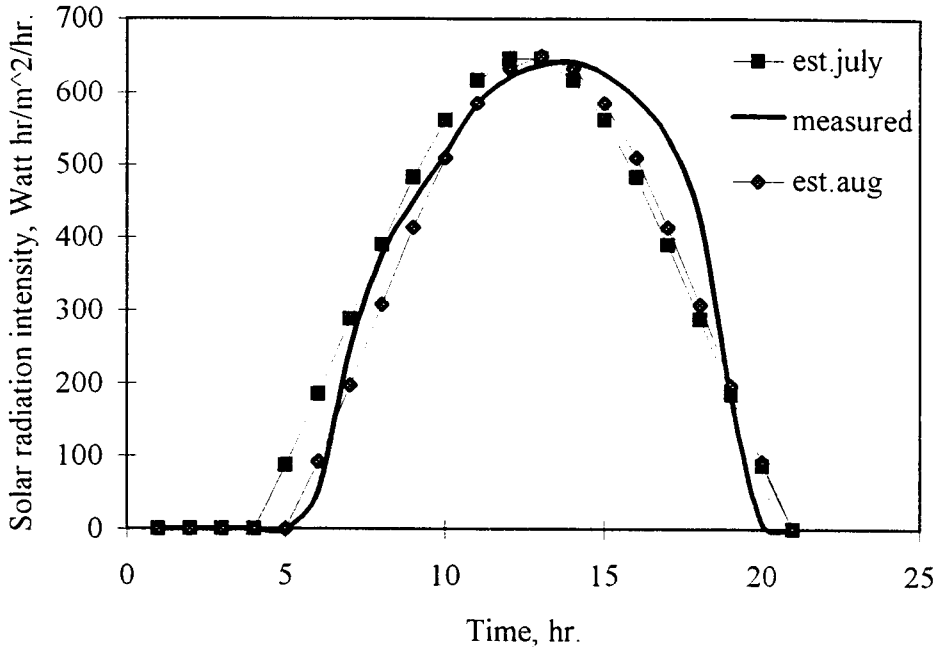

(a) Solar radiation variation

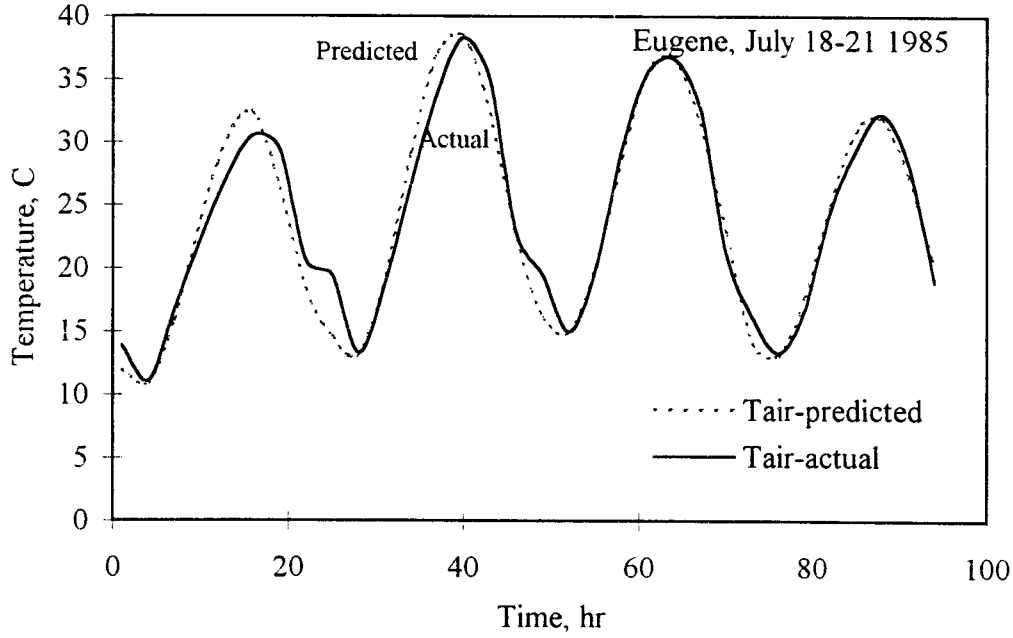

(b) Temperature variations

Figure 5.11 Comparison of environmental variations between predicted and field measurements

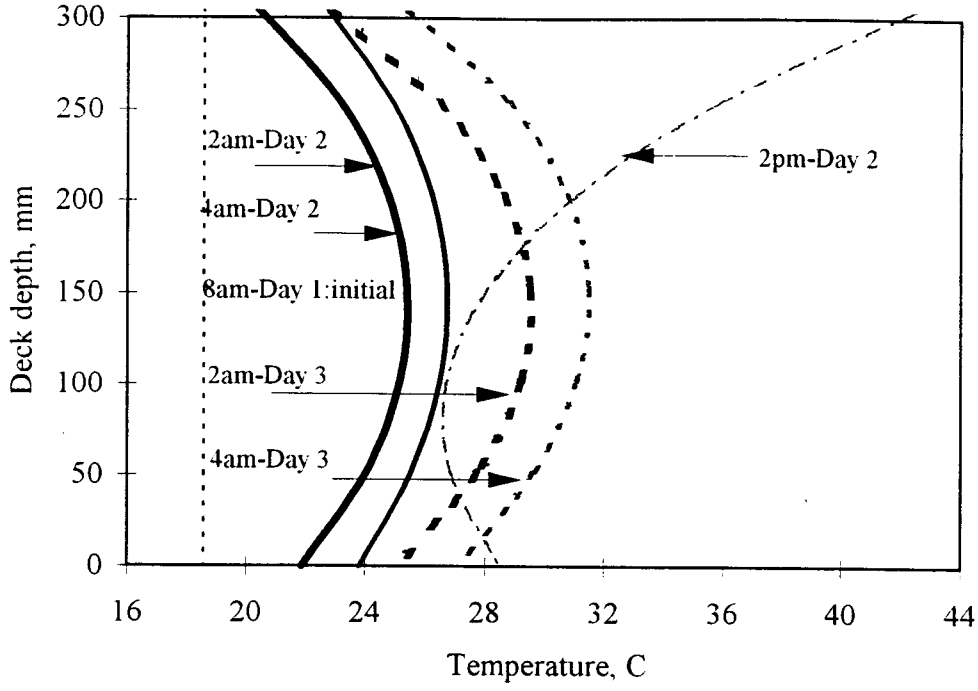

(a) Temperature distribution at different times

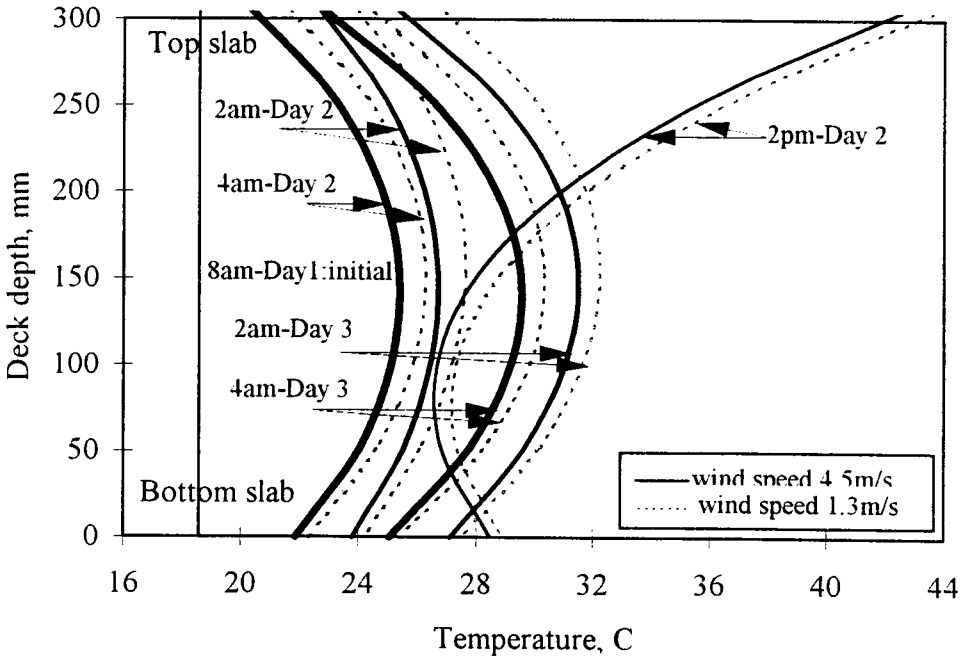

(b) Comparison of temperature distribution between normal and light wind conditions

Figure 5.12 Temperature distribution through deck depth

5.3.4 Temperature Differential Effect

A three span slab-girder bridge with a 225-250 mm thickness substrate and 51-76 mm thickness LMC overlay, spanning 7620 mm and 2540 mm in width, was used to demonstrate environmental effects at ages of 12, 24 , 36 and 48 hours. The model and material properties are shown in Figure 5.13(a).

By applying a negative unit temperature to the model, temperature differential and closing force can be calculated. This permits crack propagation to be monitored. The early age cracking behaviors of the overlay with a typical thickness of 51 mm were studied at four different ages (12, 24, 36 and 48 hours). Figure 5.14 shows the comparison of the overlay behavior due to the temperature differential effect for two conditions, cracked and uncracked surface.

The analyses indicated that age had a strong effect on temperature differential required for crack initiation/propagation, especially during the first 24 hours. At age 12 hours, the magnitude of the temperature differential that initiates or propagates cracks in the overlays for both conditions, is much lower than at later ages,. The effects of temperature differential on both uncracked and cracked overlays are approximately similar at ages 24 and 36 hours. The temperatures that initiate and propagate cracks for an uncracked overlay range between 14 to 30 °C at ages 24 and 48 hours. The range is lower, between 7 to15 °C, at 12 hours age. These findings indicated that the overlay was more sensitive to temperature differential at very early age; e.g. 12 hours, compared to later age, 24 to 48 hours. Only one-half of the temperature differential

that initiates and propagates cracks at 24-48 hours is needed to initiate cracks at 12 hours age.

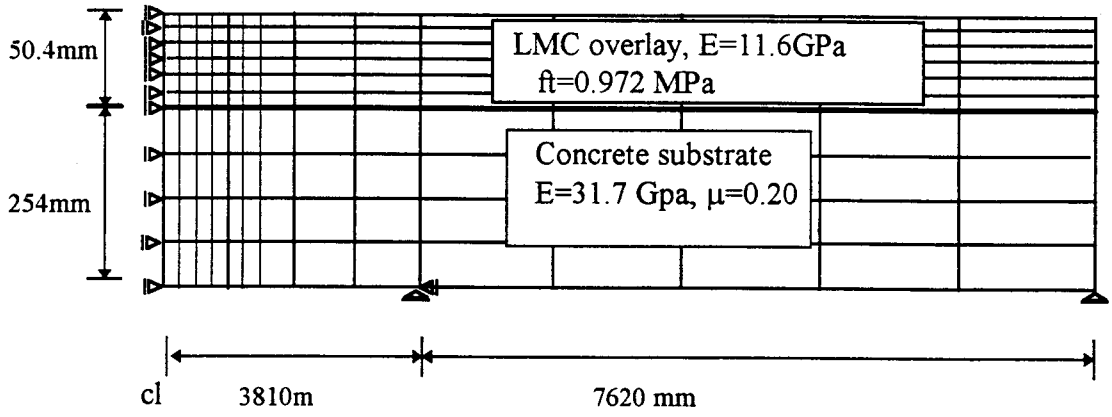

(a) F.E.mesh for three span bridge deck without crack

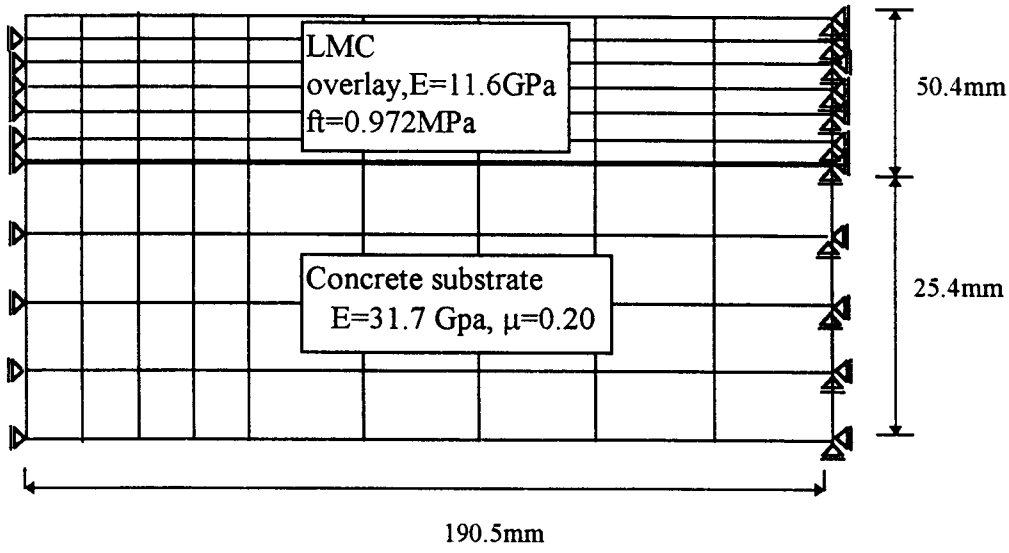

(b) model of deck with existing crack

Figure 5.13 F.E.model for deck with different conditions

The occurrence of cracks was demonstrated and compared with the case where prior cracking may be present in Figure 5.14 (cracked vs uncracked). The existence of even a shallow crack (6.35mm deep), has a significant effect in lowering the temperature differential needed for propagating the crack by approximately 30 %. However, stable crack growth was observed in both the cracked and uncracked cases. A higher temperature differential was necessary for advancing crack propagation.

The effect of structural restraint on cracking performance is also of concern. The result of the analyses at 24 hours age for a simple span condition (as modeled in Figure 5.15), compared to the continuous span condition are shown in Figure 5.16. Each point in the figure represents an element-length crack propagation. The lower initial temperature by about 30% and the flatter slopes show that the determinate structure has a higher crack sensitivity for both the temperatures to initiate cracks and to propagate cracks. Furthermore, the analyses show that once the random cracks occurred in the overlay (as modeled in Figure 5.13 (b)), and assumed 380 mm apart (26), the temperature differential required for crack propagation through the overlay thickness is significantly decreased, independent of the restraint condition (curve a in Figure 5.16). This indicated that overlays with existed random cracks have a higher risk for crack propagation through the overlay thickness.

The effect of overlay thickness on crack resistance is also of interest. Two thicknesses, 51 and 76 mm were analyzed at three different ages; 12, 24 and 36 hours. The analyses were conducted on the simple span condition for cases where the overlay surface was cracked and uncracked (Figure 5.17). The thickness of the overlay did not

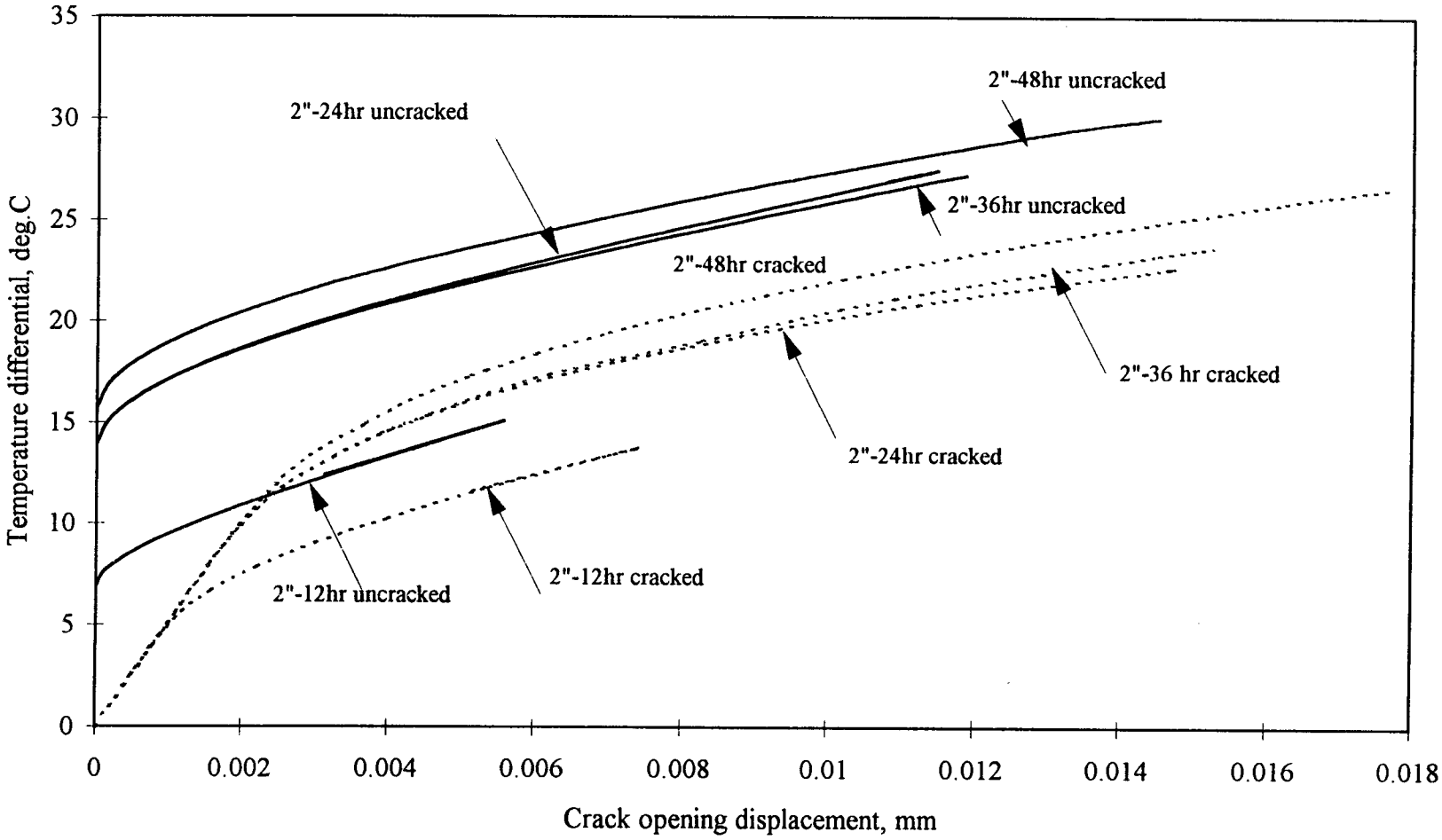

Figure 5.14 Crack performance of the 51mm overlay, for a continuous span at different ages and conditions

show any notable effect a temperature differential sensitivity. It is of interest to note that for the simple span case, the normal overlay thickness (51 mm) shows a slightly higher resistance to temperature differential, compared to the thicker overlay (76 mm). In almost all studied ages for both conditions, the thicker overlay appears to have higher sensitivity to temperature. Lower lower temperatures and flatter slopes were observed as shown in Figure 5.17. The flatter slope of the overlay with pre-existing cracks indicated a greater sensitivity to temperature, compared to the crackless overlay. In a continuous case, the cracking resistance and sensitivity are similar for both cases (Figures 5.14 and 5.18).

The stress distribution along the crack path at each temperature differential level can be traced. The plot of these stresses versus beam depth are shown in Figure 5.19.

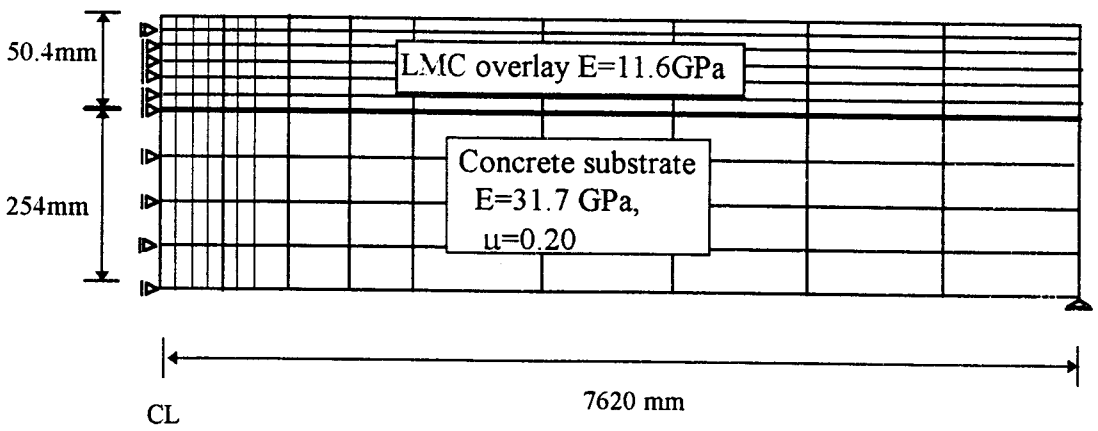

Figure 5.15 Model for simple support condition

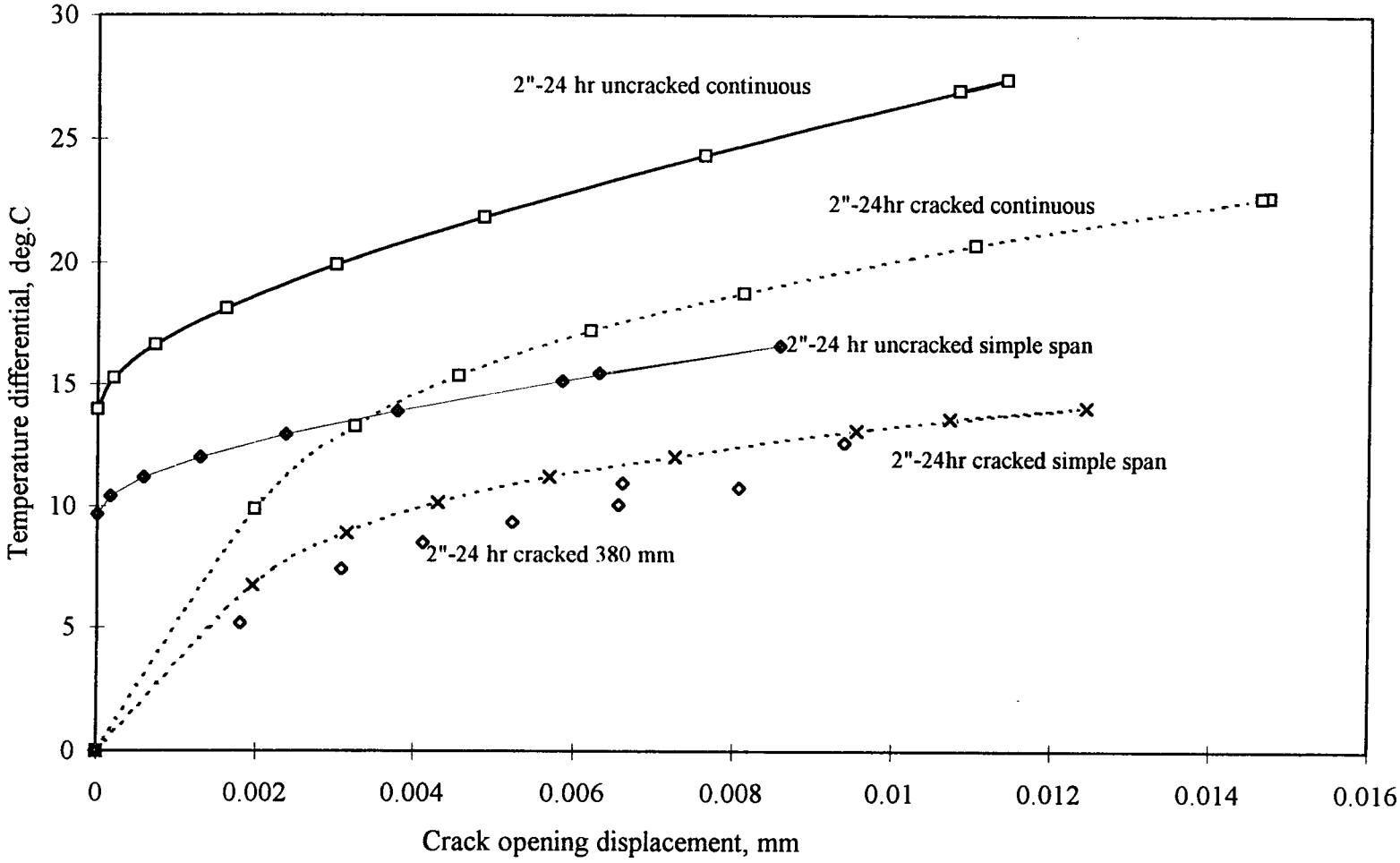

Figure 5.16 Comparison of 51 mm overlay performances with different restraint conditions

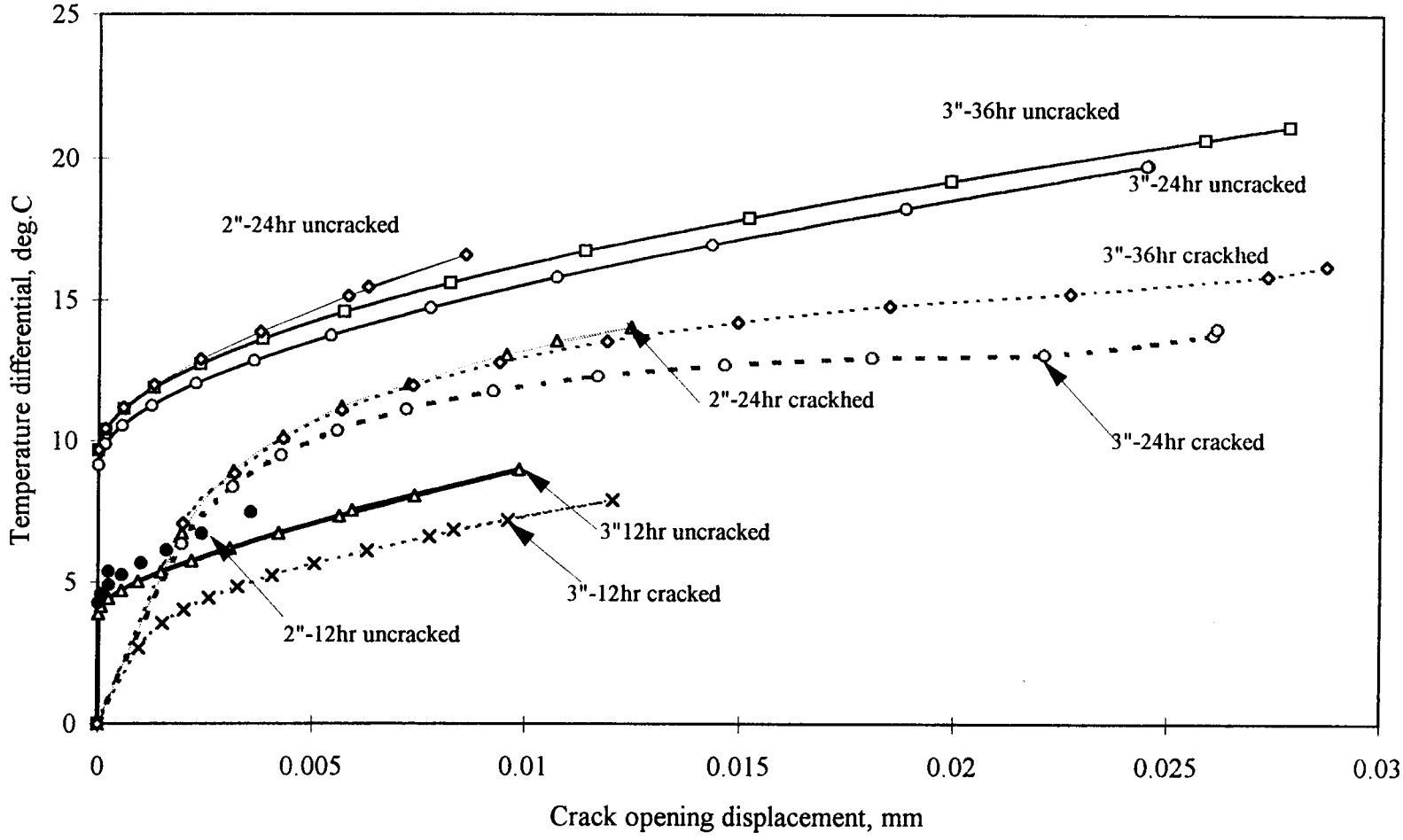

Figure 5.17 Performance comparison between two thickness overlays with different ages and conditions

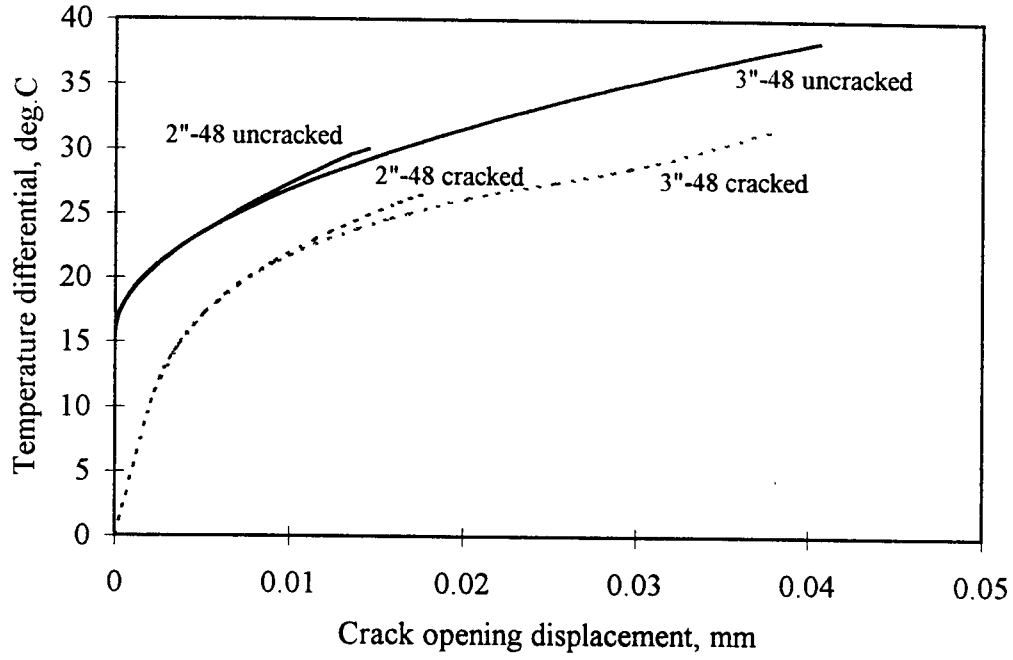

Figure 5.18 Comparison of crack resistance for similar age overlays with different thicknesses

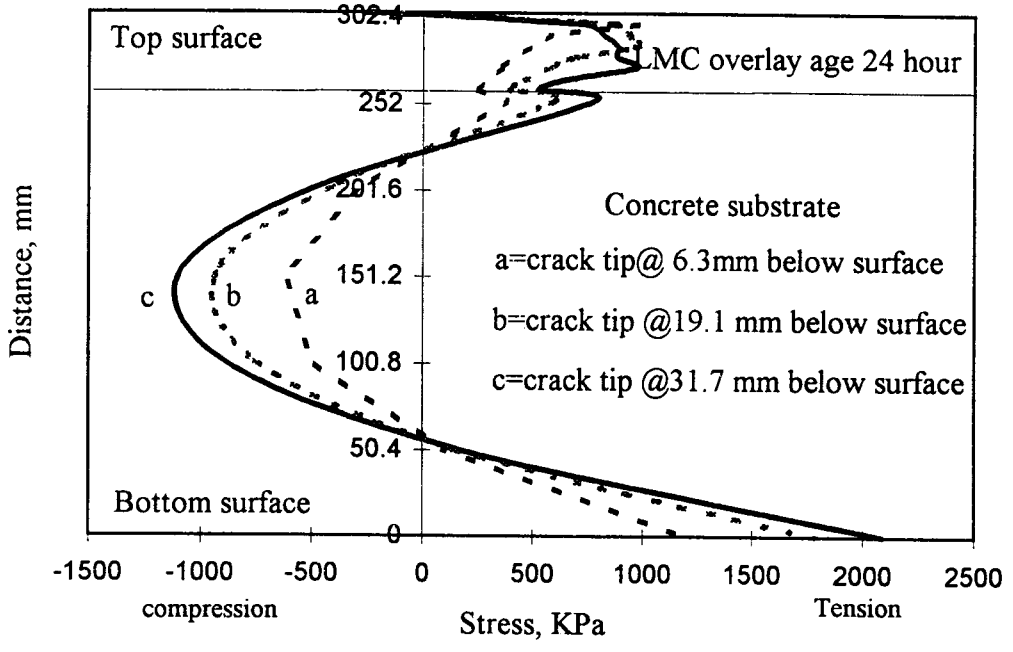

Figure 5.19 Stress distribution through the deck depth

5.4 Shrinkage Effect

To incorporate shrinkage into the model, a constant coefficient of thermal expansion of 10.3 x 10^{-6}/deg.C (4) was assumed to convert the measured shrinkage strain to an equivalent temperature differential. However, a higher (about 25%) coefficient of thermal expansion has been reported for early age conventional concrete, at 8-24 hrs., compared to later ages (86). The lower coefficient at later ages is due to an increased amount of crystalline material which results in a reduction in the potential expansion pressure. This pressure influences a part of movement which made up the coefficient of thermal expansion (18). Since the structure development of LMC also depends on the hydration process, similar to normal concrete, this effect might also be expected in LMC. Therefore, a modified coefficient (12.9 x 10^{-6}/deg.C) was used for the first 24 hours. Shrinkage strains from the low temperature test condition (12.7°C 100% RH-2 days and 50%RH 5 days) were used to simulate cool night conditions.

From the temperature distribution analysis, the maximum temperature differential 6.8°C, occurred in the third night. This value, combined with the assumed equivalent temperature difference (11.7°C) from the shrinkage effect at 24 hours resulted in an equivalent value of 18.5°C. This value is higher than the magnitude of temperature differential which may initiate crack propagation at 24 hours age for the simple span uncracked case, 9.6°C. At 36 and 48 hours, respectively, the shrinkage strain development was only slightly different from that at 24 hours. This provides a similar value for equivalent temperature differential, which also exceeds the crack initiation temperature differential.

For the continuous span uncracked condition, the equivalent temperature differential from environmental and shrinkage effects, 18.5°C, is still higher than the temperature to initiate a crack in the overlay, 14°C. This suggests a high potential for cracking in the case when the curing system is terminated at 24 hours age. These cracks, if they occur, may propagate through half of the overlay depth. Under the same severe condition, the crack depth may be even deeper in the cracked surface condition.

The value of 18.5 °C is slightly higher than the temperature that initiates cracks in the uncracked overlays at 48 hours age (15.8 °C). This suggests that if the severe condition occurs at 48 hours after placing, cracks may occur to a certain depth (12.5 mm), but may not propagate further. In the case of cracks already existing for any reason, those cracks may propagate deeper than in uncracked overlays (25.4mm).

Furthermore, it suggests that once cracks exist for any reason, the lower equivalent temperature differential, of only 5.2 °C, can further propagate those cracks. The cracks may propagate through the overlay thickness if this equivalent temperature reaches 11°C.

Based on the assumptions in this study and under the severe conditions, there is a high risk of cracking if the curing system is terminated before 48 hours after placing. However, the crack width may be very narrow. For example, when the cracks propagate through 6.25 mm depth of the initially uncracked overlay at 48 hours age, the predicted crack width is only 0.0001 mm at the overlay surface. This width crack likely would not be seen with the naked eye.

From this approximation, shrinkage appears to play a more important role than the environmental effect in the first 24 hours after placement. However, it is important to note that the assumed uniform shrinkage strain may differ slightly from actual conditions. In the field conditions, shrinkage strain may be higher at the overlay surface, compared to the inner portion. In addition, shrinkage strain may be lower for field conditions because the wet burlap used in the curing system supplies moisture during the continued hydration process. This condition differs from the controlled test environment of 12.7°C, 100% RH and with uncovered specimens. As a result, the temperature differential from environmental effects may have more importance than demonstrated by the study.

In summary, superposition appears to be a feasible technique which can be incorporated into the FCM for studying crack performance in LMC. The analyses in conjunction with a proper bilinear strain softening diagram provided satisfactory prediction of load-deflection curves, compared to the test results. The diagram shapes appear to depend on age. The bilinear shape with $s_1=f_t/6$, $w_1=0.333w_c$ and $w_2=3.66w_c$ was chosen to study early age performance.

The result of the FCM analyses, using temperature differential as a driving force, indicated that LMC cracking behaviors were strongly affected by overlay's age, especially for the first 24 hours. The thickness in the study range appeared to have less effect, compared to the first factor. To relate the environmental conditions to the overlay performance, temperature distributions through the deck depth were anlyzed at various times, using the finite difference method. The stress analyses for the severe

conditions indicated that the stress would possibly exceed the tensile strength of LMC at 24 hours.

Shrinkage effects were indirectly combined with environmental effects through an assumed constant coefficient of thermal expansion. The sum of the temperature differential from the severe environmental conditions and the equivalent temperature differential from the shrinkage effect appeared to exceed the temperature differential that initiated and propagated cracks at 24 hours age. This suggested possible early age crack occurrence if the curing system was terminated at 24 hours.

6.Conclusions

From the first phase of the study, more than 130 LMC samples were cast and tested to study the material properties at various ages ranging from 5 hours to 28 days. This information provided insights into material behavior and some necessary properties to be used for modelling in the second phase of the study. The proposed models were compared to the test data to check their appropriateness before applying them to predict the effects of material and environment on the overlay cracking performance.

The major findings from laboratory evaluations and analyses are summarized in this chapter and appropriate conclusions drawn. Finally, recommendations for further studies are provided based on the findings of this study.

6.1 Conclusions

1. The addition of latex modifies both pore structure in the matrices and interface zones of LMC through the effect of filling and sealing large voids, and film formation. These benefits bridge microcracks and improve bond strength in the interface zone. As a consequence, improvements in the material properties and the performance were observed.

2. A significant change in LMC performance occurs during the early ages, particularly in the first 24 hours after placing. Age strongly influences strength development. The rate of modulus of elasticity development is much higher than the rate of compressive strength gain.

3. Fracture behavior of LMC is slightly different than normal concrete. The high Pe/Pmax ratios (0.89-0.94) indicate increased linear behavior in the prepeak load region. The high ratio of midspan deflection at failure to midspan deflection at peak load (10-33) also indicates a ductility improvement in this material.

4. Slightly after the peak load, a bilinear relationship between midspan deflection and cmod was observed. There is no statistically significance for this relationship with time or notch depth ($p=0.50$ and 0.05, respectively), therefore this parameter is assumed constant in the study range.

5. The fracture energy of LMC varies between 2.3 to 133.1 N/m. Age appears to influence the fracture energy development. Fracture energy continues to increase for 28 days.

6. The fracture energies for unnotched beams were always higher than those for notched beams. The notch depth ratio effect was observed for a ratio of 0.1 or less. The ratios ranging between 0.2 to 0.4 did not show as significant an effect as in conventional concrete.

7. Fracture energy and compressive strength display similar trends with time. Fracture energy increased as the strength increased.

8. From the limited number of tests, the values of G_f from the cut-notch specimens were slightly higher than those from the cast notch specimens. Cutting a notch may simulate the conditions more realistically. However, the cut notch is not practical for early age studies.

9. LMC characteristic length, l_{ch}, varies between 160-2400 mm, depending on age. Large values were observed during the first 24 hours. These values decrease with time and reach the same range as for normal concrete at 28 days. However, the deformability of these two materials remains different.

10. Environmental conditions strongly affect shrinkage both in magnitude and performance. The shrinkage strains for 10 days age range between 0.0003 to 0.0005, depending on the test conditions.

11. Superposition is a feasible technique that can be incorporated into the fracture mechanics-based model, the FCM, to study cracking performance.

12. The accuracy of the model results depend on material properties; tensile strength, modulus of elasticity and fracture energy as well as the shape of the strain softening diagram.

13. A linear strain softening diagram only provides a satisfactory prediction for the load-deflection curve in the prepeak load region. A higher peak load and an inaccurate post-peak performance were observed when the linear shape was used. The bilinear shape provides a better prediction which agrees well with the test results.

14. The knee points, s_1 and w_1 of the bilinear diagram vary with age, particulary during the first 24 hours after placing. With $s_1 = f_t/6$, w_1 decreases from 0.375 w_c to 0.250 w_c as the LMC ages from 9.4 hours to 28 days.

15. In the analyses, the knee points $s_1 = f_t/6$ and w_1=0.375 w_c were used for ages less than 12 hours while $s_1 = f_t/6$, w_1=0.333 w_c were used for ages between 12 and 24 hours. Finally at ages greater than 48 hours $s_1 = f_t/6$, w_1=0.25 w_c were used.

16. The splitting tensile strength tests yielded satisfactorily predicted load-deflection curves for the later ages, 1 to 28 days. Modified f_t is necessary during the early ages (< 24 hours) when the material properties and performance change rapidly. The flexural stress- based $f_t=0.65f_f$ and $f_t=0.65f_f$ were used to study LMC at 9.4 and 12 hours ages.

17. Information from Oregon weather reports; temperature, solar radiation and wind data were used to study the environmental effects on LMC decks. During summer, the most severe conditions likely occur in July and August when temperature and solar radition are high and the wind is slight.

18. The temperature distribution analyses of the deck for three consecutive days indicated that the critical times occurred during the second and third nights when the temperature gradients reached or were close to the maximum. The stress analyses indicated that a higher stress than the tensile strength may occur at the top surface of the deck at 24 hours.

19. When only the temperature effects are of concern, the FCM is a feasible tool to study crack initiation and propagation in bridge decks.

20. The overlay's performance is influenced by age, surface conditions, the presence of cracked and uncracked sections and the degree of structural restraint.

21. LMC age has a significant effect on the temperature differential causing crack propagation and increased crack widths, particulary during the first 24 hours. The temperature differentials required for crack propagation range between 14-30°C for 24-48 hours age.The range dropped to 7-15 °C at 12 hours.

22. The presence of cracks on the overlay surface can lower the temperature differential required for further propagation by 30%, compared to crackless overlays.

23. Indeterminate structures appear to have higher crack resistance and lower crack sensitivity, compared to determinate structures. However, once the random cracks are formed, the crack resistance of the overlay is significantly decreased, independent of the degree of structural restraint.

24. The thicknesses in this study (51-76 mm) do not show any notably difference in the overlay cracking performance.

25. To relate the material effects to overlay performance, shrinkage strains were converted to an equivalent temperature differential through a coefficient of thermal expansion (12.9×10^{-6}/C).

26. At 24 hours, the combination of the environmental effect (maximum temperature gradient) and the material effect (equivalent temperature differential from shrinkage strains) indicated a high risk of cracking through one- half of the deck depth.

27. Under the same severe conditions, the analyses indicated that this high risk is reduced if the curing system is maintained for 48 hours. Cracks that may develop only propagate to shallow depth.

28. From these results, it is possible to predict the maximum temperature difference which the overlay can tolerate or, conversely determine the temperature differential at which the overlay may be expected to crack.

In summary, latex film formation affects LMC strength development, deformability and failure mechanisms. Most LMC properties; including strength, fracture, and

deformability change significantly with time, particularly at early ages. The improvements brought about through latex modification affect the overlay performance when non-structural failures are of particular concern. Fracture energy development strongly depends on time, up to 28 days. At later ages, the observed values were comparable to normal concrete.

When only temperature effects are of concern, a fracture mechanics-based model, FCM may provide a reasonable prediction for crack initiation and propagation. The study indicated that age, surface condition and structural restraint of the overlay strongly influence cracking performance. There were only slight differences from the effect of the overlay thickness. Even the shallow pre-existing cracks in the overlay can lower the temperature difference required for crack propagation.

With the available environmental information, it is possible to set up a temperature difference range for construction activities to minimize the risk of early age cracking. However, to indirectly incorporate shrinkage effects into the model, the accuracy of the predicted temperature differential also depends on other assumed properties. Therefore, further research in material properties development is necessary.

6.2 Recommendations

1. For the properties study of LMC during the early ages, considerable attention should be paid to each operation step: casting, handling, and test setting, due to the sensitive characteristics of material. This is necessary to minimize test variations.

2. Since LMC properties are time dependent and are rapidly changing during the first 24 hours after placing, accurate predictions for early age LMC performance are possible only if the true material properties are used in the model. The development of each property with time is of concern. The shape of the strain softening diagram at each age may be interpolated and can verify the predicted load deflection curve using available test results. However, better results may be obtained from the best fit appoaches when the load-deflection curves from the experiment at each testing age are used to adjust the assumed strain softening diagram until the difference between the test result and the predicted value is minimum. However, this requires a specially developed analysis program or a modification of commercial programs.

3. The fracture energy reported in this study may be slightly higher than the true value. This is due to an assumption of the RILEM method using in this study in which the consumed fracture energy is restricted to the narrow developed fracture zone in front of the notch. In the case of crack propagation in an existing cracked slab/beam, the difference may not be very large since the advanced crack path is generally close to the line for the precracked. However, for an uncracked structure, this effect may result in a significant difference.

In addition, the energy contribution during microcracking processes from the beam weight were neglected. This may have significant effects on very early age beams in which the strength properties are not sufficiently developed and the dead weight effect may be quite large compared to the external load to create crack propagation.

Therefore, further research should be performed to more accurately measure these effects.

4. To indirectly incorporate shrinkage effects in the model, experimental conditions that replicate the field condition are necessary to obtain the true strain for the equivalent temperature difference calculation. Use of these conditions will provide a more accurate prediction of the temperature difference impact.

5. Under some assumptions and the study conditions, the results of the study suggested that wet curing for new overlays should be prolonged at least 48 hours. This may reduce the high risk of cracking in the case of the severe conditions. Under some environmental conditions, such as a combination of high solar radiation, low wind and a large difference between the maximum and the minimum daily temperature, special precautions should be taken for the construction of LMC overlays. The sooner the curing system is applied after placing the overlay, the lower the risk of cracking, particularly during cool nights. Cracking prevention appears to be necessary. Once cracks are formed in the overlays, particularly random cracks, these cracks may easily propagate through the overlay thickness. Although these cracks are relatively narrow and are difficult to find, this existence affects the overlay performance.

References

1. Fontana, J. J. and Bartholomew, J., Use of Concrete Polymer Material in the Transportation Industry, *Application of Polymer Concrete: ACI Publication SP-69*, Detroit, 1981.

2. Strategic Highway Research Program, Condition Evaluation of Concrete Bridge Relative to Reinforcement Corrosion: Vol.6 Method for Field Determination of Total Chloride Content, *Technical Report SHRP-S/FR-92-108*, Washington D.C., 1992.

3. Nowak, A., Bridge Evaluation, Repair and Rehabilitation, *NATO ASI Series*, Vol. 187, London, 1990.

4. Synthesis of Highway Practice 179, *Latex-Modified Concretes and Mortars*, National Cooperative Highway Research Program, editor V.Ramakrishnan, Washington D.C., August 1992.

5. Wecharatana, M. and Shah, S.P., Prediction of Nonlinear Fracture Process Zone In Concrete, *Journal of Engineering Mechanics*, Vol.109 No.5, 1983, pp 1231-1245.

6. Chandra, S. and Ohama, Y., *Polymers in Concrete*, CRC, 1994.

7. La Fraugh, R.W. and Zinserling, M.H., Concrete Overlay for Bridge, *FHWA Report No. WA-RD-93.1*, Washington, 1987.

8. Whiting, D. and Dziedzic, W., Chloride Permeability of Rigid Concrete Bridge Deck Overlays, *Transportation Research Record 1234*, Transportation Research Board, Washington D.C., 1991, pp 24-29.

9. Dow Chemical USA, Long-Lasting Bridge Decks with Modified Concrete, *Technical paper: Form no.181-1129-87*, 1987.

10. Ohama, Y., Handbook of Polymer-Modified Concrete and Mortars:Properties and Process Technology, NOYES Publication, NJ, 1995.

11. Douglas, E.R. and Shafer, H.H., Reactions of Polymer Latex with Portland Cement Concrete, Transportation Research Record No. 542: Polymer Concrete, Washiongton D.C., 1975.

12. Parviz, S. and Atef, T., Latex Modification effects on Mechanisms of Microcrack Propagation in Concrete Material, *Transportation Research Record 1301*, Washington D.C., 1991, pp 33-39.

13. Marusin, S.L., Microstructure, Pore characteristics and Chloride Ion Penetration in Conventional Concrete and Concrete Containing Polymer Emulsion, *ACI SP-99-8*, David W. Fowler Editor, Detroit, 1987.

14. Ohama, Y., Principle of Latex Modification and Some Typical Properties of Latex Modified Concrete, *ACI Material Journal: Title no.84-M-45*, Nov./Dec. 1987, pp 511-518.

15. Ohama, Y. and Demura, K., Pore Size Distribution and Oxygen Diffusion Resistance of Polymer Modified Mortars, *Cement and Concrete Research: Vol.21 No.52/3*, March/May 1991, pp 309-315.

16. Dow Chemical, *A Handbook on Portland Cement Concrete and Mortar Containing Styrene/Butadiene Latex*, Dow' Bulletin,

17. Bean, D.L. and Husband, T.B., Latex Admixture for Portland Cement Concrete and Mortar, *Technical Report REMR-CS.3*. Missouri, 1986.

18. Neville, A.M., *Properties of Concrete*, John Wiley and Sons, 2nd ed., NJ, 1973.

19. Akihama, S., Morita, H. and Chida, H., Improvement of Mechanical Properties of Concrete through the Addition of Polymer Latex, *Polymer in Concrete: ACI SP-45*, Detroit, 1985.

20. Ohama, Y., Polymer Modified Moratars and Concretes, *Concrete Admixtures Handbook: Properties, Science and Technology*, Noyes Publication, Park Ridge, 1984.

21. Kobayashi, K. and Kimachi, Y., *Improvement of Ductility of Concrete Through the addition of Polymer Dispersion*, in Japanese, Semento-Gijutsu-Nempo, 1977.

22. Rusch, H., Jungwirth, D. and Hildorf, H., *Creep and Shrinkage: Their effect on the behavior of Concrete Structure*, Springer-Verlag, Berlin, 1979.

23. Guant, J.T. and Douglas, S. C., *Highway Bridge Vibration Studies*, School of Civil Eng. Purdue University, University Report 1983-1987, 1987.

24. Stone, J., Latex Modified Concrete: Excelsior for Bridge Deck?, Kentucky Department of Highway, March 1979.

25. Smutzer, R.K. and Hockett, R.B., Latex Modified Portland Cement Concrete - A Laboratory Investigation of Plastic and Hardened Properties of Concrete Mixtures Containing Three Formulations Used in Bridge Deck Overlays, Indiana State Highway Commission, Feb.,1981.

26. Hoff, G.G. et.al. Chemical Polymer and Fiber Additive for Low Maintenance Highway, *NOYES Data Corp.*, Newjersy. 1977.

27. Bishara, A.G., Latex Modified Concrete Bridge Deck Overlays: Field Performance Analysis. *Report No. FHWA/OH/79/004*, Ohio, October 1979.

28. ACI Committee 554, State of the Art Report on Fiber Reinforced Concrete, ACI 544.1 R-82, *Concrete International: design and Construction*, Nov. 1982.

29. Sprinkel, M.M., Twenty-Year Performance of Latex-Modified Concrete Overlay, *Virginia Department of Transportation Report No. 920883*, Washington, DC, 1992.

30. Missouri Cooperative Highway Research Program. Performance of Latex Modified and Low Slump Concrete Overlay on Bridge Decks. *Final Report 83-1*, Jefferson City, Missouri, 1983.

31. Oregon Department of Transportation. *Bridge deck overlay field reports between 1989-1994*, Oregon, 1994.

32. Chatterji., S., Probable Mechanisms of Crack Formation at Early Ages of Concretes: A Literature Survey, *Cement and Concrete Research* Vol.12, 1982.

33. Lundy, J.R. and Sujjavanich, S., Latex and Microsilica Modified Concrete Bridge Deck Overlays in Oregon, Interim Report: SPR Project No.5288, Oregon State University, 1995.

34. Kuhlmann, L.A., Cracks in Latex Modified Concrete Overlay: How They Get There, How Serious They are and What to do About Them, *Transportation Research Record 1301*, Washington, DC., 1991.

35. Ohama A., Bjorn, K. Jr. and Kamil E.K., Premature Failure of Latex Modified Concrete Bridge Deck Overlays in Ohio, Final Report, CTL Eng.Inc, Ohio, 1990.

36. *Concrete Bridge Engineering Performance and Advances*, R.J.Cope editor, Elsevier Applied Science, New York, 1987.

37. Manning, M., *Effect of Traffic Induced Vibrations on Bridge Deck Repair*, NCHRP Synthesis for Highway Practice 86, NCHRP, Washington DC, 1981.

38. Emerson, E., *The Calculation of the Distribution of Temperature in Bridges*, TRRL Report LR591, 1973.

39. Babei, K. and Hawkins, N.M., Performance of Bridge Deck Concrete Overlays, *ASTM STP 1100*, G.W.Maupin Jr., B.C.Brown and A.G.Lichtenstein editors, Philadelphia, 1990.

40. La Fraugh, R.W. and Zinserling, M.H., Concrete Overlay for Bridge, *FHWA Report No. WA-RD-93.1*, Washington, 1987.

41. Kalihaloo, B.L., Carpinteri, A. and Elices, M., Fracture Mechanics of Cement Mortars and Plain Concrete, *Advanced Cement Based Material* vol.1,1993, PP 92- 105.

42. A Report Card, Latex Modified Concrete Deck Overlays, *Public Works*, Vol. 119, No. 2, February 1988.

43. Havens, J.H., Hopwood, T. and Courtney, E.E., Bridge Decks and Overlays, *Kentucky Transportation Research Program*, Lexington, 1987.

44. Thepchatri, T., Phillip, J. C. and Matlock, H., *Prediction of Temperature and Stresses in Highway Bridges by Numerical Procedure Using Daily Weather Report*, Research report no.23-1, Texas State Department of Highway & Public Transportation, Texas, 1977.

45. Hunt, B. and Cooke, M., Thermal Calculation for Bridge Design, *ASCE Journal of Structural Div.*, vol.101 ST9, Sept. 1975, pp 1763-1781.

46. Rao, D.S.P., Temperature Distributions and Stresses in Concrete Bridges, *Journal of American Concrete Institute*, July/August, No.4, 1986, pp 588-596.

47. Elbadry, M. M. and Ghali, A., TemperatureVariations in Concrete Bridge, *ASCE Journal of Structural Engineering*, Vol.109, No.10, Oct. 1983, pp 2355- 2374.

48. Barber, E.S., Calculation of Maximum Pavement Temperatures From Weather Reports, Highway Research Board No.168, Washiongton D.C., 1957.

49. Jonasson, J.E., Analysis of Shrinkage in Concrete, Fundamental Research on Creep and Shrinkage, F.H.Wittmann editor, Martinus Nijhoff Pub., Hague, 1982.

50. Mindess, S. and Young, J.F., Concrete, Prentice Hall , Inc., NJ, 1981.

51. Bishara, A.G., Rose, J.D. and Youssef, M.A.R., Shrinkage and Creep Characteristics of Latex Modified Concrete, ACI Journal, May, 1978.

52. Gustafsson, P.J., *Fracture Mechanics Studies of Non-Yielding Material Like Concrete*: Modelling Fractrue and Applied Strength Analyses; LUTDG/(TVBM-1007)/1-422/1985.

53. Kim, S.K., The Constant Fracture Angle Model for Cementitious Material, *Dissertation* (Draft), NewJersey Institute of Technology, 1991.

54. Carpinteri, A., *Mixed Mode Crack Propagation in Concrete*, Fracture Mechanics Test Methods Test for Concrete:Rilem Report 5, S.P.Shah and A.Carpinteri, Chapman and Hall, Great Britain, Cambridge, 1991.

55. Inglis, C.E., *Stress in a Plate due to the Presence of Cracks and Sharp Corners*, Transaction of the Institute of Naval Architects 55, 1913.

56. Griffith, A.A., The Phenomenon of Rupture and Flow in Solids, Philip Transactions Royal Society of London, A-221, London, 1920.

57. Kaplan, M.F., Crack Propagation and the Fracture of Concrete, *ACI Journal* vol.58, Oct.1961 pp 591-610.

58. Brull, L. and Komlos, K., *Early Shrinkage of Hardening Cement Paste*, Fundamental Research on Creep and Shrinkage of Concrete, F.H.Wittmann editor, Martinus Nijhoff, Boston , 1982.

59. Shah, S.P., *Whiter Fracture Mechanics for Concrete*, Key note lecture in Fracture of Concrete and Rock: Recent development, S.P.Shah ans S.E Swartz and B.Barr, Elsvier Applied Science, NewYork, 1989.

60. Nallathambi, P., Karihaloo, B.L. and Heaton, B.S., Effect of Specimen and Crack Sizes, Water Cement Ratio and Coarse Aggregate Texture upon Fracture Toughness of Concrete, *Magazine of Concrete Research*, Vol.36 No.129 Dec., 1984.

61. Planas, J. and Elices, M., *Nonlinear Fracture of Cohesieve Material*, International Journal of Fracture vol.51, 1991.

62. Zaitsev, Y., Crack Propagation in a Composite Material, *Fracture Mechanics of Concrete*, F.H.Wittmann editor, Elsevier Science Publishers, Amsterdam, 1983.

63. Bazant, Z.P. and Cedolin, L., Blunt Crack Band Propagation in Finite Element Analysis, *Engineering Mechanics Division Journal*, ASCE Vol.105, April 1979, pp 297-315

64. RILEM, *Fracture Mechanics of Concrete-Application Part A*, a third draft of a report over the State of Art, RILEM, Sweden, 1988.

65. Kennedy, T., *Mechanics of Fracture and Fatigue*, Classnotes ME527 Winter 1994, OSU Book Stores Inc., Corvallis OR, 1994.

66. Du, J., A Fracture Mechanics Study of Concrete Failure, Ph.D.Dissertation, U.of Washington, Seattle, Washington, 1988.

67. Hillerborg, A., Modeer, M. and Petersson, P.E., Analysis of Crack Formation and Crack Growth in Concrete by Means of Fracture Mechanics and Finite Elements, *Cement and Concrete Research*, Vol.6, 1976

68. Brincker, R. and Dahl, H., *Fictitious Crack Model Of Concrete Fracture*, Magazine of Concrete Research Vol.41 No.147, 1989, pp 77-86.

69. Shah, S. P. and Jenq, Y.S., A Fracture Criterion for Concrete, *Engineering Fracture Mechanics Journal*, Vol.21 No.5, 1985, pp 1055-1069

70. Emborg, M., Thermal Analysis of Concrete Structures by Fracture Mechanics, RILEM Proceeding No.6, Chapman and Hall, London,1991

71. Nallathambi, P., Kalihaloo, B.L. and Heaton, B.S., *Various Size Effect in Fracture of Concrete*, Magazine of Concrete Research Vol.15, 1985, pp 117-126

72. Petersson, P.E., *Fracture Energy of Concrete:Method of Determination*, Cement and Concrete Research Vol.10, 1980.

73. Wittmann, F.H. and Hu, X., *Fracture Process Zone in Cementitious Material*, International Journal of Fracture vol.51, 1991.

74. Wittman F.H., Structure of Concrete with Respect to Crack Formation, Fracture Mechanics of Concrete, F.H.Wittman editor, Elsevier Science Pub., Amsterdam, 1983.

75. Hillerborg, A., *Analysis of one Single Crack*, Fracture Mechanics of Concrete, F.H Wittman editor, Elsevier Science Publisher, Amsterdam, 1983.

76. Carpinteri, A., Tommasso, A.D. and Ferrelli, M., *Influence of Material Parameter and Geometry on Cohesieve Crack Propagation*, Fracture Toughness and Fracture Energy of Concrete, Folker H. Wittmann editor, Elsevier Applied Science, Amsterdam, 1986.

77. Gopalaratnam, V.S and Ye, B.S., Numerical Characterization of the Nonlinear Fracture Process in Concrete, *Engineering Fracture Mechanic*, Vol.40, No.6, 1991, pp 991-1006.

78. Hillerborg, A., Results of the Three Comparative Test Series for Determing the Fracture Energy Gf of Concrete, *Materiaux et Constructions*, Vol.18, No.107, 1986.

79. Roelfstra, P.E. and Wittmann, F.H., *Fracture Toughness and Fracture Energy of Concrete: Numerical Method to link Strain Softening with Failure of Concrete*, Folker H. Wittmann editor, Elsevier Applied Science, Amsterdam, 1986.

80. Berwanger, C., *Transient Thermal Behavior of Composite bridge*, ASCE Journal of Structural Div.vol.109 no.10 October, 1983.

81. Hirst, M.J.S., Thermal Loading of Concrete Bridges, *Canadian Journal Civil Eng.*, Vol.11, No.3, Sept 1984, pp 423-429.

82. Kreith, F., *Principles of Heat Transfer*. Intext Educational Publishers 3rd edition, New York, 1973.

83. Brameshuber, W. and Hilsdorf, H.K., Development of Strength and Deformability of Very Young Concrete, *SEM/RILEM, International Conference on Fracture of Concrete and Rock*, Texas, 1987.

84. Validyne Engineer Corp., *UPC 607 PC Sensor Interface Card: Instruction Manual Revision2.0*, CA.,1990

85. American society for Testing Materials, ASTM C39-86, ASTM C496-87, 1987.

86. Properties of Set Concrete:CEA: State of Art Report, *Materiaux et Construction* vol.14 No.84, 1981, pp 411-433.

87. ASTM STP 169B. Significance of Tests and Properties of Concrete and Concrete Making Material, 1956.

88. Bruhweiler, E., Wittmann, F.H. and Rokugo, K., Influence of rate of loading on fracture energy and strain softening of concrete, *2nd Summary Report on Research Activities* compiled by F.H.Wittmann, Laboratorie des Materiaux de Construction, Lausanne, 1988.

89. Kormeling, H.A., Strain Rate and Temperature Behavior of Steel Fiber concrete in Tension, *doctoral Thesis*, Delfth University of Technology, 1986.

90. Kasai, Y., Kiyoshi, Y. and Isamu, M., *Tensile Properties of Early Age Concrete*, Proceeding International Conference of Mechanical Behavior of Material Vol.IV, Kyoto, Japan, August, 1971.

91. ANSYS, ANSYS User's Manual Revision 5.0, Swanson Analysis System, PA, 1994.

92. Carpinteri, A., Colombo, G. and Giuseppetti, G., *Fracture Toughness and Fracture Energy of Concrete: Accuracy of the Numerical Description of Cohesive Crack Propagation*, F. H. Wittmann, Elsevier Applied Science, Amsterdam, 1986.

93. Kreith, F. and Kreider, J.F., Principle of Solar Engineering, McGraw-Hill, New York, N.Y., 1978.